



INSTITUTO SUPERIOR TÉCNICO  
Universidade Técnica de Lisboa

# Performance Evaluation of UMTS/HSPA+ Data Transmission for Indoor Coverage

Ricardo José Serôdio Batista

Dissertation submitted for obtaining the degree of  
Master in Electrical and Computer Engineering

## Jury

Supervisor: Prof. Luís M. Correia

Co-supervisor: Mr. Carlos Caseiro

President: Prof. José Bioucas Dias

Members: Prof. António Rodrigues

October 2011



*To my loved ones*

“Aim for the moon. If you miss, you may hit a star.” *W. Clement Stone*

“Under promise and over deliver.” *Thomas J. Peters*



# Acknowledgements

First of all, my gratitude goes to Prof. Luís Correia, who allowed me to participate in this work a year ago when I decided to develop my thesis in collaboration with Vodafone. I will not forget his joyfulness and professionalism in our weekly meetings, sharing not only his knowledge about technical matters but also about his life experience and how to handle our future as youngsters. I also need to be thankful for being part of GROW, in which I was able to learn more about telecommunications with the other members and improve my presentation skills in the monthly meetings. Finally, a thank you for the leisure moments that Prof. Luís Correia was able to provide to all his collaborators, showing everyone how much fun this group can be.

My second dedication will be to Vodafone Portugal, more specifically to Mr. Carlos Caseiro, Mr. Marco Serrazina and Mr. Pedro Lourenço, for following my work throughout this time and sharing their knowledge about wireless communications from the operator point of view. Their availability and time spent with my doubts was crucial for the development of this work, and without their help this thesis would not be the same.

To all my professors, who provided me with tools, technical knowledge and support in my academic life, particularly to Ana Fred, António Rodrigues, Carlos Fernandes, Eduardo Pereira, João Pires, João Sobrinho, Leonel Sousa and José Figueiredo.

To my RF2 lab colleagues, Armanda Martins, Diogo Silva, João Pinto, Pedro Carreira and Tiago Gonçalves, who shared the “basement” with me, where this work was done, being a quiet place and therefore perfect to develop my work. Their help and friendship was one of the highlights of this period, not only for the mutual knowledge sharing but also for the amusing moments. Without them, this path would be tougher and I hope that my professional life can come across theirs at some point.

I will not forget all my other IST colleagues who travelled this 5-year long journey with me: Alexandre Dias, Catarina Carvalho, Duarte Martins, Henrique Silva, João Falcão, Pedro Silva, Rui Figueiredo, Sílvio Rodrigues and Tiago Jorge. A special thanks to all my other friends, such as André Gomes, Catarina Luís, Margarida Carreira and Rui Dias da Costa, who were responsible for my growth as a person and for most of the amusing moments in my life.

At last, but not the least, my family deserves all my gratitude since the day I was born: my Father and my Mother, my Sister and my Uncle Mané, and especially my Grand-Father, the latter being one of the most influencing people in my life, in every single part of it.



# Abstract

The main objective of this thesis was to study and quantify the data rate transmission performance for a UMTS/HSPA+ system in indoor scenarios, giving special emphasis to capacity and coverage aspects. These goals were accomplished through the development and implementation of two models: the Single- and Multi-User models. A measurement campaign was conducted to obtain a model for signal attenuation, which was input in both models. In order to verify the indoor data rate performance, simulations were made by changing different parameters. In DL, the most influencing factor is the presence of interference, lowering the average indoor throughput in isolated buildings. In UL, the available signal power is the key factor, in which higher buildings have greater average throughputs due to the availability of signal in the upper floors. The number of penetrated walls also decreases the data rate, as well as the desired coverage percentage. The floor height gain verified in terms of signal is also present in the data rate, with an average data rate increase of 3.25 % in DL and 8.99 % in UL. Generically, data rate reductions are greater in UL, due to the lower transmitting power and the shorter throughput range.

## Keywords

UMTS/HSPA+, Capacity, Coverage, Indoor, Data Rate Performance, Measurements

# Resumo

O principal objectivo desta tese foi estudar e quantificar o desempenho da taxa de transmissão de dados para um sistema UMTS/HSPA+ em cenários interiores, dando ênfase aos aspectos de capacidade e cobertura. Estes objetivos foram alcançados através do desenvolvimento e implementação de dois modelos: os modelos de mono- e multi-utilizador. A campanha de medições foi realizada para obter um modelo para a atenuação de sinal, que foi implementada em ambos os modelos. A fim de verificar o desempenho da taxa de transmissão de dados em ambientes interiores, as simulações foram feitas alterando vários parâmetros. Em DL, o factor de maior influência é a presença de interferência, diminuindo o rendimento médio nos edifícios isolados. Em UL, a potência do sinal disponível é o factor chave, sendo que os edifícios mais altos têm maior débito médio devido à disponibilidade de sinal nos andares superiores. O número de paredes penetradas também diminui a taxa de transmissão de dados, bem como a percentagem de cobertura desejada. O ganho de altura por piso verificado em termos de sinal está presente também na taxa de transmissão de dados, com um aumento médio de ritmo binário por piso de 3,25 % em DL e 8,99 % em UL. Genericamente, as reduções de taxa de transmissão de dados são maiores em UL devido à menor potência de transmissão e à menor gama de valores de débito possíveis.

## Palavras-chave

UMTS/HSPA+, Capacidade, Cobertura, Interior, Desempenho de Taxa de Transmissão, Medições

# Table of Contents

|                                    |       |
|------------------------------------|-------|
| Acknowledgements .....             | v     |
| Abstract.....                      | vii   |
| Resumo .....                       | viii  |
| Table of Contents.....             | ix    |
| List of Figures .....              | xii   |
| List of Tables.....                | xv    |
| List of Acronyms .....             | xvi   |
| List of Symbols.....               | xix   |
| List of Software .....             | xxiii |
| 1 Introduction .....               | 1     |
| 1.1 Overview.....                  | 2     |
| 1.2 Motivation and Contents.....   | 5     |
| 2 UMTS Aspects .....               | 7     |
| 2.1 Basic Concepts.....            | 8     |
| 2.1.1 Network Architecture .....   | 8     |
| 2.1.2 Radio Interface .....        | 9     |
| 2.1.3 Performance Analysis.....    | 14    |
| 2.1.4 HSPA Evolution .....         | 17    |
| 2.2 Services and Applications..... | 20    |
| 2.3 Interference .....             | 22    |
| 2.3.1 Basic Aspects .....          | 22    |

|          |   |           |
|----------|---|-----------|
| 2.3.2    | Intra- and inter-cell Interferences.....          | 24        |
| 2.3.3    | Interference Models.....                          | 25        |
| 2.4      | Propagation Models.....                           | 27        |
| 2.4.1    | Introduction.....                                 | 27        |
| 2.4.2    | Outdoor and Indoor Models.....                    | 29        |
| 2.5      | Throughput Models State of the Art.....           | 31        |
| <b>3</b> | <b>Model Development and Implementation .....</b> | <b>33</b> |
| 3.1      | Propagation Models.....                           | 34        |
| 3.1.1    | Outdoor Model.....                                | 34        |
| 3.1.2    | Indoor Model.....                                 | 36        |
| 3.2      | Simulator Overview .....                          | 40        |
| 3.2.1    | Single-User Model.....                            | 40        |
| 3.2.2    | Multi-User Model.....                             | 42        |
| 3.3      | Simulation Algorithms.....                        | 43        |
| 3.4      | Input and Output Parameters .....                 | 48        |
| 3.5      | Simulator Assessment.....                         | 51        |
| <b>4</b> | <b>Results Analysis .....</b>                     | <b>53</b> |
| 4.1      | Scenarios Description.....                        | 54        |
| 4.2      | Measurements.....                                 | 57        |
| 4.2.1    | Procedure .....                                   | 58        |
| 4.2.2    | Results.....                                      | 60        |
| 4.3      | Simulations .....                                 | 63        |
| 4.3.1    | Comparison with Model Results .....               | 63        |
| 4.3.2    | Urban Scenarios Simulations .....                 | 66        |
| <b>5</b> | <b>Conclusions.....</b>                           | <b>77</b> |
|          | <b>Annex A – Link Budget.....</b>                 | <b>83</b> |
|          | <b>Annex B – COST231 Walfisch-Ikegami.....</b>    | <b>87</b> |
|          | <b>Annex C – UMTS Categories.....</b>             | <b>91</b> |
|          | <b>Annex D – HSPA+ Throughput Models .....</b>    | <b>93</b> |

|   |     |
|---|-----|
| Annex E – User’s Manual.....                              | 99  |
| Annex F – Measurements Results .....                      | 103 |
| Annex G – Application Layer Throughput.....               | 113 |
| Annex H – Normal Distribution Validation.....             | 115 |
| Annex I – Indoor Signal Attenuation Model Validation..... | 117 |
| References.....   | 120 |

# List of Figures

|  |    |
|--|----|
| Figure 1.1. Evolution of HSPA maximum peak bit rate for each Release (extracted from [HoTo10]).                          | 3  |
| Figure 1.2. Data traffic and revenues trends for mobile communications (extracted from [Wire11]).                        | 4  |
| Figure 2.1. UMTS network architecture (extracted from [HoTo04]).   | 8  |
| Figure 2.2. Orthogonality factor as a function of the MT's distance to BS (extracted from [Carr11]).                     | 12 |
| Figure 2.3. DL and UL Throughputs in Pedestrian A channel for HOM (extracted from [PWST07]).                             | 18 |
| Figure 2.4. Spectral efficiency variation according to each modulation behaviour (extracted from [CEGH02]).              | 19 |
| Figure 2.5. Bit error probability in function of $E_c/N_0$ for each HSPA+ modulation.                                    | 20 |
| Figure 2.6. Different cases of interference (extracted from [Chen03]).   | 23 |
| Figure 2.7. Total interference power distribution at the reference cell (extracted from [SRAA03]).                       | 26 |
| Figure 2.8. Illustration of the outdoor and indoor losses (extracted from [Corr09]).                                     | 29 |
| Figure 2.9. Illustration of the extra attenuation parameters (adapted from [Corr09]).                                    | 30 |
| Figure 3.1. First Fresnel zone representation (extracted from [Marq08]).   | 34 |
| Figure 3.2. Different cases of outdoor path loss (extracted from [Marq08]).  | 35 |
| Figure 3.3. Different types of urban building scenarios.   | 37 |
| Figure 3.4. Example of one floor blueprint (adapted from [Marq08]).  | 37 |
| Figure 3.5. Indoor room loss model approach.   | 37 |
| Figure 3.6. Single-User simulator structure.   | 41 |
| Figure 3.7. Multi-User simulator structure.  | 42 |
| Figure 3.8. Path loss decision algorithm (adapted from [Marq08]).  | 44 |
| Figure 3.9. Single-User data rate calculation algorithm.   | 45 |
| Figure 3.10. Decision mode for the Multi-User procedure.   | 46 |
| Figure 3.11. Multi-User capacity calculation algorithm.  | 47 |
| Figure 4.1. Horizontal (blue) and vertical (red) radiation pattern for the P7755.00 antenna [Kath11].                    | 57 |
| Figure 4.2. Measurements set (laptop, cart and USB stick).   | 58 |
| Figure 4.3. Indoor and outdoor measurement process (adapted from [XaVe02]).  | 59 |
| Figure 4.4. Types of outdoor measurements of the reference signal level of each BS, depending on the accessible façades. | 60 |
| Figure 4.5. Mean throughput reductions comparison for High Integrated buildings.   | 64 |
| Figure 4.6. Mean throughput reductions comparison for High Isolated buildings.   | 64 |
| Figure 4.7. Mean throughput reductions comparison for Low Integrated buildings.  | 65 |

|  |     |
|--|-----|
| Figure 4.8. Mean throughput reductions comparison for Low Isolated buildings.....                          | 66  |
| Figure 4.9. Average DL throughput reduction along the simulated building floors. ....                      | 67  |
| Figure 4.10. Average UL throughput reduction along the simulated building floors. ....                     | 68  |
| Figure 4.11. Average DL throughput reduction along building floors with the respective trend<br>line. .... | 68  |
| Figure 4.12. Average UL throughput reduction along building floors with the respective trend<br>line. .... | 69  |
| Figure 4.13. Average throughput reduction for all simulated room types. ....                               | 70  |
| Figure 4.14. Average throughput reduction comparison for different antenna positions. ....                 | 71  |
| Figure 4.15. Average throughput reduction comparison for different distances. ....                         | 72  |
| Figure 4.16. Average throughput reduction comparison for different coverage conditions. ....               | 73  |
| Figure 4.17. Served users for the available throughput values in DL for a SISO configuration.....          | 74  |
| Figure 4.18. Average difference between outdoor and indoor served users in DL.....                         | 75  |
| Figure 4.19. Served users for the available throughput values in UL for a SISO configuration.....          | 76  |
| Figure 4.20. Average difference between outdoor and indoor served users in DL.....                         | 76  |
| <br>   |     |
| Figure B.1. Definition of the parameters used in the COST 231 - WI model (extracted from<br>[DaCo99])..... | 87  |
| Figure B.2. Definition of the street orientation angle $\varphi$ (extracted from [DaCo99]).....            | 87  |
| <br>   |     |
| Figure E.1. Main window of the UMTSIndCov simulator.....   | 99  |
| Figure E.2. Outdoor Environment window.....  | 100 |
| Figure E.3. Other Parameters window. ....  | 100 |
| Figure E.4. Coverage Simulation window. ....   | 101 |
| Figure E.5. Capacity Simulation window.....  | 101 |
| <br>   |     |
| Figure F.1. RSCP attenuation values for High Integrated buildings in floor transitions. ....               | 103 |
| Figure F.2. RSCP attenuation values for High Isolated buildings in floor transitions.....                  | 104 |
| Figure F.3. RSCP attenuation values for Low Integrated buildings in floor transitions.....                 | 104 |
| Figure F.4. RSCP attenuation values for Low Isolated buildings in floor transitions.....                   | 105 |
| Figure F.5. DL throughput attenuation values for High Integrated buildings in floor transitions. ....      | 105 |
| Figure F.6. DL throughput attenuation values for High Isolated buildings in floor transitions.....         | 106 |
| Figure F.7. DL throughput attenuation values for Low Integrated buildings in floor transitions. ....       | 106 |
| Figure F.8. DL throughput attenuation values for Low Isolated buildings in floor transitions.....          | 106 |
| Figure F.9. UL throughput attenuation values for High Isolated buildings in floor transitions.....         | 107 |
| Figure F.10. UL throughput attenuation values for High Integrated buildings in floor transitions. ....     | 107 |
| Figure F.11. UL throughput attenuation values for Low Isolated buildings in floor transitions.....         | 107 |
| Figure F.12. UL throughput attenuation values for Low Integrated buildings in floor transitions. ....      | 108 |
| Figure F.13. RSCP attenuation values in room transitions. ....   | 109 |
| Figure F.14. DL throughput attenuation values in room transitions. ....                                    | 109 |

|   |     |
|---|-----|
| Figure F.15. UL throughput attenuation values in room transitions. ....   | 110 |
| Figure F.16. DL modulation usage for High Integrated buildings.....   | 110 |
| Figure F.17. DL modulation usage for High Isolated buildings. ....  | 111 |
| Figure F.18. DL modulation usage for Low Integrated buildings. ....   | 111 |
| Figure F.19. DL modulation usage for Low Isolated buildings. ....   | 111 |
| Figure F.20. Mapping between SIR and DL throughput for the different building types. ....                                     | 112 |
|   |     |
| Figure H.1. PDF of the signal attenuation between outdoor and IW scenarios (Torre Norte, 11 <sup>th</sup> floor).....         | 115 |
| Figure H.2. PDF of the throughput attenuation distribution between outdoor and IW (Torre Norte - 11 <sup>th</sup> floor)..... | 116 |
|   |     |
| Figure I.1. Signal attenuation values for Indoor Window rooms in High Integrated buildings.....                               | 118 |
| Figure I.2. Signal attenuation values for Indoor Daylight rooms in High Integrated buildings. ....                            | 118 |
| Figure I.3. Signal attenuation values for Indoor Window rooms in High Isolated buildings. ....                                | 118 |
| Figure I.4. Signal attenuation values for Indoor Daylight rooms in High Isolated buildings. ....                              | 119 |
| Figure I.5. Signal attenuation values for Indoor Window rooms in Low Integrated buildings. ....                               | 119 |
| Figure I.6. Signal attenuation values for Indoor Daylight rooms in Low Integrated buildings. ....                             | 119 |

# List of Tables

|  |     |
|--|-----|
| Table 2.1. Comparison between different UMTS stages (adapted from [HoTo10]).....   | 19  |
| Table 2.2. UMTS traffic class parameters (extracted from [3GPP02b]).....   | 21  |
| Table 2.3. Service differentiation and characteristics (adapted from [3GPP10a]). .....   | 22  |
| Table 2.4. Standard deviations for the different MT building height cases (extracted from [Marq08]).....                         | 26  |
| Table 2.5. Standard deviations for the different distance cases (extracted from [Marq08]). .....                                 | 27  |
| Table 2.6. Wall and floor types for the MWM and weighted average loss (extracted from [Marq08]).....                             | 30  |
| Table 3.1. Characteristics of the Different cases of outdoor path loss (adapted from [Marq08]).....                              | 35  |
| Table 3.2. Parameters used for slow and fast fading margins (adapted from [Jaci09]).....   | 36  |
| Table 4.1. Measured buildings' characteristics. ....   | 55  |
| Table 4.2. Outdoor model parameters for simulations in each case scenario. ....  | 56  |
| Table 4.3. Reference parameters for all simulation scenarios. ....   | 56  |
| Table 4.4. Model parameters for the signal attenuation due to building penetration. ....   | 61  |
| Table 4.5. Correlation between throughput reduction and signal attenuation for all building types. ....                          | 66  |
| Table 4.6. Correlation coefficients for throughput reduction functions along the building floors.....                            | 69  |
| Table 4.7. Average difference of throughput reduction between floors. ....   | 70  |
| <br>   |     |
| Table A.1. Processing gain and SNR definition for HSPA+ (adapted from [Jaci09]).....   | 84  |
| <br>   |     |
| Table C.1. FDD HS-DSCH physical layer terminal categories (adapted from [3GPP10b]). .....  | 91  |
| Table C.2. FDD E-DCH physical layer terminal categories (adapted from [3GPP10b]). .....  | 92  |
| <br>   |     |
| Table F.1. Standard deviations for the measured attenuations. ....   | 108 |
| <br>   |     |
| Table G.1. Maximum physical and application throughput for different configurations in HSPA+ DL (extracted from [Preg08]). ..... | 114 |
| <br>   |     |
| Table H.1. Hypothesis test results.....  | 116 |

# List of Acronyms

|          |  |
|----------|--|
| 16QAM    | 16 Quadrature Amplitude Modulation             |
| 3GPP     | Third Generation Partnership Project           |
| 64QAM    | 64 Quadrature Amplitude Modulation             |
| AMC      | Adaptative Modulation and Coding               |
| AMR      | Adaptative Multirate                           |
| BER      | Bit Error Rate                                 |
| BLEP     | Block Error Probability                        |
| BLER     | Block Error Rate                               |
| BoD      | Bandwidth on Demand                            |
| CDF      | Cumulative Distribution Function               |
| CN       | Core Network                                   |
| CQI      | Circuit Switched                               |
| CS       | Channel Quality Indicator                      |
| DCH      | Dedicated Channel                              |
| DC-HSDPA | Dual Carrier High Speed Downlink Packet Access |
| DI       | Deep Indoor                                    |
| DL       | Downlink                                       |
| DS-CDMA  | Direct-Sequence Code Division Multiple Access  |
| DTX      | Discontinuous Transmission                     |
| DVB-H    | Digital Video Broadcasting - Handheld          |
| E-AGCH   | Enhanced Absolute Grant Channel                |
| E-DCH    | Enhanced Dedicated Channel                     |
| E-DPCCH  | Enhanced Dedicated Physical Control Channel    |
| E-DPDCH  | Enhanced Dedicated Physical Data Channel       |
| E-HICH   | Enhanced HARQ Indicator Channel                |
| EIRP     | Equivalent Isotropic Radiated Power            |
| FDD      | Frequency Division Duplex                      |
| F-DPCH   | Fractional Dedicated Physical Channel          |
| GGSN     | Gateway GPRS Support Node                      |
| GMSC     | Gateway MSC                                    |
| GPRS     | General Packet Radio Service                   |
| GSM      | Global System for Mobile Communications        |
| HARQ     | Hybrid Automatic Repeat Request                |
| HInt     | High-Integrated                                |

|          |   |
|----------|---|
| Hlso     | High-Isolated                                 |
| HLR      | Home Location Register                        |
| HOM      | Higher-Order Modulation                       |
| HSDPA    | High Speed Downlink Packet Access             |
| HS-DPCCH | High Speed Dedicated Physical Control Channel |
| HS-DSCH  | High Speed Downlink Shared Channel            |
| HSPA     | High Speed Packet Access                      |
| HSPA+    | High Speed Packet Access Evolution            |
| HS-PDSCH | High Speed Physical Downlink Shared Channel   |
| HS-SCCH  | High Speed Shared Control Channel             |
| HSUPA    | High Speed Uplink Packet Access               |
| ID       | Indoor Daylight                               |
| IP       | Internet Protocol                             |
| ISDN     | Integrated Services Digital Network           |
| IW       | Indoor Window                                 |
| L1       | Layer 1                                       |
| L2       | Layer 2                                       |
| LInt     | Low-Integrated                                |
| Llso     | Low-Isolated                                  |
| LoS      | Line-of-Sight                                 |
| MAC      | Medium Access Control                         |
| ME       | Mobile Equipment                              |
| MIMO     | Multiple Input Multiple Output                |
| MMS      | Multimedia Message Service                    |
| MSC      | Mobile Services Switching Centre              |
| MT       | Mobile Terminal                               |
| MWM      | Multi-Wall model                              |
| NLoS     | Non-Line-of-Sight                             |
| OSI      | Open Systems Interconnection                  |
| OSVF     | Orthogonal Variable Spreading Factor          |
| P-CPICH  | Primary-Common Pilot Channel                  |
| PDF      | Probability Density Function                  |
| PS       | Packet Switched                               |
| PSTN     | Public Switched Telephone Network             |
| QoS      | Quality of Service                            |
| QPSK     | Quadrature Phase-Shift Keying                 |
| RAN      | Radio Access Network                          |
| RNC      | Radio Network Controller                      |
| RNS      | Radio Network Sub-System                      |
| RRM      | Radio Resource Management                     |

|       |  |
|-------|--|
| RSCP  | Received Signal Code Power                 |
| RTT   | Round Trip Time                            |
| SF    | Spreading Factor                           |
| SGSN  | Serving GPRS Support Node                  |
| SIMO  | Single Input Multiple Output               |
| SINR  | Signal-to-Interference-plus-Noise Ratio    |
| SIR   | Signal-to-Interference Ratio               |
| SISO  | Single Input Single Output                 |
| SMS   | Short Message Service                      |
| SNR   | Signal-to-Noise Ratio                      |
| TBS   | Transport Block Size                       |
| TDD   | Time Division Duplex                       |
| TTI   | Transmission Time Interval                 |
| UE    | User Equipment                             |
| UL    | Uplink                                     |
| UMTS  | Universal Mobile Telecommunications System |
| USIM  | UMTS Subscriber Identity Module            |
| UTRAN | UMTS Terrestrial Radio Access Network      |
| VLR   | Visitor Location Register                  |
| VoIP  | Voice over IP                              |
| WCDMA | Wideband Code Division Multiple Access     |
| WI    | Walfisch-Ikegami                           |

# List of Symbols

|  |   |
|--|---|
| $\alpha_{CO}$                                      | Code orthogonality factor   |
| $\Delta\mu$  | Average value of a difference distribution                              |
| $\Delta\sigma$                                     | Standard deviation of a difference distribution                         |
| $\Delta f$   | Signal bandwidth  |
| $\frac{\Delta N_{au}}{\Delta R_b^{floor}}$         | User reduction from outdoor to indoor scenarios                         |
| $\frac{\Delta R_b^{Floor i}}{\Delta R_b^{Rooms}}$  | Average difference of throughput reduction between consecutive floors   |
| $\frac{\Delta R_b^{Rooms}}{\Delta RSCP^{Floor i}}$ | Average throughput reduction between outdoor and indoor (in floor $i$ ) |
| $\frac{\Delta RSCP^{Rooms}}{\Delta RSCP^{Rooms}}$  | Average room throughput reduction between outdoor and indoor            |
| $\eta$   | Average attenuation between outdoor and indoor (in floor $i$ )          |
| $\eta_{DL}$  | Average room attenuation between outdoor and indoor                     |
| $\eta_g$   | Load factor   |
| $\eta_{UL}$  | Downlink load factor  |
| $\mu$  | Activity factor of service $g$  |
| $\mu_{Floor i}^{IW,ID,DI}$                         | Uplink load factor  |
| $\mu^{var}$  | Average   |
| $\mu^{level}$                                      | Average attenuation concerning floor $i$ in room type IW, ID or DI      |
| $\bar{\mu}$  | Variable part of the mean attenuation, dependent on the floor number    |
| $\lambda$  | Static part of the mean attenuation, independent on the floor number    |
| $\rho$   | Mean value of a set of averages   |
| $\rho_{IN}$  | Wavelength  |
| $\rho_{corr}$                                      | Signal-to-Noise ratio   |
| $\rho_{pilot}$                                     | Signal-to-Interference-plus-Noise Ratio                                 |
| $\sigma$   | Correlation factor  |
| $\sigma_{Floor i}^{IW,ID,DI}$                      | Pilot $E_c/N_0$ when HSDPA is active                                    |
| $\bar{\sigma}$                                     | Standard deviation  |
| $\Psi$   | Standard deviation concerning floor $i$ in room type IW, ID or DI       |
| $a_{pd}$   | Quadratic mean of a set of standard deviation values                    |
| $d$  | Road orientation with respect to the direct radio path                  |
| $d_l$  | Average power decay   |
| $d_m$  | Distance between the BS and the MT                                      |
| $d_{rt}$   | Distance between the BS and the building top                            |
| $E_b$  | Horizontal distance between the MT and the diffracting edges            |
|  | Distance between the roof top and the MT                                |
|  | Energy per bit  |

|                       |  |
|-----------------------|--|
| $E_c$                 | Energy of the data chip stream   |
| $f$                   | Operating frequency  |
| $F$                   | Receiver's noise figure  |
| $F_a$                 | Activity factor  |
| $F_N$                 | Floor number   |
| $g$                   | Geometry factor  |
| $G_P$                 | Processing gain  |
| $G_{SHO}$             | Soft handover gain   |
| $G_{Rx}$              | Receiving antenna gain   |
| $G_{Tx}$              | Transmitting antenna gain  |
| $h_{base}$            | Antenna height   |
| $h_{Mobile}$          | Mobile height  |
| $h_{Roof}$            | Roof height  |
| $i_r$                 | Ratio of inter- to intra-cell interferences                              |
| $I^{Equal}$           | Interference power for a central building with equal height              |
| $I^{Far}$             | Interference power far from the base station                             |
| $I^{Higher}$          | Interference power for a central building with higher height             |
| $I_{inter}$           | Normalised inter-cell interference                                       |
| $I_{intra}$           | Normalised intra-cell interference                                       |
| $I_{DL}^{Integrated}$ | Downlink interference power for Integrated buildings                     |
| $I_{DL}^{Isolated}$   | Downlink interference power for Isolated buildings                       |
| $I^{Near}$            | Interference power near the base station                                 |
| $I^{Lower}$           | Interference power for a central building with lower height              |
| $I^{Ref}$             | Interference power for the reference scenario                            |
| $I_{UL}$              | Uplink interference power  |
| $k$                   | Propagation constant   |
| $k_a$                 | Path loss increase for antennas below the roof tops (adjacent buildings) |
| $k_d$                 | Dependence of the multi-screen diffraction loss versus distance          |
| $k_f$                 | Dependence of the multi-screen diffraction loss versus frequency         |
| $L_0$                 | Free space loss  |
| $L_c$                 | Cable loss attenuation between the emitter and the BS antenna            |
| $L_{bsh}$             | Losses due to the fact that antennas are above or below the roof level   |
| $L_f$                 | Loss due to floor attenuation  |
| $L_{glass}$           | Loss due to glass attenuation  |
| $L_{msd}$             | Multiple screen diffraction loss   |
| $L_{Ori}$             | Street orientation loss  |
| $L_P$                 | Path loss  |
| $L_{P\ ind}$          | Path loss due to indoor attenuation                                      |
| $L_{P\ m}$            | Path loss between the BS and user $m$                                    |
| $L_{P\ outd}$         | Path loss due to outdoor attenuation                                     |

|                         |  |
|-------------------------|--|
| $L_{rm}$                | Extra attenuation due to the diffraction from the roof top to the MT |
| $L_{ref}$               | Total propagation losses   |
| $L_{rts}$               | Roof-top-to-street diffraction and scatter loss                      |
| $L_u$                   | User loss attenuation  |
| $L_w$                   | Loss due to wall attenuation   |
| $M$                     | Modulation index   |
| $M_{FF}$                | Margin due to fast fading  |
| $M_I$                   | Interference margin  |
| $M_P$                   | Total margin   |
| $M_{SF}$                | Margin due to slow fading  |
| $N$                     | Total noise power  |
| $N_b$                   | Number of HS-DSCH transport block bits                               |
| $N_0$                   | Noise power spectral density   |
| $N_{adj}$               | Number of samples collected in the adjacent street side pavement     |
| $N_{au}$                | Number of active users   |
| $N_{au}^{indoor}$       | Number of indoor served users  |
| $N_{au}^{max}$          | Maximum number of served users                                       |
| $N_{au}^{outdoor}$      | Number of outdoor served users                                       |
| $N_{Floors}^{NLoS}$     | Number of floors in non line of sight                                |
| $N_{Floors}^{LoS}$      | Number of floors in line of sight                                    |
| $N_{opp}$               | Number of samples collected in the opposite street side pavement     |
| $N_{RF}$                | Noise spectral density   |
| $N_{serv}$              | Total number of services   |
| $p$                     | Desired building coverage  |
| $\overline{P_b}^{QPSK}$ | Average bit error probability for QPSK in a Rayleigh channel         |
| $\overline{P_b}^{MQAM}$ | Average bit error probability for MQAM in a Rayleigh channel         |
| $P_{adj}$               | Power samples collected in the adjacent street side pavement         |
| $P_{HSDPA}$             | HSDPA transmit power   |
| $P_{HS-DSCH}$           | BS HS-DSCH transmission power  |
| $P_{MT \rightarrow BS}$ | Transmitted power from a MT to BS                                    |
| $P_{BS \rightarrow MT}$ | Transmitted power from BS to a MT                                    |
| $P_{opp}$               | Power samples collected in the opposite street side pavement         |
| $P_{pilot}$             | Transmitting power over the pilot channel                            |
| $P_r$                   | Available receiving power at antenna port                            |
| $P_{ref}^{ind}$         | Reference value of the external power for each BS                    |
| $P_{Rx}$                | Power at the input of the receiver                                   |
| $P_{Rx min}$            | Receiver sensitivity   |
| $P_{Rx ind}$            | Indoor received signal power   |
| $P_{Rx outd}$           | Outdoor received signal power  |
| $P_{Total, BS}$         | Total transmitted power from BS to MTs within the cell               |

|                              |  |
|------------------------------|--|
| $P_t$                        | Transmitting power at antenna port                           |
| $P_{Tx}$                     | BS Transmitting antenna power                                |
| $r$                          | Cell radius  |
| $R_c$                        | Chip rate  |
| $R_b$                        | Data bit rate  |
| $R_{b/code}$                 | Physical layer throughput per code                           |
| $\overline{R_b}^{Outdoor}$   | Average throughput measured in the outdoor                   |
| $R^{Fresnel}$                | Fresnel ellipsoid radius                                     |
| $\overline{RSCP}^{Floor\ i}$ | Average RSCP measured indoors in floor $i$                   |
| $\overline{RSCP}^{Outdoor}$  | Average RSCP measured in the outdoor                         |
| $\overline{RSCP}^{Rooms}$    | Average RSCP measured indoors in room IW, ID or DI           |
| $S_b$                        | Symbols per bit  |
| $SF_{16}$                    | HS-PDSCH spreading factor of 16                              |
| $S_R$                        | Symbol rate  |
| $u(p)$                       | Function that describes the inverse indoor loss distribution |
| $w_b$                        | Building width   |
| $w_s$                        | Road width   |

# List of Software

Mathworks Matlab R2009b

Borland C++ Builder v6.0

Microsoft Excel 2007

Microsoft Word 2007

Microsoft Powerpoint 2007

Microsoft Visio 2007

TEMS Investigation v11.0

Numerical computing software

ANSI C++ Integrated Development Environment

Calculation and graphical chart tool

Text editor software

Graphical presentation software

Scheme design software

Air interface measurement and test software



# Chapter 1

## Introduction

This chapter introduces the subject of this dissertation, allowing the reader to understand the context of the work. Further on, the objectives are overviewed as well as the original contributions. At the end of the chapter, a synopsis of the work structure is provided.

## 1.1 Overview

The first experiments with radio communication by Guglielmo Marconi in the 1890s set the road to truly mobile radio communication ever since. To understand the complex mobile communication systems of today, it is also important to understand where they came from and how cellular systems have evolved from an expensive technology for a few selected individuals, to today's global mobile-communication systems used by almost half of the world's population. Developing mobile technologies has also changed, from being a national or regional concern, to becoming a very complex task undertaken by global standards-developing organisations, such as the Third Generation Partnership Project (3GPP), involving thousands of people [DPSB08].

The standardisation of Wideband Code Division Multiple Access (WCDMA) by 3GPP has brought a widely adopted air interface. Currently, third generation (3G) systems, e.g., the Universal Mobile Telecommunications System (UMTS), which is supported on WCDMA, are designed for multimedia communication: person-to-person communications can be enhanced with high-quality images and video, and access to information and services on public and private networks will be improved by higher data rates, and new flexible communication capabilities of 3G systems [HoTo07]. Many new services are based on multimedia applications, such as Voice over Internet Protocol (VoIP), video conferencing, Video on Demand (VoD), online games, and Peer-to-Peer (P2P).

3GPP is also responsible for important evolution steps on top of WCDMA: High Speed Packet Access (HSPA) for downlink (DL) in Release 5 and uplink (UL) in Release 6. The DL solution, High Speed Downlink Packet Access (HSDPA) was commercially deployed in 2005 and the UL counterpart, High Speed Uplink Packet Access (HSUPA), during 2007. The combination of HSDPA and HSUPA is referred to as HSPA. The initial peak data rate of HSDPA was 1.4 Mbps but, by the end of 2007, 7.2 Mbps were available, with the peak data rate of 14.4 Mbps foreseen for a near future, starting the mobile Internet Protocol (IP) revolution [HoTo06]. HSUPA started to be deployed at the end of 2007, with a maximum peak data rate around 6 Mbps [HoTo06].

Furthermore, Release 7, where High Speed Packet Access Evolution (HSPA+) was introduced, evolves from the previous releases in order to enable progress in terms of capacity, coverage, and latency, resulting in higher user data rates and greater spectral efficiency. HSPA+ is built on existing Release 99, Release 5 and Release 6 features and capabilities, which avoids large upgrades in network elements. The large increase in data traffic leads to a request in increasing system performance when it comes to packet data. HSPA+ introduces its new capabilities over Releases 7, 8, 9 and 10 (and more are expected). The HSPA+ development is running along with Long Term Evolution (LTE), mainly because HSPA+ is still a very promising technology for operators, since it does not require major changes in the current HSPA network. Figure 1.1 shows the new features

introduced and its maximum peak bit rate in each Release.

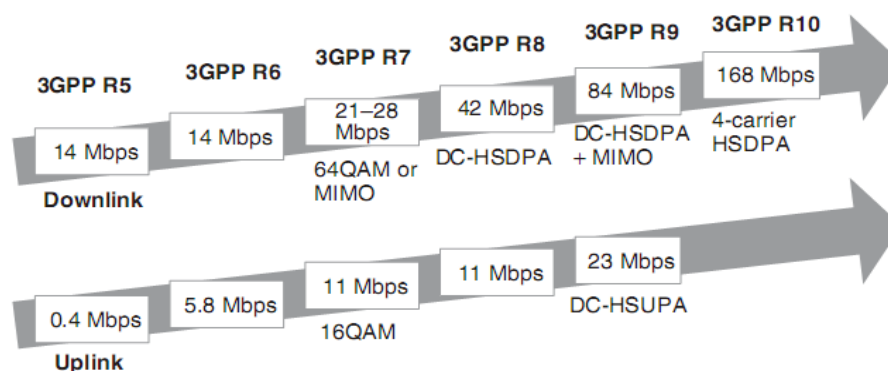


Figure 1.1. Evolution of HSPA maximum peak bit rate for each Release (extracted from [HoTo10]).

In Release 7 and Release 8, HSPA+ uses Multiple Input Multiple Output (MIMO) and Higher Order Modulation (HOM) to extend the peak data rate to 43.2 Mbps in DL and 11.5 Mbps in UL, [BEGG08] and [PWST07].

For the latest releases, DL and UL data rates improve with dual cell HSPA (DC-HSPA), with 3-carrier and 4-carrier HSPA and with higher-order modulation 64QAM DL and 16QAM UL. Multicarrier HSPA allows full benefits of 10–20 MHz bandwidths similar to LTE. DL data rate can also be increased by a multi-antenna solution (MIMO). The peak bit rate in Release 9 is 84 Mbps DL and 23 Mbps UL. The DL data rate is expected to double in Release 10 to 168 Mbps, by aggregating four carriers together over a 20 MHz bandwidth [HoTo10].

Despite all these latest releases, the scope of this thesis is to analyse the indoor coverage for a Release 7 system, mainly due to the fact that all the following releases use either the same methods to develop larger data rates (64QAM and/or MIMO) or Dual Carrier technologies, which consists of a simple scaling of Single Carrier transmissions.

Mobile phones are nowadays used everywhere, outdoors and indoors. Not only mobile phones are used for data traffic, but more and more modem dongles are spreading among users in order to get mobile data connections at high data rates. Since users spend a majority of their time inside buildings, it is important for mobile communication operators to cover indoor areas. In these environments, customers demand a good coverage and quality of service. Nevertheless, these systems were not deployed to specifically satisfy these requirements. Operator deployment requirements typically guarantee coverage, within certain quality requirements, of a minimum percent of the geographical area and population. Planning tools, key elements for the efficient dimensioning of a network, usually provide only outdoor coverage predictions. They estimate the path loss from the base station (BS) to the centre of the street where the mobile terminal (MT) is assumed to be. Therefore, an extra signal attenuation associated to building penetration is required in network planning. A specific attenuation value for building penetration can improve indoor coverage by a certain percentage of indoor

environments.

With this rapid progress of the evolutionary 3GPP roadmap from UMTS to HSPA+, new 3<sup>rd</sup> generation (3G) wireless broadband networks not only increase capacity for more users, but also offer fast and secure wireless connections to the Internet, and enable exciting new data applications for mobile devices. The perspectives are optimistic towards an exponential increase of data traffic within wireless networks, although not always being followed by a revenue increase, Figure 1.2. Operators' networks start to choke on this excessive traffic and the investments necessary to increase their capacity begin to increase exponentially too. This huge increase in data traffic is supported by the performance of certain applications, in the past classified as "killer-applications", which are now starting to be feasible, like VoD, HD video conferences and TV, gaming, other person-to-person services, or even 3DTV. In Portugal, at the moment, one has a mobile phone penetration rate of 160 %, and still growing [Voda11].

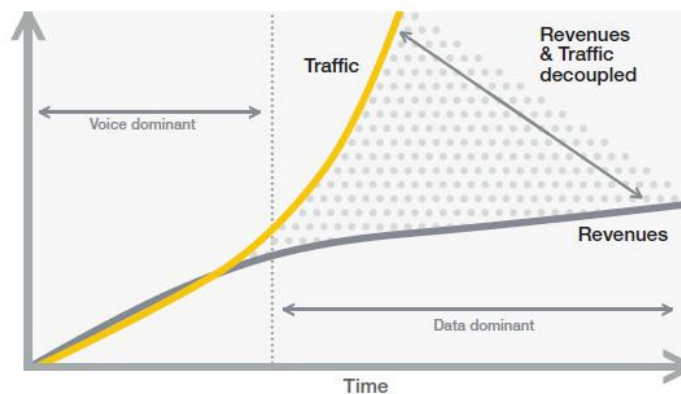


Figure 1.2. Data traffic and revenues trends for mobile communications (extracted from [Wire11]).

While the number of 3G subscribers and the traffic of 3G networks increase, indoor users generate more and more traffic. Studies show that more than 70 percent of the wireless broadband usage is generated by indoor users [ChAn08]. For such a high indoor wireless broadband usage, the indoor environment becomes a critical area for 3G network coverage. Particularly, the indoor HSDPA performance is of most interest for mobile operators and system vendors, due to the concern about the impact of building penetration loss that plagued first and second generation cellular systems [TaFi10].

The estimation of an extra signal attenuation associated to building penetration can be obtained via propagation models, or via predictions extracted from measurement campaigns. Nevertheless, building construction characteristics and city morphology have a strong impact on propagation characteristics, which makes the correct adaptation of these models and predictions a difficult task. In this particular work, a statistical approach is taken on the signal attenuation in order to quantify the throughput reductions caused by indoor penetration. The main purpose of this thesis is not the signal attenuation prediction, but the throughput reduction, which can be achieved through the available mapping models extracted from literature.

The penetration loss can be divided into two major categories: wall and floor ones, each one relative to the average path loss level outside the building. Wall loss is the penetration loss through a wall, and the loss of an external wall can be different at Non Line of Sight (NLoS) conditions compared to a perpendicular LoS situation, thus, one single external wall can have considerable different penetration losses, depending on the environmental conditions. Floor loss is the average loss in all of the rooms on the same floor in a building. In some cases, the penetration loss decreases with increasing floor level, which is commonly named as floor height gain. The height gain effect ceases to be applicable at floor levels that are considerable above the average height of the surrounding buildings.

## 1.2 Motivation and Contents

Despite the wide spreading of UMTS throughout the world, there are not enough studies and conclusions about indoor throughput coverage on it, so it is important to have a more detailed study. Especially in UMTS networks with macro cells, it is very difficult to reach sufficient indoor coverage, due to the higher carrier frequency and the higher required throughput compared to Global System for Mobile Communications (GSM). By installing extra cells and tolerating high transmitting power per link, it may be possible to reach the required coverage. However, network operators also try to avoid over dimensioning of their networks, as this results in high costs for the additional cell sites or in a waste of radio resources. Thus, in order to reach a satisfying indoor coverage without large expenses, it is necessary to have a prediction of the effective coverage. Particularly within buildings in urban areas, the prediction of the received power levels is a very complex task, due to the influence of the surrounding area, the vegetation, and for example the high attenuation of reinforced concrete walls or metallised glass façades.

The main scope of this thesis is to study indoor data transmission in UMTS as a function of urban scenario and building characteristics. These objectives are accomplished through the development of a model, and its implementation in a simulator. The indoor data transmission simulation is performed for both DL and UL, computing the theoretical received power at the terminal, and mapping it onto the adopted throughput model. The main results of the model are the indoor throughput reductions for several building types, varying the outdoor environments, and the desired building coverage. In order to obtain the indoor signal attenuation model, measurements were performed in several urban buildings that match the proposed classification, and results were input in the model implementation.

This thesis was made in collaboration with Vodafone Portugal - Comunicações Pessoais, S.A., a multinational telecom operator. Besides the scope establishment, the company was also helpful in providing three building scenarios for measurements. All measurements were performed with Vodafone Portugal support, and all the equipment was supplied by it.

The main contribution of this thesis is the developed model on indoor data transmission for several

urban scenarios and building characteristics, capable of producing an extensive analysis on a particular scenario defined one. Two models are created in order to satisfy the needs of a mobile operator. The first one performs a particular scenario characterisation for a Single-User in different room and building types, which allows a coverage study for a specific environment. The second one studies a Multi-User scenario with a random urban scenario, which is ideal for an operator to understand the impact of indoor attenuation on the desired capacity, and therefore enhance the operator's cell dimensioning procedure. To accomplish this, a new simulator is created, which can be used for radio network planning in specific indoor situations.

This work is composed of 5 Chapters, including the present one, followed by a set of annexes. Chapter 2 introduces mainly UMTS and its latest Release (HSPA+), propagation and interference models. UMTS basic concepts are explained and the architecture and radio interface are shown. Afterwards, a brief overview of propagations models is given, for outdoor models and indoors. Later on, the interference basic aspects are shown, followed by the interference models.

Chapter 3 presents all issues related to the implementation of the models in the simulator. At the beginning of the chapter, all models are presented. Then, a simulator overview is given, concerning architecture and functionality. Afterwards, detailed descriptions of propagation algorithms and models are performed, and input and output parameters are detailed. At the end of the chapter, the simulator assessment is presented.

Chapter 4 begins with a description of the scenarios to be analysed. After that, a measurements overview is given, followed by its results. Then, a comparison between measurements and simulations is presented. This chapter finishes with the presentation of the results obtain for each study case and its analysis.

Chapter 5 summarises the work in this thesis, draws the conclusions, and also discusses future work.

A set of annexes with auxiliary information and results is also included. In Annex A, the detailed link budget used throughout this thesis is presented. In Annex B, the chosen propagation model is presented together with its default values. In Annex C, the UMTS MT categories for DL and UL are listed. In Annex D, the throughput mapping model for UMTS/HSPA+ is explained. In Annex E, one presents the simulator user's manual. In Annex F, one presents results of the measurement campaign and its analysis. In Annex G, the throughput application layer overhead is calculated. In Annex H, the measurement results are tested for normality. In Annex I, one compares the measured indoor signal attenuation model with the available in previous works.

# Chapter 2

## UMTS Aspects

This chapter provides an overview of UMTS, with a focus on interference and coverage aspects, since the study is centred in indoor environments. Firstly, a basic description of the UMTS network and its radio interface is provided. Later, HSPA+ features are explored briefly and interference models are overviewed. Lastly, propagation models for outdoor to indoor coverage are analysed.

## 2.1 Basic Concepts

In this section, Release 99 basic concepts are presented, mainly based on [HoTo04], such as the network architecture, followed by a brief overview of the radio interface. Yet, a description of Releases' 5 and 6 High Speed Packet Access (HSPA) is also performed, including capacity and coverage aspects. After this, the performance of UMTS is analysed. Further on, HSPA+ features are overviewed. At last, one takes a look on UMTS services and applications.

### 2.1.1 Network Architecture

The UMTS network, defined by the 3GPP, consists of a number of logical elements, each one with a defined functionality [3GPP02a]. These network elements are grouped based on similar functionalities or on which sub-network they belong to. The network architecture is presented in Figure 2.1.

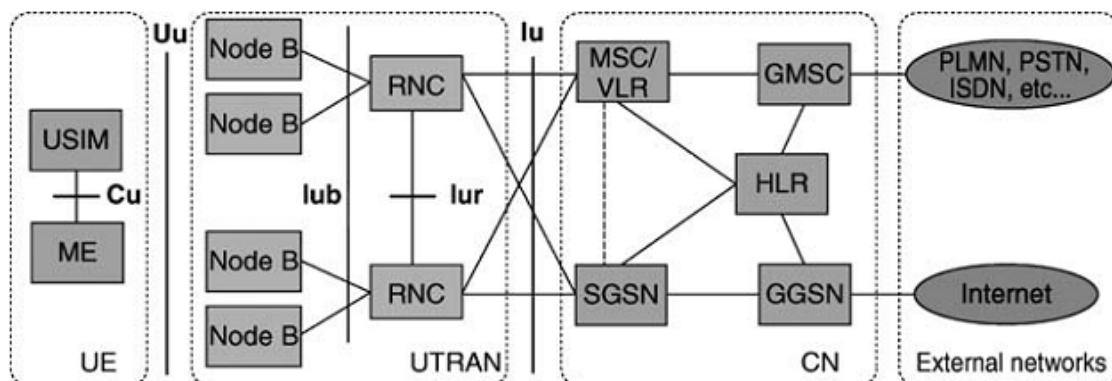


Figure 2.1. UMTS network architecture (extracted from [HoTo04]).

Functionally network elements are grouped into the User Equipment (UE), where the user and radio interface are defined, the Radio Access Network (RAN, or in this case UMTS Terrestrial RAN – UTRAN) that handles all radio-related functionality, and the Core Network (CN), which is responsible for routing and switching voice and data connections to external networks.

The UE consists of:

- Mobile Equipment (ME) - the radio terminal used for radio communications over the *Uu* interface.
- UMTS Subscriber Identity Module (USIM) – the card that holds the subscriber identity, and stores authentication and other types of information.

UTRAN consists of:

- Node B – it converts the data flow between the *Iub* and *Uu* interfaces. It also performs some

- tasks of radio resource management.
- Radio Network Controller (RNC) – it owns and controls the radio resources of the attached Node Bs. It is also the access point for all the services provided to the CN.

The UTRAN is formed by one or more Radio Network Sub-Systems (RNS) – a set of Node Bs and a RNC.

The CN is out of scope of this thesis, although it plays a very important role in UMTS architecture. It was adapted from the GSM one, and its task is to switch and route calls and data connections to external networks. These networks can either be Circuit Switched (CS), such as the existing telephony service (e.g., ISDN and PSTN), or Packet Switched (PS), such as the Internet.

## 2.1.2 Radio Interface

As specified by 3GPP in Release 99 [3GPP09], UMTS uses WCDMA, a wideband Direct-Sequence Code Division Multiple Access (DS-SS) system as the radio interface (identified as *Uu* in Figure 2.1). Its principle is to have the user information bits spread over a wide bandwidth, by multiplying the user data with quasi-random bits (called chips). The chip rate of 3.84 Mcps leads to a channel bandwidth of 4.4 MHz, with a separation between channels of 5 MHz. The network operator can deploy multiple carriers to increase capacity.

In order to achieve higher bit rates, the spreading operation (also known as channelisation) uses the Orthogonal Variable Spreading Factor (OSVF) technique. This results in spread data that maintains orthogonality among codes, according to a changeable Spreading Factor (SF), the number of channelisations codes being given by SF. In addition to spreading, scrambling codes allow the differentiation of the sectors in a cell (in DL) and the separation of mobile terminals (MTs) from each other without changing signal bandwidth.

WCDMA supports highly variable user data rates, i.e., Bandwidth on Demand (BoD) and allows Quality of Service (QoS) differentiation, with the different services and applications offered by UMTS being presented in Subsection 2.2. The user data rate is kept constant during each 10 ms frame, although the data capacity among users can change from frame to frame. This fast allocation allows the network to achieve optimum throughput for packed data services.

Despite the fact that WCDMA supports both Frequency Division Duplex (FDD) and Time Division Duplex (TDD), currently UMTS only considers the former. The UMTS band for Europe is [1920, 1980] MHz for UL and [2110, 2170] MHz for DL [Corr09].

UTRA radio interface channels can be logical, transport and physical channels. The logical channels are mapped onto transport ones, which establish the interface between the UE and the RNC [Corr09]. There are two types of transport channels: dedicated and common ones. The former use a code on a determined frequency, being reserved for a Single-User, while the latter divides the resource among a group of users in a cell. The conversion between logical and transport channels happens in the

Medium Access Control (MAC) layer, which is part of the Data Link Layer. Transport channels are again mapped onto physical ones.

Power management and handovers are also key features in WCDMA. Although the latter are not covered in this work, the former can be of two types: open loop control, to avoid the use of excessive power, thus, keeping minimum interference levels, and outer loop control, to adjust the Signal-to-Interference Ratio (SIR) of each link, in order not to waste the capacity given to a channel.

As evolution of Release 99, two new releases were added by 3GPP, respectively Release 5 and Release 6: HSDPA and HSUPA. HSDPA was designed to be deployed together with Release 99, its purpose being to increase DL packet data throughput by means of physical layer retransmission, fast scheduling, as well as fast link adaptation controlled by the Node B. While in Release 99 the scheduling was part of RNC's tasks, in HSDPA the Node B is capable of transmitting and retransmitting the packets to the ME, minimising latency and providing a whole change in Radio Resource Management (RRM). The upgrade from Release 99 to HSDPA requires only a few new software packages and hardware in the Node B and the RNC, although in the user-end a new terminal is required [Telm08].

HSDPA does not support soft handover or power control, which were two of the most fundamental features of the Dedicated Channel (DCH) in Release 99. Instead, new channels were introduced: the High Speed Downlink Shared Channel (HS-DSCH) for data, which is mapped onto the High Speed Physical Downlink Shared Channel (HS-PDSCH); and the High Speed Shared Control Channel (HS-SCCH) and the High Speed Dedicated Physical Control Channel (HS-DPCCH), for DL and UL signalling, respectively. Later, HSUPA introduced the Fractional Dedicated Physical Channel (F-DPCH) that handles power control when only packet services are active, allowing a larger number of users with lower data rates.

In order to achieve higher data rates, 16 Quadrature Amplitude Modulation (16QAM) was introduced in the HS-DSCH, together with Quadrature Phase-Shift Keying (QPSK) – which maximises coverage and robustness. The Node B's fast physical layer transmission is achieved by using Hybrid Automatic Repeat Request (HARQ) with two transmission types. HSDPA uses a fixed SF of 16 for multi-code operation, where 15 orthogonal codes are used for user data transmission and the other one for signalling (HS-SCCH), allowing a theoretical peak bit rate of 14.4 Mbps. The HS-SCCH carries the information for de-spreading of the correct codes and HARQ information providing the user's modulation and coding scheme based on received transmissions.

In Release 99, radio transmissions are structured in frames of 10 ms, and data blocks are transmitted over an integer number of these frames. For this release, the Transmission Time Interval (TTI) is usually between 10 and 80 ms. HSDPA supports a frame duration of 2 ms, obtaining lower latency and faster scheduling among all users.

With all these new features, HSDPA has enhanced the DL capabilities of UMTS. HSUPA brings in

Release 6 enhancements in UL. Just like HSDPA, HSUPA is not a stand-alone feature, rather more an add-on one, maintaining all the basic features of Release 99. The most relevant introduced features are the new interaction between Node Bs and MEs, and also the usage of QPSK. Most of HSUPA's UL enhancements were brought by its new transport channel, Enhanced DCH (E-DCH). Its main features are fast Node B based scheduling, fast physical layer HARQ, and (optionally) a shorter TTI of 2 ms. In HSUPA, the HARQ is fully synchronous, avoiding the need for sequence numbering, and it can operate in soft handover.

New operation channels were introduced. In DL, the E-DCH Absolute Grant Channel (E-AGCH) and the E-DCH Relative Grant Channel (E-RGCH) are responsible of scheduling control, and the E-DCH HARQ Indicator Channel (E-HICH) of retransmission support. In the UL, the E-DCH Dedicated Physical Control Channel (E-DPCCH) is responsible of new control information, and for carrying data the E-DCH Dedicated Physical Data Channel (E-DPDCH) was created. Contrary to HSDPA's shared channel, scheduling in HSUPA is a multipoint-to-point procedure, therefore requiring a dedicated channel (E-DCH), similar to Release 99.

Although in HSDPA one of the criteria for admitting new users is the available power, in HSUPA the common resource is the UL noise factor, directly related to the interference level. The scheduling is therefore responsible for maintaining low levels of the UL noise, in order to allow a higher cell capacity and assuring that cell overload is not reached.

In this thesis, the main performance parameters under focus are interference and coverage, since these are the issues of an indoor environment. Despite this fact, capacity is mutually related to interference, being the trade-off between both a key feature in cellular networks, and therefore being important to take into account. The interference margin is given by [Corr09]:

$$M_I [\text{dB}] = -10 \cdot \log(1 - \eta) \quad (2.1)$$

where:

- $\eta$  is the DL/UL load factor.

Increasing the load factor leads to a reduction in coverage, by increasing the interference margin, therefore, the load factor must not exceed 50 % (UL) or 70 % (DL). Since there is asymmetry in DL and UL, the load factors are given by different expressions [Corr09]:

$$\eta_{UL} = (1 + i) \sum_{m=1}^{N_{am}} \frac{1}{1 + \frac{G_{Pm}}{\rho_m F_{am}}} \quad (2.2)$$

$$\eta_{DL} = \sum_{m=1}^{N_{am}} F_{am} \frac{\rho_m}{G_{Pm}} [(1 - \alpha_{COm}) + i_{r,m}] \quad (2.3)$$

where:

- $i_r$  is the ratio of inter- to intra-cell interferences (which can be [40, 60] % in UL and 0 in DL);

- $N_{au}$  is the number of active users in a cell;
- $G_{P_m}$  is the processing gain of user  $m$ , given by:

$$G_{P_m} = \frac{R_c}{R_{b_m}} \quad (2.4)$$

with:

- $R_{b_m}$  is the data bit rate of user  $m$ ;
- $R_{c_m}$  is the chip rate, which for WCDMA is 3.84 Mcps;
- $\rho_m$  is the Signal-to-Noise Ratio of user  $m$ , given by:

$$\rho_m = \frac{E_b}{N_0} \quad (2.5)$$

- $E_b$  is the energy per bit;
- $N_0$  is the noise power density;
- $F_{a_m}$  is the activity factor of user  $m$  (which can be 50 % for voice and 100 % for data);
- $\alpha_{CO_m}$  is the code orthogonality factor of user  $m$  (which is typically in [50,90] %).

For the purpose of this work, a more realistic model is needed to describe the variation of the orthogonality factor with the distance between the MT and BS. In urban environments, the increase of multipath with the distance is not negligible, expressing influence over the orthogonality factor. [Carr11] suggests a model where a drop of the orthogonality factor can be found with the increase of distance, as shown in Figure 2.2, resulting in higher DL load factors. The model expression was interpolated by [Carr11] with high accuracy (resulting in a correlation coefficient of 0.9992):

$$\alpha_{CO} = -1.4825 \times d_{[\text{km}]}^3 + 3.1507 \times d_{[\text{km}]}^2 - 2.4152 \times d_{[\text{km}]} + 0.9891 \quad (2.6)$$

where:

- $d$  is the distance between the BS and the MT.

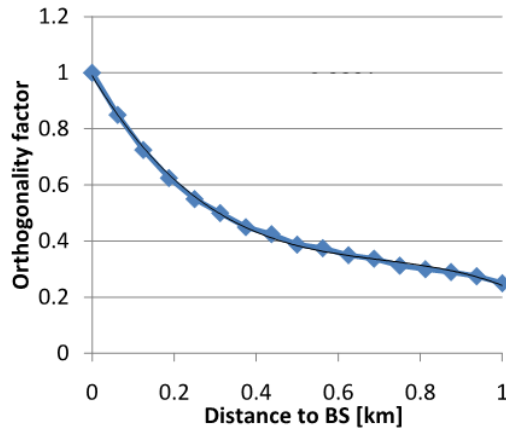


Figure 2.2. Orthogonality factor as a function of the MT's distance to BS (extracted from [Carr11]).

The difference in the load factors can be explained by the fact that in DL the maximum transmission power does not vary with the number of active users (it is shared by all users), while in the UL each MT has its own transmission power. Specifically in urban environments, where data rates are higher, capacity is limited by the DL load factor, thus, cell coverage is more load dependent in DL. Because of this sensitivity, it is important to establish the total transmission power of the correspondent BS [Corr09]:

$$P_{Tx} [\text{W}] = \frac{N_0^{MT} R_c}{1 - \eta_{DL}} \sum_{m=1}^{N_{au}} F_{a m} L_{P m} \frac{P_m}{G_{P m}} \quad (2.7)$$

where:

- $N_0^{MT}$  is the noise spectral density at the MT;
- $\overline{\eta_{DL}}$  is the average DL load factor across the cell;
- $L_{P m}$  is the path loss between the BS and user  $m$ .

Increasing the BS transmission power is not always the best solution, since it can raise the interference value across the cell. The transmission power of a macro-cell BS is usually around 30 W (44.7 dBm), but some suppliers these days can offer up to 40 W (46 dBm). The BS transmission power is shared among all MTs in the cell, whereas MTs have a service-specific transmission power, i.e., typically 21 dBm for voice, and 24 dBm for data [Jaci09].

Common control channels take some of the total power available at the transmitter for signalling and control over the network, while the remaining power goes to the dedicated channels. The power allocated to each channel group is variable according to the operating Release. In Release 99, the transmission power is shared with a ratio of 75 % for data channels, and 25 % for signalling and control. In HSPA+, the enhancements done over the network signalling result in a greater portion of power to execute these tasks properly, therefore 40 % of transmission power is delivered to the common channels, being composed of the sum of all common channels from Release 99 and on top of those the addition of the specific ones from HSPA+. The remaining 60 % is taken for the dedicated user's channels in DL. In UL, the common value for signalling and control is 15 % of the total transmitter power [Jaci09].

Concerning cell coverage, one can define its maximum distance according to the definition of path loss and the model of average power decay with distance [Corr09]:

$$\eta_{[\text{km}]} = 10^{\frac{P_{Tx} [\text{dBm}] + G_{Tx} [\text{dBi}] - P_{Rx} [\text{dBm}] + G_{Rx} [\text{dBi}] - L_{ref} [\text{dB}]}{10 a_{pd}}} \quad (2.8)$$

where:

- $P_{Tx}$  is the power fed to the transmitting antenna;
- $G_{Tx}$  is the transmitting antenna gain;
- $P_{Rx}$  is the power at the input of the receiving antenna;
- $G_{Rx}$  is the receiving antenna gain;
- $L_{ref}$  is the sum of propagation losses, (A.16);

- $a_{pd}$  is the average power decay.

In UMTS, capacity depends on the number of users and on the type of the services, via the interference margin and the transmitting power. Capacity can therefore be measured by the number of active users in the cell, for given average data bit rate and average channel conditions. Combining (2.1), (2.3), (2.8) and (A.7), one has for Release 99:

$$N_{au} = \frac{1 - 10^{\frac{10 \cdot a_{pd} \log(r_{[km]}) - P_{Tx[dBm]} - G_{Tx[dB]} + \rho_{[dB]} - G_P[dB] + N_{[dB]} - G_{Rx[dB]} + L_{ref[dB]}}{10}}}{F_a \frac{\rho}{G_p} [(1 - \alpha_{CO}) + i_r]} \quad (2.9)$$

For HSDPA/HSPA+ DL, the model presented in (2.9) is not entirely valid. In Release 99, capacity depends exclusively on the available signal power and the existing interference power. In HSPA/HSPA+ DL another limitation arises: the number of available codes is fixed, which limits the number of possible users in the cell. The model in (2.9) can therefore be used if the maximum number of served users is limited to 15.

From an operator's perspective, it is interesting to dimension the cell maximum distance according to the desired UMTS category data bit rate. These categories are presented in Annex C. Thus, the cell coverage for a given data bit rate is represented in (2.9), where the required transmission power for that same data bit rate is computed by using (2.7).

### 2.1.3 Performance Analysis

In the first release of UMTS, the metric to evaluate system performance is the Signal-to-Noise Ratio (SNR), which can be estimated by the normalised measure  $E_b/N_0$ . Depending on the service and bit rate, the associated SNR values are different: in voice (12.2 kbps) the SNR should be within the range [4.8, 8.8] dB, while for data (384 kbps) it should be [0.4, 3.2] dB [Corr09].

In Release 99, there is a requirement of SNR to achieve the bit rate for several services, while in HSDPA, due to Adaptive Modulation and Coding (AMC), the bit rate is a continuous function of HS-DSCH SINR (the bit rate can change every TTI with different modulations and coding scheme). Thus, the metric used in this case has to be different from the one used in Release 99. The method to evaluate HSDPA performance is the average HS-DSCH Signal-to-Interference-plus-Noise Ratio (SINR),  $\rho_{IN}$ , after despreading the HS-PDSCH, for a single-antenna Rake receiver [HoTo06]:

$$\rho_{IN} = SF_{16} \frac{P_{HS-DSCH}}{(1 - \alpha_{CO}) I_{intra} + I_{inter} + P_{noise}} \quad (2.10)$$

where:

- $SF_{16}$  is the HS-PDSCH spreading factor of 16;
- $P_{HS-DSCH}$  is the received power of the HS-DSCH summing over all active HS-PDSCH codes;

- $\alpha_{CO}$  is the DL orthogonality factor;
- $I_{intra}$  is the received intra-cell interference;
- $I_{inter}$  is the received inter-cell interference;
- $P_{noise}$  is the received noise power at the radio-frequency band.

Despite the HSDPA SF of 16, only 15 codes can be allocated for data transmission, since one is needed for the HS-SCCH transmission. This HS-DSCH SINR metric measures the SINR required per-TTI on the HS-DSCH in order to accomplish a certain Block Error Rate (BLER) for a given HS-PDSCH number of codes, type of modulation and coding scheme. [HoTo06] plots continuous functions of the average HS-DSCH throughput and the average HS-DSCH SINR for 5, 10 and 15 HS-PDSCH codes: for the same value of SNR, the throughput increases with the increase in the number of HS-DSCH allocated codes.

The use of link adaptation allows the link scheme to change depending on the radio channel quality. Using the Channel Quality Indicator (CQI), the MT can provide the BS feedback on the DL channel quality; for UL, the BS can estimate the channel quality, based on the received SINR. The CQI is calculated at the MT based on the SNR of the received common pilot. Instead of expressing the CQI as a received signal quality, the CQI is expressed as a transport-block size, taking also the receiver performance into account [DPSB08]. Subsequently, the SINR is settled with the purpose of extracting the higher throughput and the lowest delay possible. Note that network capacity depends on the type of user and the respective scenario, and on the type of service provided.

In order to estimate the achievable HSDPA single-user throughput, aiming at network dimensioning, it is possible to use the wideband average Primary-Common Pilot Channel (P-CPICH)  $E_c/N_0$  pilot. The average SINR can be expressed as a function of the average P-CPICH:

$$\rho_{IN} = SF_{16} \frac{P_{HSDPA}}{\frac{P_{pilot}}{\rho_{pilot}} - \alpha_{CO} P_{Tx}} \quad (2.11)$$

where:

- $P_{HSDPA}$  is the HSDPA transmit power;
- $P_{Tx}$  is the total BS transmit power;
- $P_{pilot}$  is the P-CPICH transmit power;
- $\rho_{pilot}$  is the P-CPICH  $E_c/N_0$  when HSDPA is active.

It is possible to express the BS HS-DSCH transmit power as a function of SINR, rearranging (2.11):

$$P_{HS-DSCH} \geq \frac{P_{Total}}{SF_{16}} \left[ \frac{1}{g} + 1 - \alpha_{CO} \right] \cdot \rho_{IN} \quad (2.12)$$

where:

- $P_{HS-DSCH}$  is the BS HS-DSCH transmission power;
- $g$  is the so-called geometry factor,

$$g = \frac{I_{\text{intra}}}{I_{\text{inter}} + P_{\text{noise}}} \quad (2.13)$$

returning a wideband ratio between the total power received by the MT from the serving cell and the other cell interference plus noise power, [HoTo10]. This association is made because the intra-cell interference is the total transmitter power of the serving cell multiplied by the average power attenuation. Thus, due that, the  $g$  factor reflects the distance of an MT to the associated BS, which decreases when distance increases and the required transmission power has to be increased to balance the lower SINR obtained. To assure enough HS-DSCH throughput at the cell edge, (2.12) can be used to calculate the minimum required HS-DSCH transmission power to guarantee a certain service, assuming that the geometry factor at the cell edge is known. The  $\rho_{IN}$  values are taken from Figure 2.3, depending on the service requested throughput.

Similar to HSDPA, performance in HSUPA depends on network algorithms, deployment scenario, type of traffic, Node B receiver performance and capability, and ME transmitter capability. The performance metric used by HSUPA is the energy per chip to noise spectral density ratio  $E_c/N_0$ , similar to Release 99 due to the absence of AMC. A high  $E_c/N_0$  at the BS is necessary in order to achieve higher data rates, which leads to an increase of the UL noise, thus, decreasing the cell coverage area. Concerning this, a maximum level for UL noise may be defined for macro-cells, though it limits high data throughputs.

The capacity increase from HSUPA is mainly due to the use of Layer 1 (L1) HARQ and BS based scheduling. The use of L1 HARQ has two main advantages: faster retransmissions at L1 than in L2 RLC-based, and the use of soft combining of retransmissions. Faster retransmissions lead to a decrease of  $E_b/N_0$ , which increases spectral efficiency, while the combining techniques can improve BS performance. UL spectral efficiency can be improved by increasing the Block Error Probability (BLEP) at first transmission, which leads to a lower  $E_b/N_0$  requirement. Assuming realistic traffic, the cell throughput gain due to the use of L1 HARQ is approximately 15 to 20 % [HoTo06].

Regarding Node B based scheduling, it can provide tighter control of total received UL power, as well as faster reallocation of radio resources among users, with the former allowing faster adaptation to interference variations, and the latter dynamically take resources from users with low usage of allocated radio resources, and redistribute them among users with high usage. Node B based scheduling provides a cell throughput increase of approximately 15 to 20 % on top of the gain from L1 HARQ [HoTo06].

From an operator's view point, system performance is not only given by the average SINR of the channel, but most importantly by the throughput provided to the user. Annex D shows the equations that relate the SINR of a system to the data bit rate it can achieve for a different modulation and antenna configuration.

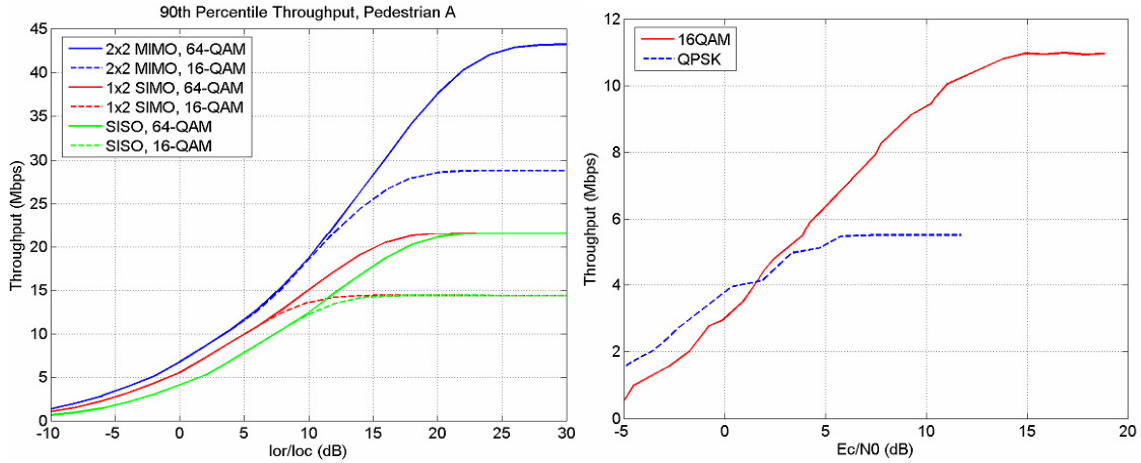
## 2.1.4 HSPA Evolution

The aim of HSPA evolution is to further improve the performance of UMTS, through higher peak rates, lower latency, greater capacity, increased battery times, better support for VoIP, and improved multi/broadcast capabilities. In Release 7 and 8, HSPA+ several new features are introduced, such as Higher-Order Modulation (HOM) in both DL and UL, Multiple Input Multiple Output (MIMO), advanced G-rake Receivers, Layer-2 (L2) protocol enhancements, Multimedia Broadcast Multicast Service single-frequency network, enhanced Cell Forward Access Channel and support optimisation for Voice over IP (VoIP).

Release 7 introduces 64QAM in DL, increasing the peak data bit rate by 50 %, from about 14.4 Mbps to 21.1 Mbps. In UL, the introduction of 16QAM, allows peak data rates to reach about 11.5 Mbps, featuring an increase of 100 % compared with the 5.74 Mbps of the enhanced UL in Release 6, with QPSK. Release 8 states that the theoretical peak data rate is 42.2 Mbps for DL and 11 Mbps in UL (per 5 MHz carrier) [BEGG08]. For further releases, 3GPP is planning multi-5 MHz-carrier transmission that will offer a wider bandwidth (until this date, 4 carriers are provided in Release 10), altogether with the usage of MIMO systems, boosting up the theoretical peak data rate up to 168 Mbps in DL and 23 Mbps in UL [HoTo10].

MIMO can increase the data rates, i.e., transmitting multiple transport blocks in parallel using multiple antennas to a Single-User, taking advantage of spatial multiplexing. Using the channel properties exploits multipath, providing higher data throughput and simultaneously link reliability and higher spectral efficiency, all without consuming extra radio frequency. Within separate streams, these are encoded, modulated and transmitted with different transmit weights, estimated in the Node B/ME, spatially spread, and by different antenna ports. MIMO uses advanced receivers, allowing a superior interference cancellation and expected boost of performance. In order to update the network with these features, 3GPP updates several physical channels, like HS-SCCH, HS-DPCCH, E-AGCH and E-DPCCH to incorporate and update signalling information, like ACK/NACK, MIMO information (pre-coding weigh, number of streams, modulation), to allow larger transport block sizes and a larger range for the CQI in {1,...,30}.

With the usage of MIMO configurations, the theoretical peak data rates grows linearly with the number of transmitted data streams [HoTo07], from 14.4 to around 28 Mbps in a 2x2 MIMO configuration. Additionally, HOM brings the opportunity of even higher throughputs, incorporating new digital modulations, 16 QAM for UL and 64 QAM on DL. In Release 8, HSPA+ reaches in DL around 42 Mbps with a 2x2 MIMO configuration and 64 QAM [BEGG08], while in UL doubles from 5.7 Mbps to 11 Mbps with 16 QAM per 5 MHz carrier. One should notice that these values refer to the peak rates in the cell. The average cell capacity improvement is far less, because 64QAM and dual stream MIMO can only be utilised when SNR is good enough. The capacity gain of these features is 10–50 % depending on the network loading. With full loading the gain is typically below 10 % both for 64QAM and with MIMO [HoTo10]. Figure 2.3 shows some data rates achieved with detailed configuration information.



(a) The 90<sup>th</sup> percentile throughput for DL.

(b) Throughput as a function of  $E_c/N_0$  for UL.

Figure 2.3. DL and UL Throughputs in Pedestrian A channel for HOM (extracted from [PWST07]).

Still concerning Release 8, the 42 Mbps peak data rate can also be achieved by using Dual Carrier HSDPA (DC-HSDPA) instead of the MIMO configuration. MIMO can improve spectral efficiency due to two antennas transmission, while the DC-HSDPA brings some improvement to the high loaded case with frequency domain scheduling and a larger trunking gain. The dual carrier solution looks attractive because the data rate improvement is available over the whole cell area equally, while MIMO improves the data rates mostly close to the Node B. Also, dual carrier HSDPA tends to be easier to upgrade the network since it can be implemented with single 10 MHz power amplifier per sector, while MIMO requires two separate power amplifiers [HoTo10].

The SNR and  $E_c/N_0$  are important metrics used in the link budget, Annex A. The expressions for the DL and UL curves obtained in the scope of this thesis are presented in Annex D.

HSPA+, as HSDPA, makes use of AMC, or link adaptation, which adjusts the modulation and coding scheme according to the radio channel instantaneous conditions, returning the best modulation with the possible higher user data rate. The fundamental parameters to be settled in are modulation scheme, coding levels, among several others, e.g., power levels, spreading factors, signalling bandwidth and so on. The transmission power is kept constant, but the data rate varies, with the transmission radio channel conditions. The AMC link, incorporated over the Node B scheduler, is influenced by the feedback strength received from the ME, taking the CQI instantaneous reports into account, stood on the P-CPICH signal. CQI and P-CPICH analysis is not under the scope of this thesis. Figure 2.4 shows the dynamic allocation of the most efficient modulation according to the available signal strength, in which green plots the perfect channel adaptation, returning the best spectral efficiency.

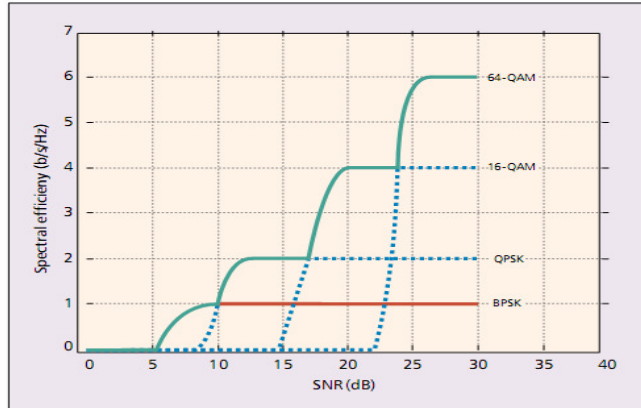


Figure 2.4. Spectral efficiency variation according to each modulation behaviour (extracted from [CEGH02]).

To sum up, a comparison between the key features of the major UMTS releases up to Release 7 is shown in Table 2.1.

Table 2.1. Comparison between different UMTS stages (adapted from [HoTo10]).

| Feature                   | Release 99     | Release 5 (HSDPA) | Release 6 (HSUPA) | Release 7 (HSPA+ DL) | Release 7 (HSPA+ UL) |
|---------------------------|----------------|-------------------|-------------------|----------------------|----------------------|
| Variable Spreading Factor | Yes            | No                | Yes               | No                   | Yes                  |
| Adaptive Modulation       | No             | Yes               | No                | Yes                  | Yes                  |
| Soft Handover             | Yes            | No                | Yes               | No                   | Yes                  |
| Fast Power Control        | Yes            | No                | Yes               | No                   | Yes                  |
| Node B based scheduling   | No             | Yes               | Yes               | Yes                  | Yes                  |
| Fast Physical Link HARQ   | No             | Yes               | Yes               | Yes                  | Yes                  |
| Higher Order Modulation   | No             | No                | No                | Yes                  | Yes                  |
| MIMO                      | No             | No                | No                | Yes                  | No                   |
| TTI length [ms]           | 80, 40, 20, 10 | 2                 | 10, 2             | 2                    | 10, 2                |
| Maximum Data Rate [Mbps]  | 0.384          | 14.4              | 5.7               | 21.1                 | 11.5                 |

The use of adaptive modulation brings issues concerning BER, since a change in the active modulation will affect its value. The UMTS/HSPA+ performance analysis is therefore influenced by the change in BER. Equation (2.14) for QPSK and (2.15) for rectangular M-QAM (M being the modulation index) show the average bit error probability for a given modulation in a Rayleigh channel [Gold05], namely for the HSPA+ current modulations: QPSK, 16QAM and 64QAM, the latter being only available for DL. For each of these modulations, Figure 2.5 shows the BER as a function of SNR for the HSPA+ available modulations. One can notice that higher order modulations require higher SNRs in order to accomplish a determined BER. This fact must be taken into account when using AMC.

$$\overline{P}_b^{QPSK} = \frac{1}{2} \left[ 1 - \sqrt{\frac{10^{\frac{\overline{\rho}_{[dB]}}{10}}}{1 + 10^{\frac{\overline{\rho}_{[dB]}}{10}}}} \right] \quad (2.14)$$

$$\overline{P}_b^{M-QAM} = \frac{2(\sqrt{M} - 1)}{\sqrt{M} \times \log_2(M)} \left[ 1 - \sqrt{\frac{1.5 \times \log_2(M) \times 10^{\frac{\overline{\rho}_{[dB]}}{10}}}{M - 1 + 1.5 \times \log_2(M) \times 10^{\frac{\overline{\rho}_{[dB]}}{10}}}} \right] \quad (2.15)$$

where:

- $M$  is the modulation index;
- $\overline{\rho}$  is the average energy per chip to noise spectral density ratio,  $E_c/N_0$ .

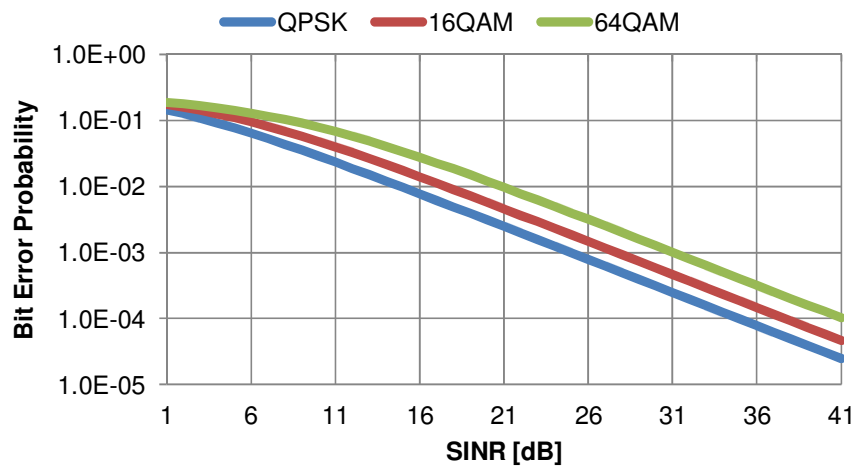


Figure 2.5. Bit error probability in function of  $E_c/N_0$  for each HSPA+ modulation.

The deployment of HSPA+ from the service providers' view point should be simple, since the majority of changes are mostly software features, comparing to other available technologies that are not WCDMA based.

## 2.2 Services and Applications

UMTS networks were designed from the beginning for a flexible delivery of any type of service. Prioritisation becomes mandatory when the system load gets higher, and services must be differentiated according to their requirements, i.e., QoS differentiation should be applied. 3GPP defined different QoS classes, i.e., Conversational, Streaming, Interactive and Background. These four traffic classes are distinguished mainly on the basis of delay sensitivity. This differentiation is shown in Table 2.2, where the different characteristics of each class are brought up.

The Conversational class is the most delay-sensitive one, since it is intended for real-time communication, where traffic is nearly symmetric between UL and DL, and end-to-end delay has to be less than 400 ms [HoTo04], this being the maximum acceptable delay for human perception of video and audio conversation. One can set as example in this class the traditional voice service running under CS, or VoIP which runs over IP, therefore on the PS domain. VoIP requires QoS differentiation and IP header compression in order to achieve low delays. Video telephony has BER requirements even tighter than voice, due to video compression, and it can be transmitted in CS or PS. The speech codec used in UMTS employs the Adaptive Multirate (AMR) technique with eight source rates, namely 12.2 kbps. Discontinuous Transmission (DTX) is used in the AMR codec, in order to reduce the average required bit rate, leading to a lower interference level, hence, increased capacity.

Table 2.2. UMTS traffic class parameters (extracted from [3GPP02b]).

| Service Class          | Conversational | Streaming        | Interactive         | Background      |
|------------------------|----------------|------------------|---------------------|-----------------|
| <b>Real time</b>       | Yes            | Yes              | No                  | No              |
| <b>Symmetric</b>       | Yes            | No               | No                  | No              |
| <b>Switching</b>       | CS/PS          | CS               | PS                  | PS              |
| <b>Guaranteed Rate</b> | Yes            | Yes              | No                  | No              |
| <b>Delay</b>           | Minimum Fixed  | Minimum Variable | Moderately Variable | Highly Variable |
| <b>Buffer</b>          | No             | Yes              | Yes                 | Yes             |
| <b>Bursty</b>          | No             | No               | Yes                 | Yes             |
| <b>Example</b>         | Voice          | Video Streaming  | Web Browsing        | E-mail          |

Streaming class services are based on the multimedia streaming technique, which enables the end user to access data before the transfer is complete. This is achieved through a continuous stream transmission and the use of buffers in the final applications. Information is real-time delivered in a continuous stream preserving time relation between packets, however, it is not delay-sensitive as voice from Conversational class. In this case, traffic is not symmetric; hence, DL traffic is the most significant one.

Web browsing and online multiplayer games are examples of applications from the Interactive class, as well as push-to-talk and location-based services. This class is based on PS connections with a very asymmetric traffic, being tolerant to delay. Web browsing may support large delays, but still, in order to accomplish a good communication, the delay should be lower than 4 to 7 s [Lope08]. For multiplayer games, the Round Trip Time (RTT) is a very important parameter, especially in real time action games, where the end-to-end delay should be below 100 ms [Lope08].

The main distinguishable characteristic between the Interactive class and the Background one is that in the former the end user is waiting for a response within a certain time, while in the latter one is not. Resource transmissions are only used in Background, when none of the other classes are active, making it the most delay-insensitive one. This class, like the Interactive one, is intolerant to transmission errors. Some of the applications in this class are the Short Message Service (SMS), Multimedia Message Service (MMS), and e-mail. These traffic classes are flexible, which means that a

multimedia application might belong to different classes according to its delay requirements on a given moment. QoS differentiation becomes useful for the network efficiency during high load, when there are services with different delay requirements.

It is also important to categorise the service profiles to be able to serve the different demands on the network. Establishing these categories can be done in several different ways, therefore, one was chosen to fulfil the scope of this thesis. Table 2.3 shows each application characteristics and its QoS priority level, as well as its maximum service delay and required bandwidth.

Table 2.3. Service differentiation and characteristics (adapted from [3GPP10a]).

| Service         | Bit Rate [kbps] |            | QoS Priority Level | Delay [s] |
|-----------------|-----------------|------------|--------------------|-----------|
|                 | DL              | UL         |                    |           |
| Chat            | [64, 384]       |            | 7                  | -         |
| E-mail          | [384, 1536]     | [128, 512] | 5                  | < 4       |
| FTP             | [384, 2048]     | [128, 512] | 6                  | < 10      |
| P2P             | [128, 1024]     | [64, 384]  | 8                  | < 10      |
| Streaming       | [512, 1024]     | [64, 384]  | 4                  | < 10      |
| Video-Telephony | [32, 384]       |            | 2                  | < 0.4     |
| Voice           | [4, 25]         |            | 1                  | < 0.4     |
| Web             | [384, 1536]     | [128, 512] | 3                  | <4/page   |

One needs to notice that these traffic classes, as well as the service classes, are affected by the rise of new radio technologies and therefore are not static in time. Nevertheless, nowadays there still are some services that need a perfect RRM to be performed in a satisfactory way, like push-to-talk, video share and high definition video (DVB-H), multi-player games with low RTT and other person-to-person services [Jaci09].

## 2.3 Interference

Interference is one of the big issues in mobile communications. There are several works on this subject that study to avoid or minimise interference. In this chapter, interference basic aspects are briefly explained. Later, different approaches to interference calculation are shown and interference models are presented.

### 2.3.1 Basic Aspects

In the early days, interference was not a great problem in mobile communication systems. With the growth of these systems and the number of users, interference is nowadays a great issue for an operator. Smaller size cells and less transmitting power are needed in order to reduce the number of users per cell, allowing more bandwidth and less power per user. Still, interference remains an issue,

because of the large number of users in urban areas.

There are several types of interference, though in this thesis it is only expressed in the form of co-channel and adjacent channel ones, because of its importance in mobile radio systems. Both them can be intra- and/or inter-cell interferences.

Adjacent channel interference occurs when operators maximise spectrum efficiency: channels are kept very close to each other in the frequency spectrum, therefore, a channel can be overlapped by another. Co-channel interference is caused by another signal operating in the same channel. Since in UMTS there is a 5 MHz separation between each 4.4 MHz radio channel, co-channel interference is more relevant, and therefore being the main focus of this work.

Channel interference can be divided into UL (caused by MTs on BSs) and into DL (caused by BSs on MTs), Figure 2.6.

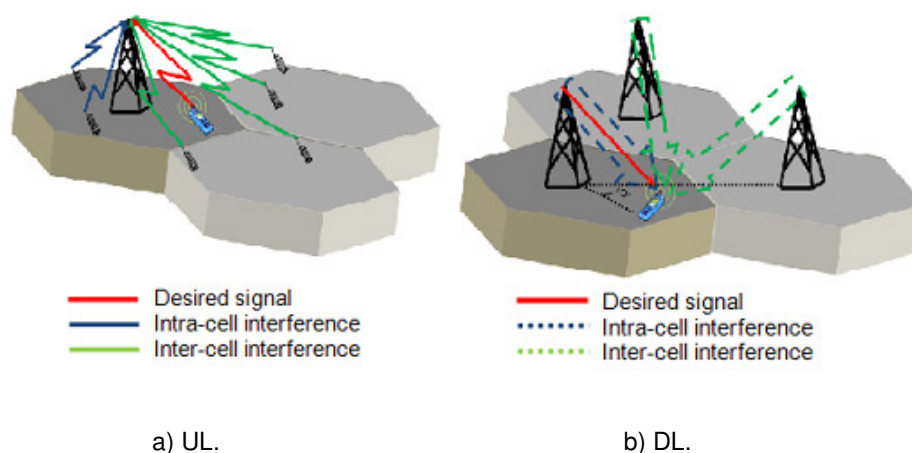


Figure 2.6. Different cases of interference (extracted from [Chen03]).

Intra-cell interference in UL is caused by the signals sent by MTs within the cell, as shown in Figure 2.6.a). Assuming the power control is well performed, UL interference is strictly related to the load distribution within the network. On the other hand, in DL, intra-cell interference occurs when a signal from the BS interferes with the signal of the served MT, as shown in Figure 2.6.b), which can happen if the orthogonality of the codes is somehow not maintained. Summing up, the main interference factor is the loss of code orthogonality between users.

In UL, inter-cell interference is caused by the signals sent by MTs in other cells, as shown in Figure 2.6.a). On the other hand, DL inter-cell interference occurs when a signal from another cell's BS interferes with the desired signal, as shown in Figure 2.6.b). Since BSs are independent from each other (i.e., not synchronised), the received signal may be influenced by other BS's signals [EsPe06].

Since UMTS uses FDD, interference among BSs does not exist, as different frequency bands are used in DL and UL. Also interference does not occur among MTs, because each MT has its own

identifying code when transmitting to the BS.

Fading must be introduced. The distribution that best fits slow fading is the Log-Normal Distribution, with standard deviation in the range of 4 to 10 dB. On the other hand, treating fast fading is not so simple since it is required to know if the MT and the BS are in Line-of-Sight (LoS) or in Non-Line-of-Sight (NLoS). For NLoS, fast fading can be described by a Rayleigh Distribution, while for LoS fast fading follows a Ricean Distribution.

Both [EsPe06] and [Marq08] offer an extensive analysis of different inter- and intra-cell interference models. However, most of them are similar, the propagation models in which they are based and the statistical distribution that characterize slow fading being the main differences between each work.

### 2.3.2 Intra- and inter-cell Interferences

As for DL intra-cell interference, (2.16) describes for MT  $i$  the interference power considering the total BS transmitted power for other MTs within the cell, the orthogonality factor and the path loss [SKYM03].

$$I_{\text{int } ra, i}^{DL} [w] = (P_{\text{Total, BS}} [w] - P_{BS \rightarrow MT_i} [w]) \times \alpha_{CO} \times L_P [w] \quad (2.16)$$

where:

- $P_{\text{Total, BS}}$  is the total transmitted power from the BS to the MTs within the cell;
- $P_{BS \rightarrow MT_i}$  is the transmitted power from the BS to a single MT  $i$  where the interference is calculated;

$$P_{\text{Total, BS}} - P_{BS \rightarrow MT_i} = \sum_{j=1, j \neq i}^{N_{au}} P_{BS \rightarrow MT_j} \quad (2.17)$$

with:

- $P_{BS \rightarrow MT_j}$  being the transmitted power from BS to the other MTs  $j$  within the cell;

For intra-cell interference in UL on cell  $j$  the calculation is done according to (2.18), [Nguy05]. This model considers the MT transmitted power, the service activity factor, the number of users using the service as the MT in study and the path loss.

$$I_{\text{int } ra, j}^{UL} [w] = \sum_{n=1}^{N_{serv}} (P_{MT \rightarrow BS_j} [w]) \times \eta_n \times L_P [w] \times N_{au, j, n} \quad (2.18)$$

where:

- $P_{MT \rightarrow BS_j}$  is the transmitted power from the MT to the desired BS  $j$ ;
- $\eta_n$  is the activity factor of the used service  $n$ ;
- $N_{au, j, n}$  is the number of users using the service  $n$  within the cell that contains BS  $j$ ;
- $N_{serv}$  is the total number of services.

For DL inter-cell interference, the interference in MT  $i$  is calculated according to (2.19), taking into account the total transmitting power of all BSs that are causing interference, as well as the orthogonality factor and path loss [EsPe06], based on [Chen03].

$$I_{inter,i}^{DL} [\text{W}] = \sum_{j=2}^{N_{NodeB}} P_{Total, BS j} [\text{W}] \times \alpha_{CO} \times L_P [\text{W}] \quad (2.19)$$

where:

- $P_{Total, BSj}$  is the total transmitting power of BS  $j$ ;
- $N_{BS}$  is the number of interfering BSs.

In case of inter-cell interference in UL, calculation on BS  $j$  is given by (2.20), [Marq08]. This depends on the transmitting power of the MTs outside the cell, the path loss, service activity factor and the distance relation between the cell in which the MT is causing interference and the cell that is serving it.

$$I_{inter,i}^{UL} [\text{W}] = \sum_{k=1, k \neq j}^{N_{NodeB}} \sum_{m=1}^{N_{serv}} \sum_{k=1}^{N_k} P_{MT_k \rightarrow BS_j} [\text{W}] \times L_P [\text{W}] \times \eta_m \times \sum_{n=1}^{N_{au k, g}} \frac{r_{j,n}^a}{r_{k,n}^a} \quad (2.20)$$

where:

- $P_{MTk \rightarrow BSj}$  is the power of MT  $k$  transmitted to BS  $j$  in an adjacent cell;
- $N_{au k, m}$  is the number of users using service  $m$  in the interfering cell  $k$ ;
- $r_{j,n}^a$  is the distance from the MT  $n$  using service  $g$  to BS  $j$ ;
- $r_{k,n}^a$  is the distance from the MT  $n$  using service  $g$  to BS  $k$ .

### 2.3.3 Interference Models

In order to analyse system performance, a reference outdoor interference power should be used for the SINR calculation, two models being suggested.

For the first model, a set of measurements were extracted from a BS in downtown Sevilla, Spain [SRRA03], where 250 users were scattered in the scenario. The total received interference power includes intra-cell, inter-cell and noise components, from which only the intra- and inter-cell interferences were desirable. Since it was not possible to remove the noise power from the total received power, this was the implemented set in the indoor interference calculation. Moreover, this set was implemented for both DL and UL, since no other model was available. This set was then summarised in a histogram, Figure 2.7, from where the average and standard deviation values were extracted and input into the simulation default parameters. The average outdoor interference power is -97.64 dBm and the standard deviation is 0.54 dB.

The second model is based on the simulations performed in [Marq08]. Several parameters were analysed during the simulation procedure, namely the distance between the BS and the MT, the MT building height, the street width and the BS antenna tilt. For the purpose of this thesis, only the MT building height and the distance are included, since the rest of the parameters are not so relevant for

the desired analyses.

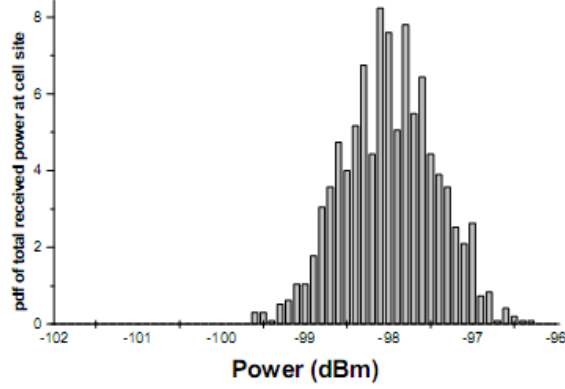


Figure 2.7. Total interference power distribution at the reference cell (extracted from [SRAA03]).

For the MT building height, three configurations were tested in the simulation procedure: the MT building height being higher, equal and lower than the remaining buildings height. In the first scenario, the MT building height was 33 m and the results are split in two cases, LoS and NLoS, being given by (2.21). For the second scenario the MT building height was 21 m and is provided in (2.22). For the third scenario the MT building height was 12 m, and is given by (2.23).

$$I_{DL}^{Higher} [\text{dBm}] = \begin{cases} 1.23 \times F_N - 93.97, & \text{NLoS} \\ 3.27 \times F_N - 80.05, & \text{LoS} \end{cases} \quad (2.21)$$

$$I_{DL}^{Equal} [\text{dBm}] = \begin{cases} 0.98 \times F_N - 95.38, & \text{DL} \\ -0.01 \times F_N - 111.15, & \text{UL} \end{cases} \quad (2.22)$$

$$I_{DL}^{Lower} [\text{dBm}] = \begin{cases} 1.38 \times F_N - 95.82, & \text{DL} \\ -0.01 \times F_N - 111.81, & \text{UL} \end{cases} \quad (2.23)$$

where:

- $F_N$  is the floor number.

The standard deviations for the given scenarios are presented in Table 2.4.

Table 2.4. Standard deviations for the different MT building height cases (extracted from [Marq08]).

| Standard Deviation [dB] |              |       |       |        |       |       |
|-------------------------|--------------|-------|-------|--------|-------|-------|
| DL                      |              |       |       | UL     |       |       |
| Higher (NLoS)           | Higher (LoS) | Equal | Lower | Higher | Equal | Lower |
| 6.65                    | 7.15         | 6.62  | 6.43  | 2.58   | 2.61  | 2.32  |

Concerning the interference variation with the distance between the BS and MT, three scenarios were simulated: the MT positioned at half the cell coverage distance, near the BS and on the cell edge. Since no information was found regarding the simulated distances, the models are presented as

previously stated: (2.24) shows the interference power in the reference scenario, (2.25) is referred to the near BS scenario, and (2.26) to the far BS scenario.

$$I_{\text{[dBm]}}^{\text{Ref}} = \begin{cases} 2.52 \times F_N - 97.29, & \text{DL} \\ -0.09 \times F_N - 111.16, & \text{UL} \end{cases} \quad (2.24)$$

$$I_{\text{[dBm]}}^{\text{Near}} = \begin{cases} 2.31 \times F_N - 87.82, & \text{DL} \\ -0.06 \times F_N - 110.79, & \text{UL} \end{cases} \quad (2.25)$$

$$I_{\text{[dBm]}}^{\text{Far}} = \begin{cases} 2.68 \times F_N - 102.77, & \text{DL} \\ -0.07 \times F_N - 111.42, & \text{UL} \end{cases} \quad (2.26)$$

The standard deviations for the given scenarios are presented in Table 2.5. UL expressions are similar, because the building height does not have a direct influence in UL, i.e., the interference in UL depends on the number of users served. With building height variation the number of users during the simulation is almost equal, therefore interference behaviour does not present variations [Marq08].

Table 2.5. Standard deviations for the different distance cases (extracted from [Marq08]).

| Standard Deviation [dB] |      |      |      |      |      |
|-------------------------|------|------|------|------|------|
| DL                      |      |      | UL   |      |      |
| Ref                     | Near | Far  | Ref  | Near | Far  |
| 6.82                    | 7.11 | 6.91 | 2.58 | 2.54 | 2.60 |

## 2.4 Propagation Models

### 2.4.1 Introduction

The surrounding environment is a key factor in mobile communications. Wave propagation models are extremely important to guarantee a good coverage and capacity planning, since one can use them to determine propagation characteristics. Propagation models can be theoretical or empirical. The theoretical ones provide an approximation of the real environment based on assumptions that simplify the problem; however, when the scenario changes these models show low versatility. The empirical ones are based on measurements through the use of best fit equations; the disadvantage of these models is the limitation of boundaries in the parameters, since a set of equations is only valid under certain circumstances. It is not uncommon to find combinations of both types of models, as the resulting model is less sensitive to parameter accuracy and shows good results.

The model to be selected depends on the type of environment, because each type differs in some parameters: terrain undulation, building density and height, vegetation and open areas density. These environments can be of three types: rural, suburban and urban. The rural environment is characterised

by the largest open area, flat terrain without obstacles. Suburban type consists of terrain with few obstacles, such as small residential areas. The urban type is a highly dense environment, with buildings higher than four floors, such as large cities and industrial areas.

It is also important to point out the classification of the cells, which is done according to their radius range and to the relative position of the BS antennas. Four types of cell arise: large macro-, small macro-, micro- and pico-cells. Relevant to this work are the small macro-cells, since they are used for outdoor in urban scenarios. They are built above the medium roof-top level, therefore LoS is not guaranteed in some areas. Their coverage radius range is between 0.5 and 3 km.

Because it is not reasonable to measure radio propagation in every single building, indoor models are important to reduce interference in this environment, since the characteristics that degrade performance are quite different from the outdoor ones. It is a complex multipath study, taking into account several variables, such as the variation of building size, shape and structure, room layouts, and the most important one, construction materials. Therefore, these models show up as a suitable alternative, without the need of performing signal measures on site. The next sections give a detailed description of the existing models, for both outdoor and indoor environments. For a correct analysis, the selected models take into account the fact that this work is dealing with UMTS in urban small macro-cells. Two models were chosen, as suggested in [Marq08]: COST231 – Walfisch-Ikegami [DaCo99] for outdoor; COST231 – Multi-Wall [DaCo99] for indoor.

One needs also to calculate link budget, i.e., the maximum loss that the system can tolerate due to propagation. Annex A shows this characterisation in further detail. However, it might be useful to introduce the generic path loss expression [Corr09]:

$$L_p [\text{dB}] = P_{Tx} [\text{dBm}] + G_{Tx} [\text{dBi}] - P_{Rx} [\text{dBm}] + G_{Rx} [\text{dBi}] \quad (2.27)$$

This path loss expression can also be achieved by the combination of outdoor and indoor losses, as shown in Figure 2.8:

$$L_p [\text{dB}] = L_{p \text{ outd}} [\text{dB}] + L_{p \text{ ind}} [\text{dB}] \quad (2.28)$$

where:

- $L_{p \text{ outd}}$  is the path loss attenuation given by the outdoor model;
- $L_{p \text{ ind}}$  is the path loss attenuation given by the indoor model.

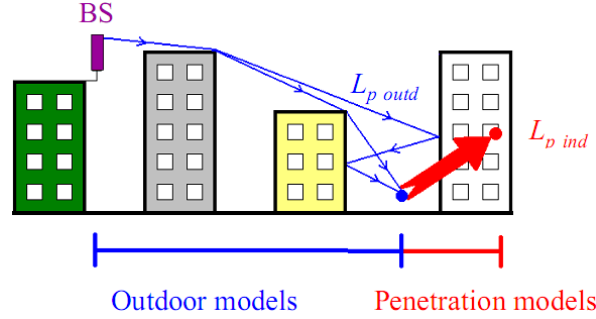


Figure 2.8. Illustration of the outdoor and indoor losses (extracted from [Corr09]).

## 2.4.2 Outdoor and Indoor Models

Two outdoor models are suggested by [Corr09], COST231 – Okumura-Hata and COST231 – Walfisch-Ikegami. The Okumura-Hata is based on Hata [Hata80] and Okumura [OkOh68] models, and Walfisch-Ikegami is the result of the combination of Walfisch-Bertoni [WaBe88] with Ikegami [IkYo84] models. They were developed for urban, suburban and rural environments, but with particular specificities: Okumura-Hata handles large distances, usually more than 5 km, while Walfisch-Ikegami (WI) is used for cases where the distances are less than 5 km in urban and suburban environments. Since the distances to the BSs in urban environments are most of the times less than 5 km, the latter model was chosen over the former. It is thoroughly described in Annex B.

When the MT is not between buildings and the BS is on the building top adjacent to the MT, the path loss is calculated according to the Walfisch-Bertoni model [Corr09]. In this case the reflected ray in the building no longer exists, therefore one cannot use the WI model. This particular situation is used when the MT is indoors and there is only one ray connecting the MT and the BS. An extra attenuation factor should be taken into account when the signal is diffracted from the roof to the MT. This factor is added to the free space loss factor of the path loss expression (B.2) and it is given by:

$$L_{rm}[\text{dB}] = -20 \log \left[ \frac{1}{\sqrt{\pi \cdot k \cdot d_{rr}[\text{m}]}} \left( \frac{1}{\Psi[\text{rad}]} - \frac{1}{2\pi - \Psi[\text{rad}]} \right) \right] \quad (2.29)$$

where:

- $\Psi$  is angle between the MT and roof top corner defined by (2.30) and as shown in Figure 2.9;

$$\Psi = \arctan \left( \frac{\Delta h_{\text{Mobile}}[\text{m}]}{d_m[\text{m}]} \right) \quad (2.30)$$

with:

- $\Delta h_{\text{Mobile}}$  being the difference between the roof height and the mobile height, (B.5);
- $d_m$  being the horizontal distance between the MT and the diffracting edges.
- $k$  is the propagation constant given by:

$$k = \frac{2\pi \cdot f_{[\text{MHz}]}}{300} \quad (2.31)$$

- $d_{rt}$  is the distance between the roof top and the MT, as shown Figure 2.9 and given by:

$$d_{rt}[\text{m}] = \sqrt{(\Delta h_{\text{Mobile}}[\text{m}])^2 + (d_m[\text{m}])^2} \quad (2.32)$$

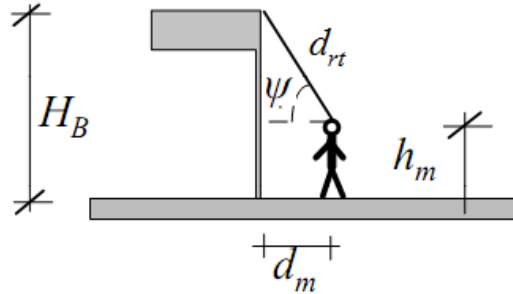


Figure 2.9. Illustration of the extra attenuation parameters (adapted from [Corr09]).

For indoor models, one can consider one of the three models investigated by COST231 [DaCo99]. The One-Slope model assumes a linear dependence between path loss and the logarithmic distance. The Multi-Wall model (MWM) takes the free space loss into account plus losses like walls and floors penetration loss by the direct path between transmitter and receiver. The Linear Attenuation model gives the path loss as a linearly dependence with the distance plus free space loss.

The most interesting model for this study is the MWM, since it can take the wall and floor penetrations into account, expressed in (2.33). The wall and floor types and their average loss are shown in Table 2.6.

$$L_{p \text{ ind}} [\text{dB}] = L_0 [\text{dB}] + L_{\text{glass}} [\text{dB}] + \sum_{i=1}^{N_{\text{wall}}} k_{wi} \times L_{wi} [\text{dB}] + k_f \times L_f [\text{dB}] \quad (2.33)$$

where:

- $L_{\text{glass}}$  is the glass loss attenuation;
- $N_{\text{wall}}$  is the number of wall types;
- $k_{wi}$  is the number of penetrated walls of type  $i$ ;
- $L_{wi}$  is the attenuation per penetrated wall of type  $i$ ;
- $k_f$  is the number of penetrated floors;
- $L_f$  is the attenuation per penetrated floor;

Table 2.6. Wall and floor types for the MWM and weighted average loss (extracted from [Marq08]).

| Loss category      | Description  | Factor [dB] |
|--------------------|--|-------------|
| $L_f$              | Typical floor structures (i.e. offices): hollow pot tiles, reinforced concrete, thickness type < 30 cm | 2           |
| $L_{w i}$          | Light internal walls (<10cm): plasterboard, walls with large numbers of holes (e.g. windows)           | 10          |
| $L_{\text{glass}}$ | Typical glass  | 1           |

## 2.5 Throughput Models State of the Art

A brief overview of the state of the art is presented in this section, in order to show what has been done in this field up to now, thus, emphasising the importance of this work.

Several works present statistical studies on the indoor signal attenuation in urban scenarios, comprehending both GSM and UMTS bands, but not taking the building type into consideration. Tanis and Pilato [TaPi93] showed an average penetration loss of 19.2 dB for 880MHz and 15.7 dB for 1922 MHz, resulting in a difference between the two bands of 3.5 dB. A similar study was made by Toledo et al. [ToTP98], which showed a penetration loss of 14.2 dB, 13.4 dB and 12.8 dB for 900 MHz, 1800 MHz and 2300 MHz respectively. This study realises a 0.8 dB difference between 900 and 1800 MHz, and a 1.4 dB difference between 900 and 2300 MHz. [ToTP98] also investigated the average attenuation per floor and found a number of 1.4 dB per floor, below the 6th floor. On higher floors, they saw a 0.4 dB decrease per floor, although no distinction was made between the per floor penetration losses between lower and higher floors. COST231 [DaCo99] reports an increase in loss for GSM1800 of 2 dB.

Other studies take into account the building type in the attenuation results (also statistical). [XaVe02] and [SLCM05] performed measurements in four types of buildings (the same approach as this work) on both GSM and UMTS bands. For UMTS, [XaVe02] presents an average attenuation of 13.3 dB, 2.6 dB, 12.8 dB and 15.8 dB for High Integrated, High Isolated, Low Integrated and Low Isolated buildings, respectively, resulting in 10.2 dB of average attenuation. [SLCM05] presents an average attenuation of 7.5 dB, 3.9 dB, 7.7 dB and 11 dB for High Integrated, High Isolated, Low Integrated and Low Isolated buildings, respectively, resulting in 7.6 dB of average attenuation. It can be observed in both studies that Low-Isolated has the highest attenuation and High-Isolated the lowest one. The average discrepancy between the two studies is 2.6 dB, mainly due to a smaller set of measured BSs per building in [XaVe02].

Although the presented works are useful to create a signal attenuation model, the main subject of this thesis is the throughput analysis, more specifically its indoor reduction for different types of buildings. Few studies can be found on this specific subject, although some indoor throughput analyses are available. [BrHo10] performs measurements and simulations inside a shopping centre, varying the distance to the BS in DL. When the maximum distance is reached (30 m), the authors notice an average throughput decrease of 69 % and 94 % for the simulated and measured results, respectively. [IsLe07] studies the performance of HSDPA in indoor environments, coverage improvement using distributed antenna systems being the main subject. Although the focus of this thesis is not the study of distributed antenna systems, [IsLe07] presents some throughput measurements with distance variation: the average throughput decreases 94 % from the start to the end point (100 m away).

[TaFi10] studies the impact of building penetration on HSDPA throughput, being the work that most resembles this thesis' subject. Indoor and outdoor HSDPA performance measurements were carried

out in a live HSDPA network for a mobile located near the cell edge in a suburban environment. Measurements results show that the greatest difference between indoor and outdoor data rates occur during the low load period (when the system is noise-limited, and therefore the building penetration loss has the greatest impact). In this period, the outdoor data rate is higher than the indoor data rate by 20 % to 40 %. During the high traffic (high cell load) periods, the difference between indoor and outdoor performance is minimal, due to full power transmission from all BSs resulting in an interference-limited environment. Under these circumstances, the building penetration loss impacts the wanted and interfering signal equally. For this period, the outdoor data rate is no greater than 10 % higher than the indoor one.

# Chapter 3

## Model Development and Implementation

This chapter provides a thorough analysis of the models used in the scope of this thesis. The first section is used to describe the developed indoor and outdoor models used in the simulator. An overview of both simulation modes (Single- and Multi-User) is given in the following section. Further on, the simulation algorithms behind the two modes are explained. After this, the simulator input and output parameters are described. The chapter concludes with the simulator assessment.

## 3.1 Propagation Models

In this section, the propagation model is overviewed. This propagation model is composed of two parts: outdoor and indoor. A set of urban scenarios is chosen to accommodate all propagation possibilities concerning the BS and the MT positions.

### 3.1.1 Outdoor Model

In order to decide if there is LoS between BS and MT, the first Fresnel zone principle criterion is used [RMSP87], as shown in Figure 3.1. The direct ray between BS and MT is calculated, and then it is verified through (3.1) if the first Fresnel zone is obstructed by the top of the last building before the MT. If it is, the MT is in NLoS, if it is not, the MT is in LoS with BS.

$$R_{[m]}^{Fresnel} = \sqrt{\frac{d_1(d-d_1)}{d}}\lambda \quad (3.1)$$

where:

- $d$  is the distance between the BS and the MT;
- $d_1$  is the distance between the BS and the building top.

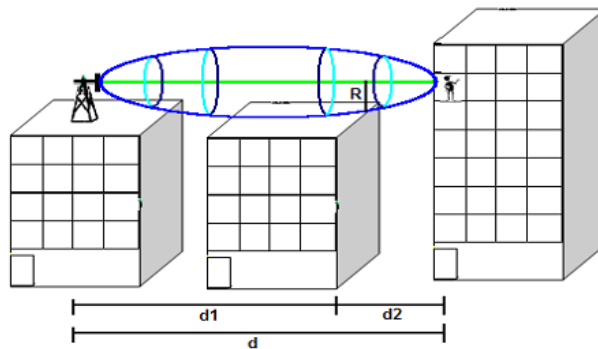


Figure 3.1. First Fresnel zone representation (extracted from [Marq08]).

Concerning outdoor path loss, there are 6 situations that can be identified [Marq08]:

- When the MT is served by one BS on the building top, Figure 3.2, case 1. The calculation is done according to (3.2). In this particular case, the outdoor reference position is on the building rooftop and not on the middle of the street;
- When the distance between BS and MT is less than 20 m and there is LoS, Figure 3.2, case 2, free space attenuation (B.3) plus indoor loss (3.2) are the propagation models used to obtain the total loss;
- When the BS is located on the top of an adjacent building, the distance between BS and MT is

less than 20 m and BS is in NLoS with MT, the path loss is calculated by free space plus extra attenuation (2.29) added to (3.2), Figure 3.2, case 3;

- When the BS is in the adjacent building façade and there is LoS with all the floors, the path loss is calculated according to (B.3) if the distance is less than 20 m, and (B.1) if it is more than 20m, plus (3.2), Figure 3.2, case 4;
- When the BS is in LoS and more than 20 m far away to the MT, COST 231 - Walfish-Ikegami (B.1) plus (3.2) are the models applied, Figure 3.2, case 5;
- For last situation, Figure 3.2, case 6, when the BS is in NLoS and more than 20 m far away to the MT, the calculation is done according to (B.2) plus (3.2).

All these methods are summarised in Table 3.1.

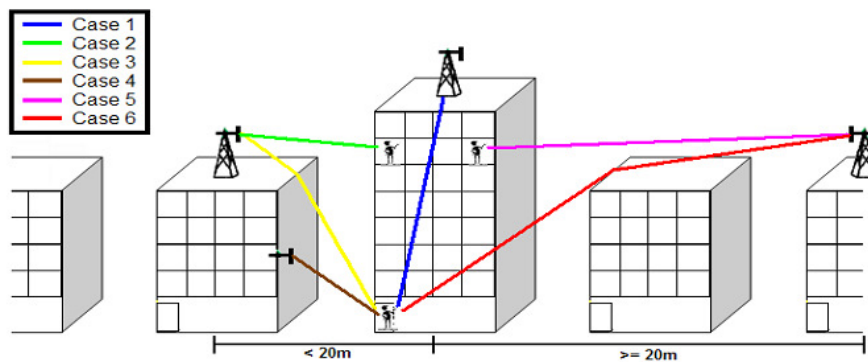


Figure 3.2. Different cases of outdoor path loss (extracted from [Marq08]).

Table 3.1. Characteristics of the Different cases of outdoor path loss (adapted from [Marq08]).

| Path Loss Cases | Description   | LoS/NLoS | Model   | Equations            |
|-----------------|---|----------|---|----------------------|
| 1               | BS on the top of the same building as MT                                    | NLoS     | Indoor Model                                  | (3.2)                |
| 2               | Distance between BS and MT is less than 20m                                 | LoS      | Free Space + Indoor Model                     | (B.3)+(3.2)          |
| 3               | BS on adjacent building top, distance between BS and MT is less than 20m    | NLoS     | Free Space + Extra Attenuation + Indoor Model | (B.3)+(2.29) + (3.2) |
| 4               | BS on adjacent building façade, distance between BS and MT is less than 20m | LoS      | Free Space + Indoor Model                     | (B.3)+(3.2)          |
|                 | BS on adjacent building façade, distance between BS and MT is more than 20m | LoS      | Walfish-Ikegami + Indoor Model                | (B.1)+(3.2)          |
| 5               | Distance between BS and MT is more than 20m                                 | LoS      | Walfish-Ikegami + Indoor Model                | (B.1)+(3.2)          |
| 6               | Distance between BS and MT is more than 20m                                 | NLoS     | Walfish-Ikegami + Indoor Model                | (B.2)+(3.2)          |

In an indoor scenario, slow fading is mainly static whereas the fast fading is stochastic due to outdoor multipath. Therefore, the fast fading is characterised by the corresponding Rayleigh distribution in a pedestrian environment, and the slow fading is characterised by a margin that accounts for the

outdoor environment. Table 3.2 shows the parameters used to describe the fading phenomena, according to the criteria explained above.

Table 3.2. Parameters used for slow and fast fading margins (adapted from [Jaci09]).

| Fading Type | Parameter Type     | Value [dB] |
|-------------|--------------------|------------|
| Fast Fading | Standard Deviation | 4          |
| Slow Fading | Margin             | 7.6        |

### 3.1.2 Indoor Model

The MWM model given by (2.33) is the general expression, though a statistical approach is used in this work: the mean value and the standard deviation are inserted for each loss type. One glass and up to two walls were set for this model, since it covers most of the urban scenarios, given the measurement campaign experience. The number of floors depends on the MT position inside the building,  $k_f$  being referred to the building base, i.e., its value is zero at the ground floor.

In order to obtain a representative range of different types of buildings existing in an urban environment, a selection of buildings was created according to defined classes. For the characterisation of signal penetration into buildings, four different typical scenarios were considered, based on [XaVe02], Figure 3.3:

- High-Integrated (HIInt): a building with more than 6 floors, being surrounded by other buildings with similar height (possibly contiguous);
- High-Isolated (HIso): a building with more than 6 floors, being surrounded by other buildings with lower height;
- Low-Integrated (LIInt): a building up to 6 floors, being surrounded by other buildings with similar height (possibly contiguous);
- Low-Isolated (LIso): a building up to 6 floors, not being surrounded by other buildings.

For each floor of a given building, three categories of rooms were considered, as defined in [XaVe02]:

- Indoor Window (IW): a room with a window facing the outdoors;
- Indoor Daylight (ID): a room with one wall separation to the outdoors;
- Deep Indoor (DI): a room with two walls separation to the outdoors.

An example of these room categories is shown in Figure 3.4, where the crosses represent a possible path to be followed in the measurement procedure.

The calculation of the indoor loss is done according to (3.2). The indoor loss is referred to the outdoor signal power (in the middle of the street, as modelled by the outdoor model) for each room type, as shown in Figure 3.5. It is modelled as a function of the coverage percentage,  $p$ ,  $u(p)$  being the inverse function of the indoor loss distribution. In order to model the received signal power by (3.2), one has to assume a Log-Normal distribution for the RSCP.

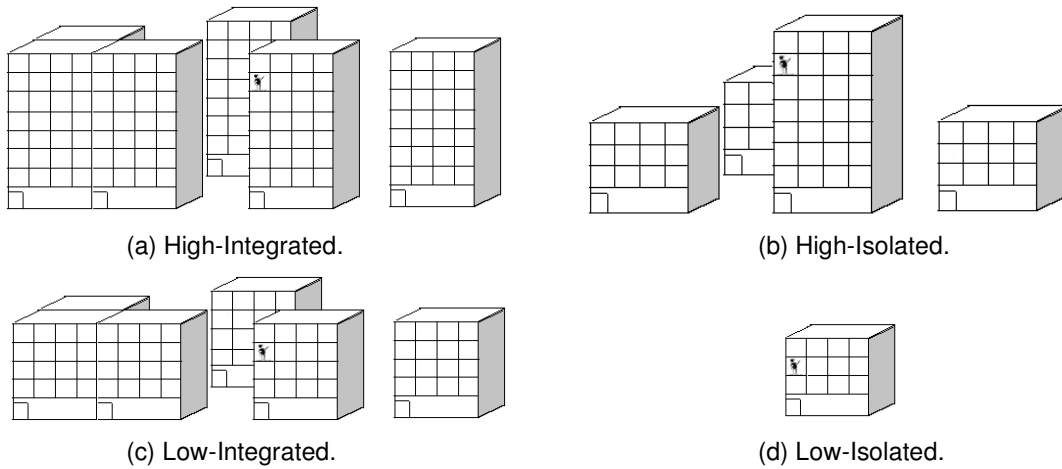


Figure 3.3. Different types of urban building scenarios.



Figure 3.4. Example of one floor blueprint (adapted from [Marq08]).

The indoor model covers not only the depth of the building but also its height. In other words, the indoor propagation model is composed of horizontal propagation (room attenuation) and vertical one (floor attenuation). Therefore, each mean and standard deviation value in (3.2) is referred to one specific floor.

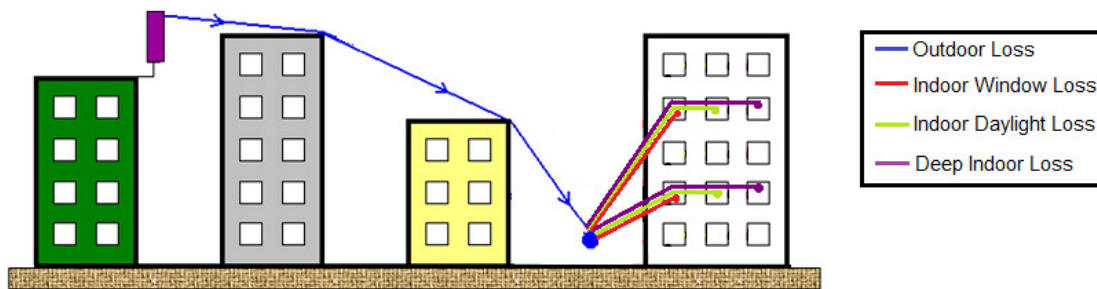


Figure 3.5. Indoor room loss model approach.

$$L_{p\ ind} [\text{dB}]_{\text{Floor } i}^{IW, ID, DI} (p) = \mu_{[\text{dB}]_{\text{Floor } i}^{IW, ID, DI}} + u(p) \times \sigma_{[\text{dB}]_{\text{Floor } i}^{IW, ID, DI}} \quad (3.2)$$

where:

- $\mu_{\text{Floor } i}^{IW, ID, DI}$  is the mean attenuation concerning floor  $i$  in room type IW, ID or DI;
- $p$  is the desired building coverage (in percentage);
- $u(p)$  is the function that describes the inverse indoor loss distribution;
- $\sigma_{\text{Floor } i}^{IW, ID, DI}$  is the standard deviation concerning floor  $i$  in room type IW, ID or DI.

A linear model was created for the mean value of each room type, with a floor dependency on each trend, (3.3). The choice for a linear trend curve is due to the desire to define a trend of the attenuation along the building floors, allowing extrapolations to be performed.

$$\mu_{[\text{dB}]_{\text{Floor } i}^{IW, ID, DI}} = \mu_{[\text{dB}]_{\text{var}}} \times F_N + \mu_{[\text{dB}]_{\text{level}}} \quad (3.3)$$

where:

- $\mu^{\text{var}}$  is the variable part of the mean attenuation, depending on the floor number;
- $\mu^{\text{level}}$  is the static part of the mean attenuation, independent of the floor number.

The interference power is also variable with the distance to the BS: the DL model in (3.2) accounts for a distance-dependent reference value (in UL, the variation with distance is not so evident). This model was based on the reference values in (2.24), (2.25) and (2.26). Although no information was provided on the simulated distances, the 30 m, 120 m and 250 m distances were assumed and a model was interpolated using a quadratic function. This interpolation was performed with a high correlation coefficient (0.99). The standard deviation values were left unchanged, since the two interference models (variable with MT building height and variable with distance) have similar standard deviation values, as shown in Table 2.4 and Table 2.5.

A minor change was introduced in (2.21), as shown in (3.3): the interference power in LoS was too high, causing the SINR to be too low in the upper floors. A change in the interference offset was performed, assuring continuity between the NLoS and the LoS cases. This change required a correction in the standard deviation value for the higher buildings in DL, Table 2.4. Therefore, the quadratic mean was performed using (3.10) and the result is an average standard deviation of 6.91 dB. The remaining standard deviations were left unchanged, Table 2.4.

$$\begin{cases} I_{DL}^{\text{Isolated}} [\text{dBm}] = 1.23 \times N_{\text{Floors}}^{\text{NLoS}} + 3.27 \times N_{\text{Floors}}^{\text{LoS}} + 286.7 \times d_{[\text{km}]}^2 - 148.2 \times d_{[\text{km}]} - 83.63 \\ I_{DL}^{\text{Integrated}} [\text{dBm}] = 1.23 \times N_{\text{Floors}}^{\text{NLoS}} + 286.7 \times d_{[\text{km}]}^2 - 148.2 \times d_{[\text{km}]} - 83.63 \\ I_{UL} [\text{dBm}] = -0.01 \times N_{\text{Floors}} - 111.15 \end{cases} \quad (3.4)$$

where:

- $N_{Floors}^{NLoS}$  is the number of floors in NLoS;
- $N_{Floors}^{LoS}$  is the number of floors in LoS.

In order to obtain the indoor signal power, the outdoor reference power is affected by the indoor loss, as shown in (3.5). Only the signal power is affected by this loss, since the proposed interference power in (3.4) is already referred to the indoor case.

$$P_{Rx\ ind} [\text{dBm}] = P_{Rx\ outd} [\text{dBm}] - L_{p\ ind} [\text{dB}] \quad (3.5)$$

where:

- $P_{Rx\ ind}$  is the indoor received signal power;
- $P_{Rx\ outd}$  is the outdoor received signal power.

The indoor and outdoor capacity model is based on the derived capacity model (2.9) in Subsection 2.1.2. Although (2.9) accounts for the available received signal power and the nearby interference power (through SINR computation), the capacity also depends on the number of available codes given by the BS. The main inclusion is the adjustment of the capacity expression to the number of codes available in HSPA+ DL. Although the number of served users can be higher, the 15 available codes for data transmission only allow the same number of users in the respective BS. For UL, the same approach is chosen, since UL requests are made from the same users that require DL capabilities. Other small adjustments had to be included, such as the exclusion of negative number of users. Equation (3.6) shows the expression to be included in the model.

$$\left\{ \begin{array}{l} N_{au} = \min \left( 15, \frac{1 - 10^{\frac{10 \cdot a_{pd} \log(r_{[km]}) - P_{Tx} [\text{dBm}] - G_{Tx} [\text{dB}] + P [\text{dB}] - G_P [\text{dB}] + N [\text{dB}] - G_{Rx} [\text{dB}] + L_{ref} [\text{dB}]}{10}}}{F_a \frac{\rho}{G_p} [(1 - \alpha_{CO}) + i_r]}}, N_{au} > 0 \right), \\ N_{au} = 0, \quad N_{au} \leq 0 \end{array} \right. \quad (3.6)$$

Concerning the variable  $i_r$  in (3.6), the chosen approach is a uniform distribution between the suggested values in Subsection 2.1.2. Regarding  $\alpha_{CO}$ , the model suggested in (2.6) is used for the computation of this value.

In both DL and UL, the outdoor capacity is calculated using the outdoor signal and interference powers, whereas the indoor capacity is computed using the indoor signal and interference powers.

## 3.2 Simulator Overview

In order to implement the described models, the *UMTSIndCov* simulator was developed following the work of [Marq08]. The simulator was developed in C++ using the Borland C++ Builder software [Code11]. Two different models were implemented: the Single-User and the Multi-User. The former concerns the modelling of the available resources for a Single-User in the network, whereas the latter gives information about the total capacity in a multiple user network, given a desired data rate for each user. These two models are explained further on in the respective subsections.

For this simulator, several simulation parameters can be modified, such as:

- BS building height;
- BS antenna height and tilt;
- MT building height and number of floors;
- Distance between BS and MT;
- BS and MT transmission power;
- BS radiation pattern;
- MT antenna gain;
- Frequency;
- Fading margins/distributions;
- Room and building types;
- Desired coverage (in percentage);
- Building's number of floors.

Different approaches are used for the signal and throughput losses. The focus of this work is to analyse the indoor throughput loss, i.e., the signal power loss is only needed to produce the simulated throughput through the mapping shown in Annex D. Because the existing indoor signal power loss models are not extensive, the indoor signal power loss is extracted from the measurements and inserted in the model, allowing it to produce the available throughput by a theoretical mapping. It is then possible to compare this result with the measured one.

### 3.2.1 Single-User Model

The objective of this application is to calculate the indoor data rate in different UMTS typical scenarios. The simulator can be split into four main blocks, as shown in Figure 3.6: configuration, measurements, simulation and results. The simulation type adopted for the simulator was the statistical approach (snapshot).

The initial block gives the user the possibility to define the characteristics of the BS (building and antenna height). One can choose the number of obstacle buildings between the BS and MT buildings and their characteristics (street width, building separation and building height), according to the WI

model described in Annex B. The MT building characterisation is another input of the simulator: the number of floors, the room category, the building type, and the building coverage percentage. Furthermore, outdoor parameters are to be set, such as frequency, standard deviation for fading distributions, BS antenna tilt and radiation pattern, BS and MT transmission power, MT antenna gain, receiver noise figure, cable and user losses, as defined in Annex A.

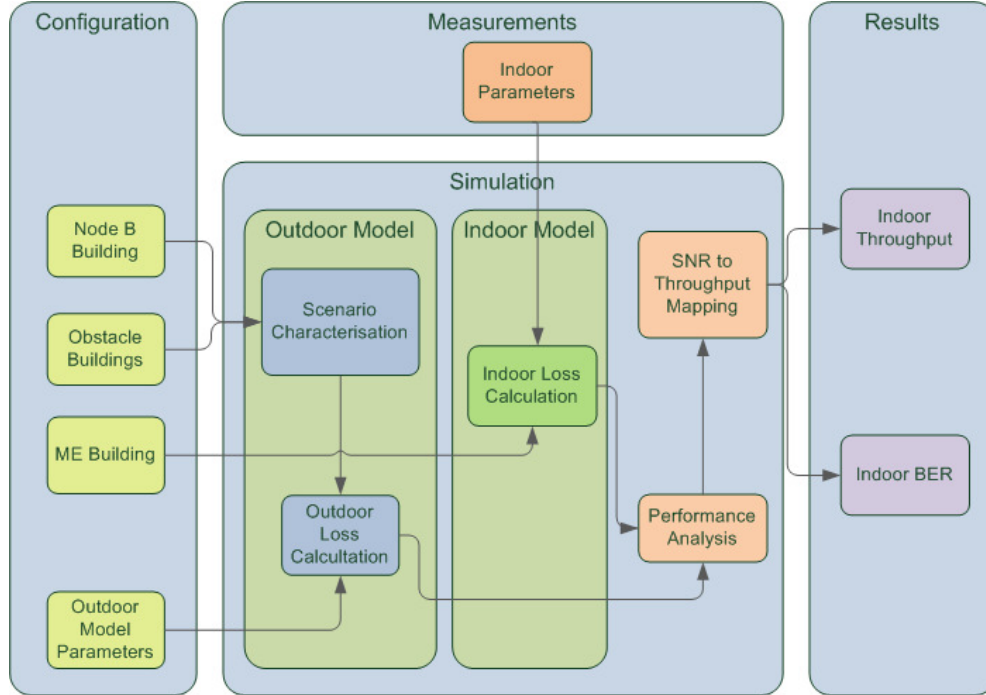


Figure 3.6. Single-User simulator structure.

In the measurements block, the set of parameters used in the indoor path loss model are identified, such as the signal power loss between floors ( $L_f$ ) and the signal power loss between walls ( $L_{glass}$ ,  $L_{w1}$  and  $L_{w2}$ ). Additionally, due to the lack of theoretical knowledge on the modulation usage, the percentage of each of the possible modulation schemes used in the measurements is identified. These parameters are extracted from the measurements, as shown in Section 4.1, and are included in the simulation block, more specifically in the indoor loss calculation, given by (3.2) and (3.3).

In the simulation block, the outdoor path loss scenario is determined depending on the MT position in relation to the BS and LoS/NLoS conditions, Table 3.1. Outdoor and indoor path losses are calculated according to the criteria shown in Section 3.3. The indoor interference power is also computed, according to (3.4). The total path loss value is deducted from the transmission power, using (3.5). The performance analysis is done depending on the link, using (A.9) for UL and (A.10) for DL. After this, the modulation is chosen using the results shown in Annex F. The last step is to perform the SINR to throughput mapping, according to Annex D.

In the results block, the simulation output is saved in files, such as the indoor physical and application throughput (according to Annex G) and the bit error probability.

### 3.2.2 Multi-User Model

The objective of this application is to calculate the number of indoor and outdoor served users in UMTS, considering the losses due to the presence of a building environment. The simulator can be split into four main blocks, as shown in Figure 3.7: configuration, measurements, simulation and results. The simulation type adopted for the simulator was the statistical approach (snapshot).

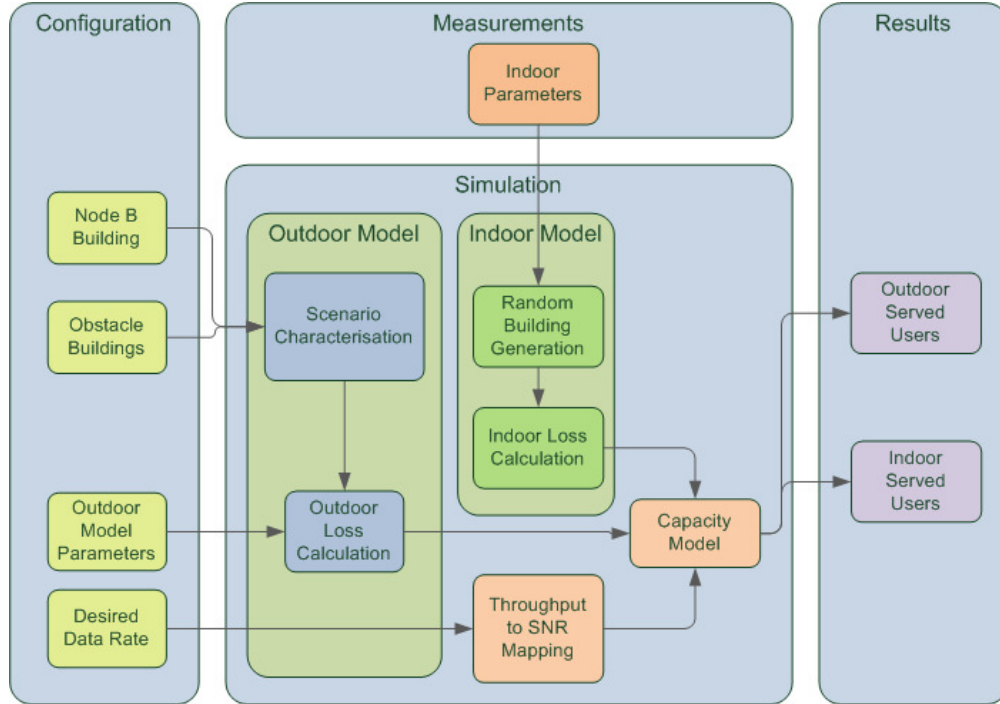


Figure 3.7. Multi-User simulator structure.

The initial block gives the user the possibility to define the characteristics of the BS (building and antenna height). One can choose the number of obstacle buildings between the BS and MT buildings, and their characteristics (street width, building separation and building height), according to the WI model described in Annex B. The MT building characterisation is another input of the simulator: the number of floors, the room category, the building type, and the building coverage percentage. Furthermore, outdoor parameters are to be set, such as frequency, standard deviation for fading distributions, BS antenna tilt and radiation pattern, BS and MT transmission power, MT antenna gain, receiver noise figure, and cable and user losses, as defined in Annex A.

In the measurements block, the set of parameters used in the indoor path loss model is identified, such as the signal power loss between floors ( $L_f$ ) and the signal power loss between walls ( $L_{glass}$ ,  $L_{w1}$  and  $L_{w2}$ ). Additionally, due to the lack of theoretical knowledge on the modulation usage, the percentage of each of the possible modulation schemes used in the measurements is identified. These parameters are extracted from the measurements, as shown in Section 4.1, and are included in the simulation block, more specifically in the indoor loss calculation, given by (3.2) and (3.3).

In the simulation block, the outdoor loss scenario is determined depending on the MT position in relation to the BS and LoS/NLoS conditions, Table 3.1. The outdoor and indoor path losses are calculated according to the criteria shown in Section 3.3. The indoor scenario is generated randomly, considering uniform distributions for the following parameters: number of floors (up to 12, depending on the building type), building coverage percentage (from 0 to 100 %), building and room type. The total path loss value is deducted from the transmission power. Before applying the capacity model, the desired data rate is mapped onto SINR according to the expressions in Annex D and the modulation is chosen using the results shown in Annex F. The capacity model is done according to (3.6), considering the outdoor and indoor losses, the distance between the BS and MT, and the SINR required for the desired data rate per user.

In the results block, the simulation output is saved in files: the indoor and outdoor number of served users.

### 3.3 Simulation Algorithms

The path loss calculation is fundamental for estimating the attenuation between the BS and the MT, and vice-versa. For this estimation to be accurate, an algorithm that combines different propagation models was created [Marq08], Figure 3.8.

The algorithm starts by verifying the Node and MT location. If they are in the same building the path loss calculation is done according to (3.2). If not, the algorithm begins with the search of the outdoor model that best fulfils the situation. So, in the first step, the distance between BS and MT is calculated. If it is more than 20 m far away from each other, WI is the model applied. WI presents two ways, i.e., when they are in LoS the calculation is performed by (B.1), when they are in NLoS the calculation is done according to (B.2). When they are less than 20 m, the BS location is evaluated. If it is not on a building roof, the free space model (B.3) is the one used. If it is, free space (B.3) is applied in case of LoS and free space plus extra attenuation (2.29) in case of NLoS. All LoS conditions are verified through first Fresnel zone principle (3.1). Once the outdoor model is selected, it is combined with the indoor model (3.2), the total path loss is achieved and the algorithm ends.

Regarding the data rate computation used in the Single-User model, the algorithm adopted for the simulator is shown in Figure 3.9. The simulator runs this algorithm a great number of times for each building floor, in order to guarantee statistical significance concerning the random variables, namely the indoor interference power and the fast fading.

After choosing the path loss case, using the algorithm in Figure 3.8, and computing the outdoor loss, LoS is tested in the current floor. The simulation for the current floor starts with the indoor interference power calculation. After this, the outdoor path loss is influenced by the indoor loss calculation, as

defined in (3.5). The next verification is the building type, which can be Integrated or Isolated (as shown in Figure 3.3). It also takes the indoor wall type into account: Indoor Window, Indoor Daylight or Deep Indoor. The result from both the interference and signal loss is inserted into the SINR calculation algorithm, which is done according to either (A.10) for UL or (A.11) for DL. For the data rate calculation, the SINR was mapped onto throughput according to the antenna configuration scheme and the modulation. The former can be set by the simulator user, whereas the latter is defined by the distribution extracted from the measurement campaign. The iteration ends after the throughput calculation and returns to the starting point, moving on to the next building floor.

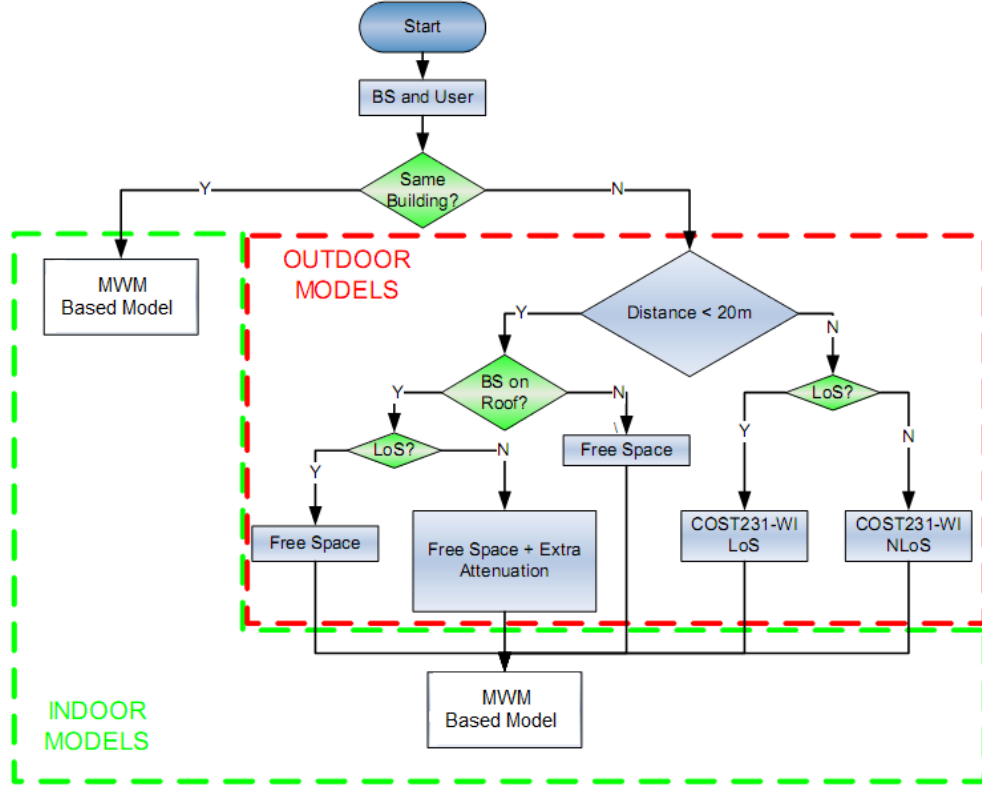


Figure 3.8. Path loss decision algorithm (adapted from [Marq08]).

For the indoor loss calculation in the Multi-User model, a similar approach is set although some changes have to be distinguished. Firstly, the user is able to choose between an automatic and a manual mode. The former computes the output for a range of available data rates, depending on the antenna configuration scheme and the link, as shown in (3.7). The latter performs the computation based on the desired data rate value input by the user in the application. Figure 3.10 shows the decision tree for the Multi-User simulation.

$$\begin{cases} R_b \in [0, 21.6] \text{ Mbps,} & \text{for DL SISO \& SIMO} \\ R_b \in [0, 43.2] \text{ Mbps,} & \text{for DL MIMO} \\ R_b \in [0, 11.5] \text{ Mbps,} & \text{for UL SISO} \end{cases} \quad (3.7)$$

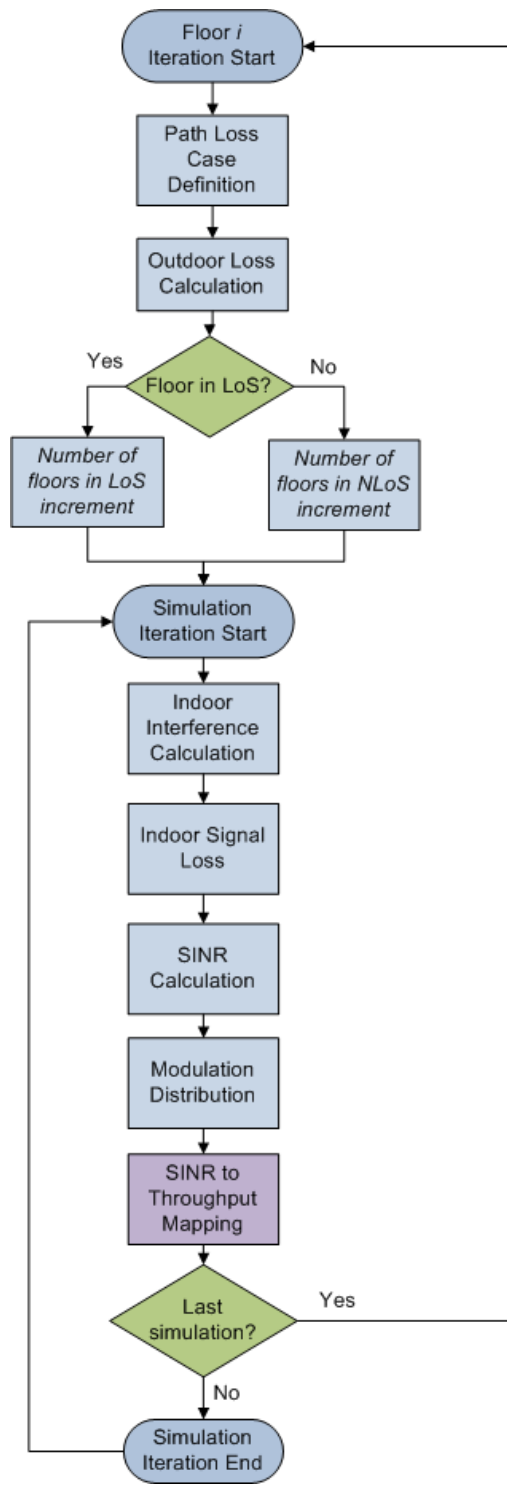


Figure 3.9. Single-User data rate calculation algorithm.

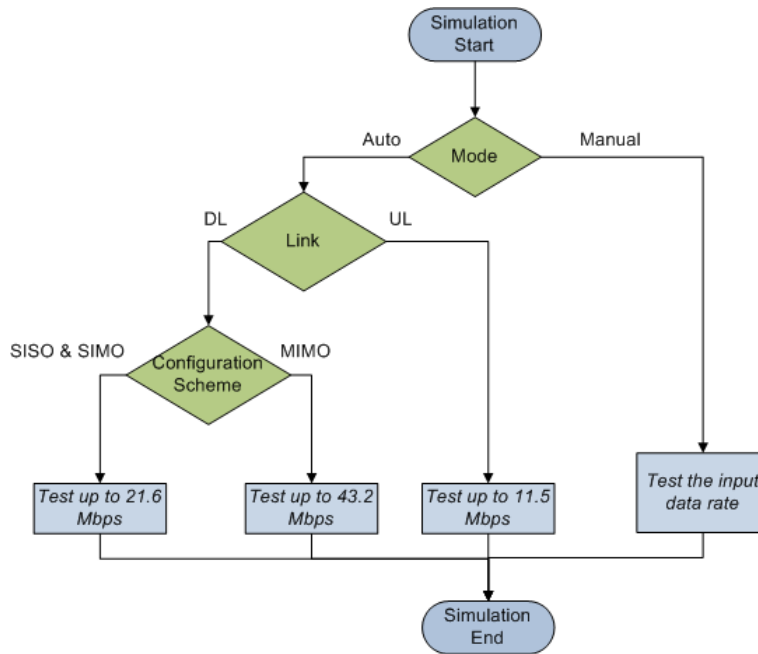


Figure 3.10. Decision mode for the Multi-User procedure.

Concerning the capacity calculation loop, Figure 3.11 shows the algorithm to be applied to the data rate tests. Similarly to the Single-User implementation, the simulator runs the algorithm several times in order to ensure statistical significance. Some steps differ from the Single-User model, mainly due to the inverse approach adopted concerning SINR and throughput. While the Single-User model calculates the path loss and informs the available data rate to be given to a Single-User, the Multi-User model defines a data rate to be given to each user and calculates the number of users that can be served with that same data rate. As in the Single-User model, the outdoor scenario is defined by the simulator user. Concerning the indoor scenario, the approach is quite different: in the Multi-User every single parameter in the indoor scenario is randomised, such as the number of floors (up to 12, depending on the building type), the building coverage percentage (from 0 to 100 %), the MT building and room types. This choice creates a richer environment, because the operator is most of the times not able to characterise every detail of an indoor scenario.

More specifically, the procedure is composed of the outdoor loss calculation, followed by the simulation loop start. The defined throughput and a chosen modulation (according to its distribution), together with the randomised indoor scenario, are inserted in the mapping procedure of the desired data rate into the required SINR. After verifying LoS/NLoS, in order to define the interference model to be used, the indoor loss is computed using the same steps as the Single-User model but with the previously stated corrections. Equation (3.6) is then used to calculate the indoor and outdoor capacity of the network for a given distance and outdoor loss. The outdoor capacity is calculated using the outdoor signal and interference powers, whereas the indoor capacity is computed using the indoor signal and interference powers. Two additional parameters are randomised: the code orthogonality factor, using the previously defined model (2.6), and the ratio of inter- to intra-cell interferences, each

of them belonging to their respective typical range. One should also take into account that the BS antenna gain was not corrected for the indoor environment.

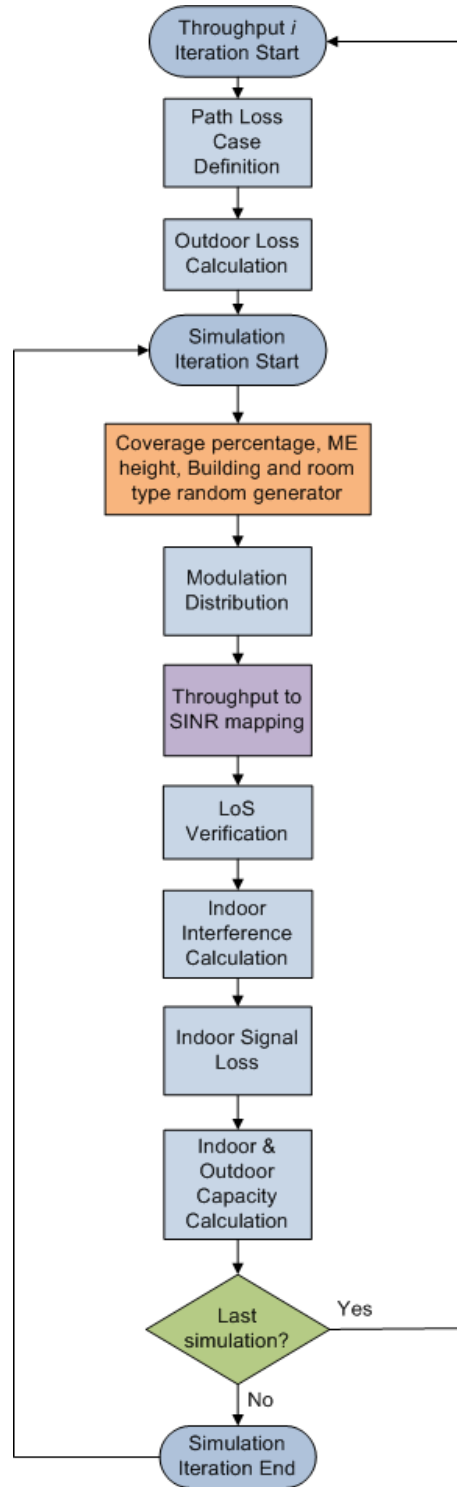


Figure 3.11. Multi-User capacity calculation algorithm.

### 3.4 Input and Output Parameters

It is not necessary to insert any input file in the UMTSIndCov application in order to run the simulator. During execution, the user can load the BS antenna radiation pattern. The radiation pattern file is based on the files from the base station antennas supplier Kathrein [Kath11]. All parameters required for simulation are filled in the program by the tool user. For more details about these input parameters, refer to the user's manual in Annex E.

In the end of the simulation, all parameters/results are written in \*.xls files. These files contain all the necessary information to perform a thorough analysis. Depending on the used model, the output files differ in their name. For the Single-User model, the application creates the following files:

- conditions.xls: this file contains the input parameters in the application run.
- results.xls: this file contains the main output of the application, where each row indicates the computed values for each iteration in the algorithm.

An extra .xls file, dataprocess.xls, is available to process the data from the previously indicated files, converting the information inside those files in numerical data and automatically creating plots of each of the main indicators, such as the BS antenna gain, indoor SINR, indoor interference, indoor physical and application throughput, among others.

For the Multi-User model Auto mode, the files are similar but contain the “\_cap” suffix in order to be distinguished from the Single-User model ones. An extra .xls file is also available in this case, dataprocess\_cap.xls, which is capable of computing the mean values and standard deviation for each data rate value.

Several parameters are extracted from the simulation in order to perform a complete analysis. This analysis requires knowledge on some statistical indicators, such as [Corr09]:

- Average,  $\mu$

$$\mu = \frac{1}{n} \sum_{i=1}^n x_i \quad (3.8)$$

where  $x_i$  is the value of sample  $i$  and  $n$  the total number of samples.

- Standard deviation,  $\sigma$

$$\sigma = \sqrt{\frac{1}{n} \sum_{i=1}^n x_i^2 - \left( \frac{1}{n} \sum_{i=1}^n x_i \right)^2} \quad (3.9)$$

- Mean of a set of average values,  $\bar{\mu}$

$$\bar{\mu} = \frac{1}{n} \sum_{i=1}^n \mu_i \quad (3.10)$$

- Quadratic mean of a set of standard deviation values,  $\bar{\sigma}$

$$\bar{\sigma} = \sqrt{\frac{1}{n} \sum_{i=1}^n \sigma_i^2} \quad (3.11)$$

The main output values are signal attenuation and throughput reduction. As stated in Section 3.1, the attenuation values are referred to the average outdoor RSCP. Equation (3.12) shows the adopted approach for the RSCP attenuation, so that a positive value represents attenuation and a negative one stands for gain. The DL/UL average throughput drop is similar to the RSCP one.

$$\left\{ \begin{array}{l} \overline{\Delta RSCP}^{Floor\ i}_{[dB]} = \overline{RSCP}^{Outdoor}_{[dBm]} - \overline{RSCP}^{Floor\ i}_{[dBm]} \quad , \text{ Floor Attenuation} \\ \overline{\Delta RSCP}^{Rooms\ IW, ID, DI}_{[dB]} = \overline{RSCP}^{Outdoor}_{[dBm]} - \overline{RSCP}^{Rooms\ IW, ID, DI}_{[dBm]} \quad , \text{ Room Attenuation} \end{array} \right. \quad (3.12)$$

where:

- $\overline{RSCP}^{Outdoor}$  is the average RSCP measured in the outdoor;
- $\overline{RSCP}^{Floor\ i}$  is the average RSCP measured indoors in floor  $i$ ;
- $\overline{\Delta RSCP}^{Floor\ i}$  is the average attenuation between the outdoor and indoor values (in floor  $i$ );
- $\overline{RSCP}^{Rooms\ IW, ID, DI}$  is the average RSCP measured indoors in room IW, ID or DI;
- $\overline{\Delta RSCP}^{Rooms\ IW, ID, DI}$  is the average attenuation between the outdoor and indoor values (in room IW, ID or DI).

Concerning throughput variation, the focus is on relative values rather than the absolute ones, giving an estimate of the throughput variation in percentage. This is due to the desire to scale these results to any HSPA+ configuration, since the throughput percentage drop shows the same variation as its absolute values. The average DL/UL throughput drop in percentage is given by (3.13).

$$\left\{ \begin{array}{l} \overline{\Delta R_b}^{Floor\ i} [\%] = \frac{\overline{\Delta R_b}^{Floor\ i} [\text{Mbps}]}{\overline{R_b}^{Outdoor} [\text{Mbps}]} \times 100 \quad , \text{ Floor Reduction} \\ \overline{\Delta R_b}^{Rooms\ IW, ID, DI} [\%] = \frac{\overline{\Delta R_b}^{Rooms\ IW, ID, DI} [\text{Mbps}]}{\overline{R_b}^{Outdoor} [\text{Mbps}]} \times 100 \quad , \text{ Room Reduction} \end{array} \right. \quad (3.13)$$

where:

- $\overline{R_b}^{Outdoor}$  is the average throughput in the outdoor;
- $\overline{\Delta R_b}^{Floor\ i}$  is the average throughput reduction between outdoor and indoor values (in floor  $i$ );
- $\overline{\Delta R_b}^{Rooms\ IW, ID, DI}$  is the average throughput reduction between outdoor and indoor values (in room IW, ID or DI).

Also interesting is the average throughput drop between room types, expressed by:

$$\overline{\Delta R_b}^{room\ types} [\%] = \frac{1}{N_{transitions}} \sum_{i \neq j}^{N_{transitions}} \frac{\overline{\Delta R_b}^{type\ i \rightarrow type\ j} [\text{Mbps}]}{\overline{R_b}^{type\ i} [\text{Mbps}]} \times 100 \quad (3.14)$$

The comparison between simulated and measured results is performed by means of a correlation factor. The correlation coefficient between two random variables X and Y with their respective expected values and standard deviations is given by [Rahm68]:

$$\rho_{corr}(X,Y) = \frac{\sum_{i=1}^n (x_i - \mu_X) \cdot (y_i - \mu_Y)}{\sqrt{\sum_{i=1}^n (x_i - \mu_X)^2 \cdot \sum_{i=1}^n (y_i - \mu_Y)^2}} \quad (3.15)$$

The correlation coefficient assumes a positive unitary value in case of a perfect positive correlation and a negative unitary value in case of negative correlation; the null value indicates total absence of correlation. All in all, the closer the coefficient is to -1 or 1, the stronger the correlation is between the variables. Excel includes a function to calculate the correlation factor therefore all computations are performed using this software.

The average difference of throughput reduction between consecutive floors, defined as the extra reduction going one floor up, is given by:

$$\overline{\Delta R_b^{floor}} = \overline{R_b^{floor(i)}} - \overline{R_b^{floor(i-1)}} \quad (3.16)$$

The throughput reduction can be defined with dependence on signal attenuation, given by:

$$\overline{\Delta R_b [\%]} = \Psi_{[\% \cdot \text{dB}^{-1}]} \times \overline{\Delta RSCP [\text{dB}]} + \zeta_{[\%]} \quad (3.17)$$

where:

- $\Psi$  is the variable part of throughput reduction, depending on signal attenuation;
- $\zeta$  is the static part of throughput reduction, independent of signal attenuation.

For the Multi-User analysis, an indicator was computed to measure the user reduction from outdoor to indoor scenarios:

$$\Delta N_{au} (\%) = \frac{N_{au}^{outdoor} - N_{au}^{indoor}}{N_{au}^{max}} \times 100 \quad (3.18)$$

where:

- $N_{au}^{outdoor}$  is the number of outdoor served users in the cell;
- $N_{au}^{indoor}$  is the number of indoor served users in the cell;
- $N_{au}^{max}$  is the maximum number of served users in the cell (15 for HSPA+ DL).

## 3.5 Simulator Assessment

This section addresses the assessment made to validate the simulator, so that the simulator gives results within a certain degree of confidence. Several parts of the indoor and outdoor models were tested, namely the antenna gain, the outdoor propagation scenarios, the fast fading average value, the losses between room types and the difference between the outdoor and indoor number of served users. Although the first two tests were already performed in [Marq08], new tests were considered in order to test the integration of those functions in the global simulator.

For the antenna gain test, the default radiation pattern, shown in Figure 4.1, was used. Four were placed in the antenna coverage area: the first right below the antenna, the second in the ground floor of a building placed some meters in front of the antenna, the third inside the same building but at the same height as the antenna, and the fourth placed in the same building but at double height of the antenna. The result is the expected one: the first MT has an average gain of -19.23 dBi, because it is positioned below the antenna, where nulls in the radiation pattern can be found; the second MT should have a similar gain as the fourth, since the radiation pattern is symmetrical, which is verified by the output values -9.97 dBi and -12.33 dBi, respectively; and the third MT should have a much higher gain, close to the maximum value (18.1 dBi), which is verified by the output value 15.43 dBi.

For the outdoor propagation scenarios presented in Section 3.1, four tests were performed to ensure the correct functioning of the path loss algorithm. The four tests correspond to the six cases of Figure 3.2, in which the NLoS and the LoS cases were merged for distances lower and greater than 20 m. In the first test, the BS was placed on the top of the MT building, assuring that only the indoor model was called. In the second test, the BS was placed in a building façade with the MT being placed inside the front building, and either (B.3) or (B.1) was used as outdoor models, depending on the distance of the MT (less or more than 20 m, respectively). Concerning cases 2 and 3, these were merged in one single test, by inserting the BS antenna obstructed by the BS building corner, creating a NLoS scenario in the lower floors. This test was also successful: the simulator was able to make the transition from cases 2 to case 3 when LoS was available. The same procedure was made for cases 5 and 6 by inserting an obstacle building that obstructed the signal propagation in the lower floors in the MT building. After performing all these tests, the conclusion was that all path loss models are working properly.

In order to test the fading average values, one should take in consideration the input values. The slow fading is inserted in the simulator as a margin, therefore the average value is the margin itself, which can be seen in the output file. As for the fast fading, it is generated according to its Rayleigh distribution and its mean value is approximately 5 dB. The expression for the theoretical mean value of a Rayleigh distribution is shown in [Corr09], which for the standard deviation given in Table 3.2 gives an average value of 5.01 dB. The theoretical value is very similar to the simulated one, therefore the simulator ensures the correct calculation of the fading output values.

After testing the outdoor variables, the indoor model needs to be assessed too. Starting by testing the losses between room types, the test comprehends a Low Isolated building with a MIMO antenna configuration scheme. In the outdoors the average RSCP was -82.75 dBm and the average DL throughput was 33.63 Mbps; for the Indoor Window room the average RSCP on all building floors was -83.25 dBm and the average DL throughput was 28.06 Mbps; for the Indoor Daylight room the average RSCP on all building floors was -91.25 dBm and the average DL throughput was 21.14 Mbps; for the Deep Indoor room the average RSCP on all building floors was -93.27 dBm and the average DL throughput was 19.52 Mbps. These results show the correct functioning of the indoor loss model, since an inner room has lower average signal power and throughput than the outer one.

The capacity model must be assessed too. Since most of the parts of the capacity model are used in the Single-User model, there is only the need to assess the output of the Multi-User simulator. The most important aspect is the average difference between the outdoor and indoor number of served users, which must be greater or equal to zero. In fact, all results show that the average difference between the number of outdoor and indoor users is always non-negative, mostly because the average indoor room losses are always positive. Another important aspect is the decreasing variation of served users with the increase of the desired data rate, which was verified in every simulation output.

Only DL was considered in the assessment; UL was not assessed, since the link is similar to the DL one, despite the differences in frequency bands, noise figure and the SINR-throughput correspondence, which was already assessed in previous works. Nevertheless several debug sessions were performed to accurate the results.

Due to the simplicity of the simulation procedure, the number of simulations can be high without reducing the simulation performance. Therefore, the number of simulations was set to 1000 runs for each floor in the Single-User implementation, and 1000 runs for each data rate value in the Multi-User implementation, ensuring statistical significance for the random variables.

# Chapter 4

## Results Analysis

In the first part of the chapter, a general description of the measured and simulated scenarios is given. In the second part, the measurement campaign is reviewed, giving an overview of the adopted measurement procedure and the measurements results, taking the building and floor characterisations for each of the scenarios into account. In the third part, several simulations are performed: firstly, the simulated results are compared with the measured ones for similar propagation scenarios, and then different urban scenarios are simulated and its results are analysed.

## 4.1 Scenarios Description

The scenario for all evaluations is a pedestrian environment, considering an almost static user at the street level (3 km/h as defined in ITU Pedestrian A channel). This environment is situated in urban cells, with the associated fading margins considered in Table 3.2. This scenario accounts for Isolated and Integrated buildings, Figure 3.3, with their height assuming values in the recommendations of COST231-WI, Annex B. In order to fit better with the city of Lisbon's characteristics (where the measurements were made), the lack of very high buildings forced the reduction of the building height range to [4, 36] m. Although the outdoor scenario is defined, it only serves the purpose of establishing a reference outdoor throughput value. The MT is set inside the studied building, both in Single and Multi-User analyses. The indoor scenarios comprehend all the available room types in Figure 3.4.

Two types of analysis are performed in this chapter: in the first part, the measurement campaign results are overviewed, while in the second part, the measurement results are compared with the simulation results for a reference urban scenario. Later, several simulations are performed and their results analysed, using a reference urban scenario and then changing some parameters. Both single and Multi-User models are simulated: the Single-User scenario considers that there is only one user in the cell, therefore all available resources are dedicated to this user, whereas in the multiple users scenarios one considers that users are uniformly distributed up to a certain radius, performing different services with different associated throughputs.

Three important outputs of the measurement campaign arise: firstly, the signal attenuation model extraction allows the creation of the proposed indoor model in Subsection 3.1.2; secondly, the modulation usage defines the system probability of using a certain modulation, depending on the building and room type; lastly, the measured DL/UL throughputs allow a throughput reduction comparison with the Single-User model output, being possible to assess the model with real results.

The measurement campaign was performed in the city of Lisbon. The selected spots were the buildings inside the IST campus, such as Pavilhão Central, Pavilhão Interdisciplinar, Pavilhão Civil, Torre Norte and Torre Sul, and three other buildings in dense urban areas of the city, namely Anjos, Avenida da República and Rua Castilho. These scenarios are highly representative of the different urban scenarios, and fit the different building types represented in Figure 3.3.

In order to characterise the measured buildings, several parameters are taken into account, such as the number of floors, the proximity to other buildings, and the position of the building in relation to the BS. The first three buildings (Anjos, Avenida da República e Rua Castilho) are inserted between other two buildings in highly dense streets, therefore being classified as High Integrated. Both Torre Norte and Torre Sul are 11-floor high buildings, the campus being composed of low buildings, resulting in High Isolated buildings. As for Pavilhão Civil and Pavilhão Central, these low buildings are located in areas without any surrounding ones that may cause the loss of LoS, therefore being Low Isolated buildings. Concerning Pavilhão Interdisciplinar and Pavilhão de Matemática buildings, both are

integrated between themselves, and therefore are Low Integrated buildings. A brief characterisation of the measured buildings is presented in Table 4.1.

Table 4.1. Measured buildings' characteristics.

| Building Type   | Building                  | Total number of floors | Measured floors                  | Number of measured rooms |    |    |
|-----------------|---------------------------|------------------------|----------------------------------|--------------------------|----|----|
|                 |                           |                        |                                  | IW                       | ID | DI |
| High Integrated | Anjos                     | 8                      | 0, 1, 3, 4, 5, 6, 7              | 7                        | 13 | 0  |
|                 | Avenida da República      | 10                     | 0, 3, 5, 6, 7, 8, 9              | 20                       | 13 | 0  |
|                 | Rua Castilho              | 11                     | 0, 1, 2, 3, 4, 5, 6, 7, 8, 9, 10 | 15                       | 14 | 0  |
| High Isolated   | Torre Norte               | 12                     | 0, 4, 5, 6, 7, 8, 9, 10, 11      | 25                       | 8  | 16 |
|                 | Torre Sul                 | 12                     | 0, 2, 4, 5, 6, 7, 8, 9, 10, 11   | 26                       | 8  | 16 |
| Low Integrated  | Pavilhão de Matemática    | 5                      | 0, 1, 2, 3, 4                    | 15                       | 4  | 6  |
|                 | Pavilhão Interdisciplinar | 4                      | 0, 1, 2                          | 9                        | 3  | 0  |
| Low Isolated    | Pavilhão Central          | 2                      | 0, 1                             | 8                        | 2  | 0  |
|                 | Pavilhão Civil            | 4                      | 0, 1, 2, 3                       | 4                        | 12 | 4  |

The number of measured rooms is quite variable due to permission restrictions, since some rooms were not accessible for the measuring procedure, being left out of the analysis. Only rooms presenting more than 100 samples are considered in the present study, in order to guarantee statistical significance. For all available rooms, the number of collected samples was between 120 and 150, corresponding to 4 to 5 minutes of data collection.

Concerning outdoor measurement types, the single façade option was applied to all buildings, Figure 4.4. This is due to the desire to acquire the signal from a single BS, avoiding handovers during measurements. Only with this configuration the purpose of this work is ensured: analysing the influence of indoor penetration between a single BS and the MT.

Measured results are compared with simulated ones in Subsection 4.3.1 in order to evaluate the simulator. In Subsection 4.3.2, different urban scenarios are simulated, accounting for a variation of the outdoor configuration between BS and MT, Figure 3.2, the indoor desired coverage and both room and building type. For the purpose of the different analyses, a reference simulation scenario is created. It considers a MT average distance to the BS in a dense urban area [Voda11], approximately 120 m, with an obstacle building between them. The adopted antenna configuration scheme is SISO and the building coverage is 50 %, Table 4.2. The antenna height is set to 2 m above a 5-floor building, representing the average height of the buildings analysed in the reference scenario (with the exception of case 4 where the antenna is on the building façade). All presented values belong to the recommended values of COST231-WI in a typical urban situation, which is described in Annex B.

The urban scenarios presented in Subsection 3.1.1 were proposed for an extensive throughput reduction analysis. Case 1 in Figure 3.2 was excluded from the simulation set, since it does not

comply with reality: the signal does not go through building floors, but instead it is reflected in the surrounding buildings and penetrates building walls, degenerating in cases 2, 3 or 4. Therefore, the case 1 signal attenuation model was not available, since the required measurement procedure was not performed. For the remaining case scenarios, the simulations on cases 2, 3 and 4 were performed with 95 % building coverage due to the short distance to the BS. Otherwise, the analyses would be inconclusive, since at such short distance (less than 20 m) SINR is high enough to obtain a saturated throughput, which does not evidence the throughput variation along the floors/rooms. Concerning cases 5 and 6, a different approach is taken, in which different distances between the BS and MT are tested in order to understand the throughput variation along the cell. The respective parameters for all simulated scenarios are shown in Table 4.2.

Table 4.2. Outdoor model parameters for simulations in each case scenario.

| Path Loss Case          | 2  | 3  | 4  | 5  | 6<br>(Reference) | 6   |
|-------------------------|----|----|----|----|------------------|-----|
| Coverage [%]            | 50 | 50 | 50 | 50 | 50, 90, 95       | 50  |
| Outdoor Distance [m]    | 18 | 18 | 18 | 30 | 120              | 250 |
| Building separation [m] | 36 | 36 | 36 | 60 | 80               | 100 |
| Street width [m]        | 34 | 30 | 30 | 50 | 60               | 70  |
| Number of obstacles     | 0  | 0  | 0  | 0  | 1                | 2   |
| Antenna height [m]      | 17 | 17 | 10 | 17 | 17               | 17  |
| BS building height [m]  | 15 | 15 | 15 | 15 | 15               | 15  |

The general characteristics of the simulated scenario are described in Table 4.3, which were used in both measurement comparison and urban scenarios simulations. Most of the reference values were extracted from [Jaci09] and [Corr09] or explained in the previous chapter.

Table 4.3. Reference parameters for all simulation scenarios.

|                           |                       |                          |      |          |
|---------------------------|-----------------------|--------------------------|------|----------|
| <b>Outdoor Parameters</b> | Fast Fading           | Standard Deviation [dB]  |      | 4        |
|                           | Slow Fading           | Margin [dB]              |      | 7.6      |
|                           | BS                    | Transmission Power [dBm] |      | 42.48    |
|                           |                       | Radiation Pattern        |      | P7755.00 |
|                           | Mobile Equipment      | Transmission Power [dBm] |      | 23.29    |
|                           |                       | Antenna Gain [dBi]       |      | 1        |
|                           | Noise Figure [dB]     | DL                       | 9    |          |
|                           |                       | UL                       | 5    |          |
|                           | User Body Losses [dB] | 1                        |      |          |
|                           | Cable Losses [dB]     | 2                        |      |          |
|                           | Frequency [MHz]       | DL                       | 2110 |          |
|                           |                       | UL                       | 1920 |          |
|                           | BS Antenna Tilt [deg] | -5                       |      |          |

The real BS radiation pattern is not known, therefore P7755.00 was chosen [Kath11], the same as selected in [Marq08], since it is the most common one on the network under analysis. Its radiation pattern is shown in Figure 4.1, the vertical pattern (in red) being the one used in this work. Its maximum gain is 18 dBi, with a vertical 6° half power beam width. To compensate the uncertainty in the BS antenna tilt, a five degrees variation was inserted in the antenna tilt and the average gain was applied in the SNR calculation.

The MT antenna gain was set to 1 dBi, since it only performs data services. The BS transmission power depends on the equipment, but a generic 44.7 dBm macro-cell equipment was defined for this simulator [Telm08]. Since in HSPA+ 40 % of the total transmitter power is for control and signalling [Jaci09], the available power for data services is 42.48 dBm. For UL, the typical MT transmitter power is 24 dBm, although the 15 % usage for signalling and control [Jaci09] reduces the maximum available power to 23.29 dBm. The antenna efficiency is also affected by the losses, due to the human body, the common margin being set to 1 dB. Feeders, connectors and all external equipment between the antenna and the BS receiver also introduce a loss, considered to be 2 dB.

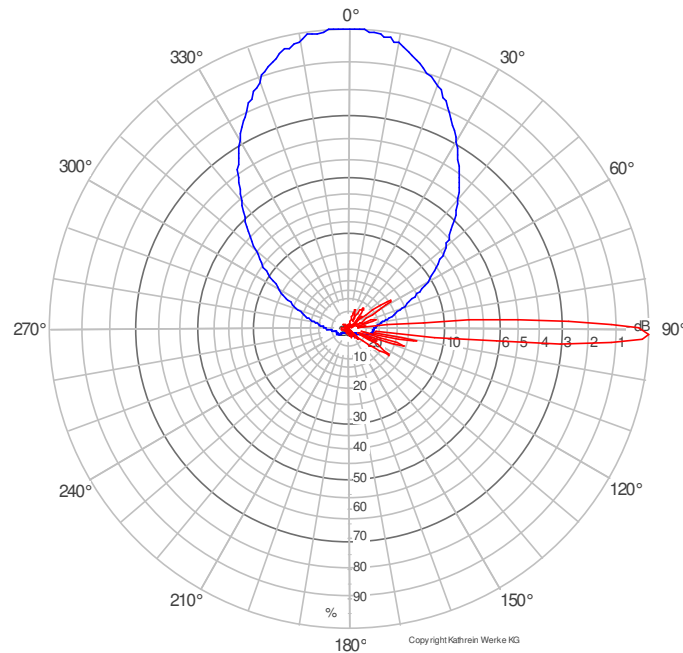


Figure 4.1. Horizontal (blue) and vertical (red) radiation pattern for the P7755.00 antenna [Kath11].

## 4.2 Measurements

Measurements in indoor environments were made in order to develop the transmission model. Through the measurements in different building scenarios, a set of values could be extracted as parameters in the indoor model, namely wall and floor signal attenuations. As for the measured throughput attenuations, those are to be compared with the theoretical model results in Section 4.3. Creating diversity in the type of building scenarios allows for a more comprehensive analysis and therefore a more realistic model.

## 4.2.1 Procedure

All measurements were made with equipment provided by Vodafone Portugal. The measurement set is composed by one MT (Huawei K4505 USB Stick), one USB cable, one laptop and a cart. In order to avoid undesired attenuation, the cart is made of plastic. The measurement equipment was placed 1.5 m above floor level. Figure 4.2 shows all equipment used in the measurements.



Figure 4.2. Measurements set (laptop, cart and USB stick).

The available measurement software was TEMS Investigation 11.0 [Asco11], which allows measuring and monitoring the air interface of mobile networks. More information, such as user interface, system and equipment specifications, can be found in [Asco11].

Besides measuring the signal power, commonly designated as Received Signal Code Power (RSCP), the physical layer throughput was also measured, in order to evaluate its variation along the building and across the several floors. Both values were extracted from the software log files. For most of the sites, it was possible to measure both DL and UL throughputs, but in Anjos the DL/UL throughput was not measured at all and in Rua Castilho only DL throughput was measured (through a FTP server), because the testing software was yet not fully mastered by the author.

DL and UL throughputs testing software was TPTTest 3.1 [TPTe11], which uses TCP/UDP servers spread around Stockholm, Sweden, to test the data transmission rate. For the measurements in this work, only UDP was used, because it allows a more realistic approach in terms of data rate, since UDP does not include retransmissions and slow start procedure.

The adopted measurement procedure was based on [XaVe02], being described in Figure 4.3 and consisting of two distinct stages. On the first stage, the cart was displaced along the accessible outside building façades, although in integrated building some of the façades were not accessible for measurements. When possible, outside measurements were taken on both sides of the street, with the mean values of both sides of the street providing a good estimation of the mean power in the middle of the street. In these cases, the reference value for each BS is given by:

$$P_{ref}^{ext} [dBm] = \frac{P_{adj} [dBm] + P_{opp} [dBm]}{N_{adj} + N_{opp}} \quad (4.1)$$

with:

- $P_{adj}$  is the sum of the power samples collected in the adjacent street side pavement.
- $P_{opp}$  is the sum of power samples collected in the opposite street side pavement.
- $N_{adj}$  is the number of samples collected in the adjacent street side pavement.
- $N_{opp}$  is the number of samples collected in the opposite street side pavement.

In the cases where only the adjacent pavements could be measured, the external power is:

$$P_{ref}^{ext} [dBm] = \frac{P_{adj} [dBm]}{N_{adj}} \quad (4.2)$$

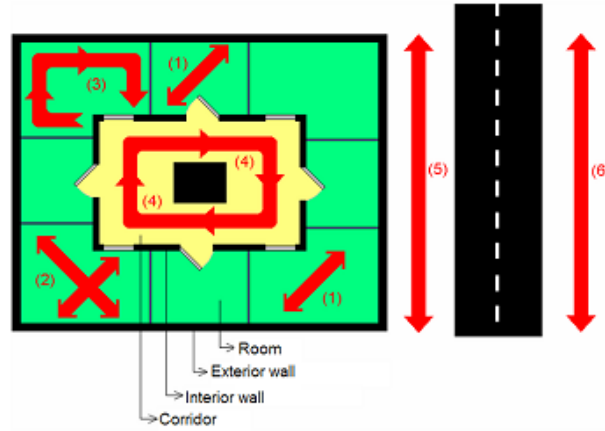


Figure 4.3. Indoor and outdoor measurement process (adapted from [XaVe02]).

The second stage consisted of measuring the signal inside buildings, namely in rooms, followed whenever possible an “X” trajectory (marked (2) in Figure 4.3), although in most cases, due to the room’s furniture or geometry, alternative trajectories (marked (1), (3) and (4) in Figure 4.3) had to be followed. The cart was pushed (manually) along the measuring places with a speed around 0.05 m/s. The criterion to choose/reject the measurements of a BS is the number of collected samples for that BS, being considered that there was no statistical relevance if less than 100 samples were collected. The indoor attenuation,  $L_{P_{int}}$ , is given by:

$$L_{P_{int}} [dBm] = P_{ref}^{ext} [dBm] - P_{int} [dBm] \quad (4.3)$$

where  $P^{int}$  is the power of the signal of a certain BS measured in a specific room of the building.

It can be seen in Figure 4.4 that the measurement of the reference level outdoors may follow different configurations. The type of configuration has a considerable influence on the reference level. Ideally, the best would be the square measurement. Nevertheless, when buildings are integrated, this is not possible. An integrated building can typically only be measured at one façade, or at another potentially

existing one, such as an interior courtyard, which may not be accessible for measurements. Nevertheless, this non accessible façade has rooms with windows, where some BSs signals can be received at levels higher than on the street, depending on the position of the measured BS. This introduces a large dependency on the configuration, a large number of measured BS and measurements, being needed to avoid dependence of results on this phenomenon.

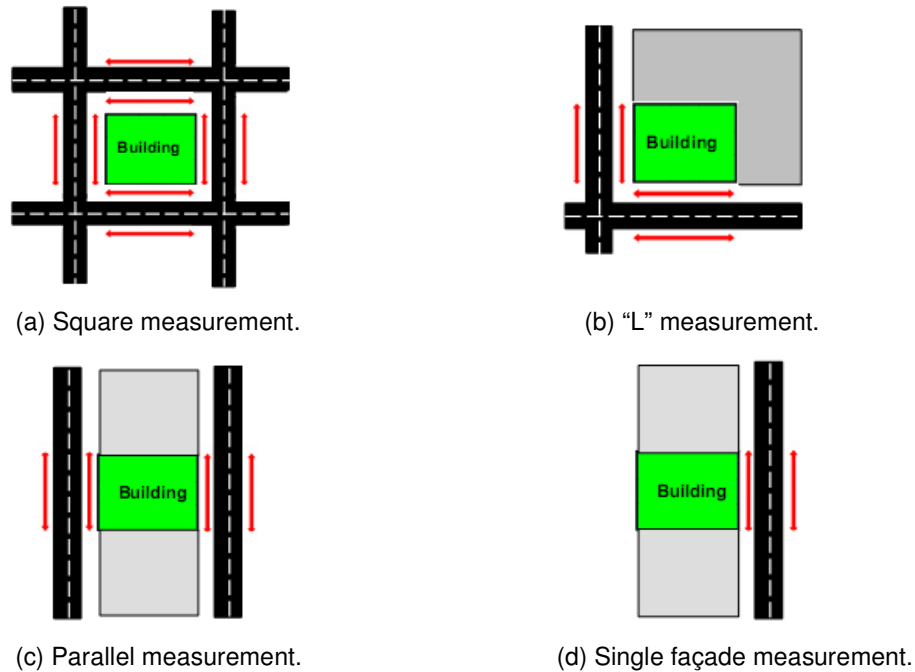


Figure 4.4. Types of outdoor measurements of the reference signal level of each BS, depending on the accessible façades.

## 4.2.2 Results

In this Section measurement results are discussed. For each of the measured buildings, results are analysed in the user's perspective, i.e., the analysis is performed not taking into account the network load and the scheduler's options, such as the modulation, the TTI and the number of codes given to the user.

The results obtained during the measurement campaign were processed statistically. The existing figures and tables were produced by Excel, extracting the information from the output log files from TEMS Investigation. The criteria for determining the loss between walls and floors was the average value measured in each building, since there is a great variability in the measured values due to the specific conditions in each floor/wall. Not only was the average value presented, but also the standard deviation in order to understand the more or less precision of the measured values.

In order to estimate the difference between the measured values of two consecutive floors/rooms, it was assumed that the distribution of the measured values follows a normal distribution, given the high

number of measured values. Nevertheless, this assumption is tested in Annex H. Given this, the difference between the two floors/rooms is given by a normal distribution, with an average value given by the difference between the average values of the two floors/rooms distributions, and the standard deviation being the sum of the two standard deviations from each floor/room distribution.

For each building, the average DL/UL throughput and RSCP values are calculated, computing the arithmetic mean value of all the average values for each floor/room, according to (3.10), and the standard deviation quadratic mean value for each floor/room, according to (3.11).

A comprehensive study of the measurement results for each building is performed in Annex F. Several analyses are performed:

- Attenuation values and trend curves for each building type, considering the received signal power (RSCP) and the DL/UL throughputs losses;
- DL modulation usage, in percentage, for each building type;
- SIR mapping onto DL throughput.

After this analysis, the RSCP attenuation values and the DL modulation usage are inserted in the indoor model implementation, using (3.2) and (3.3). The UL modulation usage is based on the DL one, although not considering the usage of 64QAM. Table 4.4 shows the mean and standard deviation attenuation for each building type. As for the DL modulation usage, Figure F.16, Figure F.17, Figure F.18 and Figure F.19 show the usage values (in percentage) for each building type.

For each equation, the  $\rho_{corr}$  value is presented, (3.15). As expected, the goodness-of-fit is not high due to the linear model choice. One should notice that each  $\mu^{var}$  value needs to be negative, since the signal power suffers a gain when moving upper in the building. Most of the presented models were extracted from [SLCM05] due to three reasons:

- The room type was not available in the measured set;
- The results showed growing attenuation trend, which is contrary to the expected trend since the signal power is higher when LoS increases;
- The comparison between room types show inconsistent results, i.e., the average attenuation should be increasingly higher when going inner inside the building.

Table 4.4. Model parameters for the signal attenuation due to building penetration.

| Building Type | Room Type       |               |                    |               |                 |               |                    |               |                 |               |                    |               |
|---------------|-----------------|---------------|--------------------|---------------|-----------------|---------------|--------------------|---------------|-----------------|---------------|--------------------|---------------|
|               | Indoor Window   |               |                    |               | Indoor Daylight |               |                    |               | Deep Indoor     |               |                    |               |
|               | $\mu^{IW}$ [dB] |               | $\sigma^{IW}$ [dB] | $\rho_{corr}$ | $\mu^{ID}$ [dB] |               | $\sigma^{IW}$ [dB] | $\rho_{corr}$ | $\mu^{DI}$ [dB] |               | $\sigma^{DI}$ [dB] | $\rho_{corr}$ |
|               | $\mu^{var}$     | $\mu^{level}$ |                    |               | $\mu^{var}$     | $\mu^{level}$ |                    |               | $\mu^{var}$     | $\mu^{level}$ |                    |               |
| <b>HInt</b>   | -2.37           | 15.19         | 9.4                | 0.97          | -2.89           | 21.08         | 9.3                | 0.94          | -3.19           | 28.63         | 9.4                | -             |
| <b>HIso</b>   | -0.56           | 4.55          | 15.7               | 0.58          | -0.92           | 10.43         | 15.4               | 0.74          | -0.79           | 14.92         | 11.5               | 0.81          |
| <b>LInt</b>   | -1.98           | 13.79         | 5.2                | 0.44          | -4.42           | 20.68         | 12.9               | 0.81          | -5.97           | 26.59         | 11.5               | 0.92          |
| <b>LIso</b>   | -0.94           | 11.62         | 11.2               | 0.75          | -0.06           | 11.2          | 9.0                | 0.02          | -0.07           | 15.21         | 10.2               | -             |

With these requirements, the measured rooms included in the model were High Isolated's IW and ID rooms and Low Integrated's IW rooms. The rest was extracted from [SLCM05], fulfilling the requirements. A particular note goes to the ID room values in Low buildings, which show a poor  $\rho_{corr}$  value, and therefore should be analysed with caution: because the Deep Indoor rooms' trend line in High Integrated and Low Isolated buildings was not available in both this work's measurement set and [SLCM05], two models were extrapolated taking into account the variations in the available buildings. Despite this, these models should also be taken into account with caution. Annex I shows the validation of the results extracted from [SLCM05].

The measured RSCP is referred to the DL channel, although it is considered to be roughly the same in the UL. This assumption is based on the proximity of the two different frequencies on the radiofrequency spectrum and the frequency independence of the indoor materials. In fact, computing the difference in path loss between the two frequencies, considering free space propagation (B.1), shows a value of approximately 0.82 dB. This ensures a correct application of this assumption, since the error is lower than 1 dB, even in the worst propagation scenario for frequency variation – the LoS case.

As stated before, the signal power (RSCP) and the DL and UL physical throughputs were measured in most of the buildings. Concerning DL throughput, its sensitiveness to the number of codes given by the BS scheduler is noticeable, and therefore this is not taken into account, since the results are to be analysed in the user's perspective. As for UL, it is very sensitive to the TTI value given by the BS scheduler and, similarly to the DL, it is not taken into account.

Another important point is the incapability of the software equipment to lock the desired BS. Therefore, measurements from several rooms were left out of the analysis, because of the undesired handovers to other BSs.

Concerning throughput, its analysis is not only greatly dependent on the signal power, but also on the adopted modulation and the network load, which might not be constant, showing a greater variability than the RSCP. Therefore, a cautious analysis is required, since throughput might be variable for the same channel conditions. Specifically in the UL throughput, it is dependent not only on the modulation but also on the chosen TTI, which affect greatly the available physical throughput. The measurements on UL show that a TTI of 2 ms can achieve a maximum physical throughput of 4.297 Mbps whereas a TTI of 10 ms can only achieve a maximum physical throughput of 1.448 Mbps, values that are in accordance with the maximum theoretical ones in category 6 of Table C.2. 16QAM is not used in this category, therefore one cannot test the full potentialities of HSPA+ UL.

## 4.3 Simulations

In this section, simulation results are presented. In the first part, simulation and measured results are compared; in the second part, several representative urban scenarios are simulated and analysed.

### 4.3.1 Comparison with Model Results

In order to evaluate the simulator, several scenarios based on the measurements environments are created. One should take in consideration that the analysis is done mostly comparing the curves variation and not their absolute value, since the latter is due to the outdoor model itself, which is not the main scope of this work. The outdoor model is responsible by defining the path loss between the BS and the MT at the centre of the street, which is defined by parameters that are unknown and specific for each scenario, such as fading distributions, antenna tilt, and so on. More specifically concerning throughput, it is variable with the number of codes given to the user and the instantaneous network load. All these factors affect the magnitude of the RSCP/throughput to be analysed, therefore, these comparisons only consider the throughput reduction trend between the measured room types, and not their actual values. Furthermore, these actual values' analysis is performed for the same reference scenario in Subsection 4.3.2.

The compared throughputs may also differ: in the simulation a maximum of 21.6 Mbps were available, considering a SISO scheme on a HSPA+ implementation, since the measurements were made with equipment prepared for a theoretical maximum of 21.6 Mbps. Despite the eventual difference in the throughput values, the chosen approach is to consider only the variations and not the absolute values, similarly to the RSCP one.

A typical urban scenario is chosen for all simulations, as described in Section 4.1. In order to be compared with the measurements results, the simulation is run with 50 % building coverage, therefore the results represent the median attenuation in each case. Each comparison is followed by the corresponding correlation factor, as defined in (3.15). This complements the qualitative analysis with a quantitative one.

The next analysis is the average throughput reduction per room type. As described in Section 3.4, the mean and standard deviation reductions are calculated for each room type, taking the average floor value into account, according to (3.10) and (3.11). Since it is possible to define average attenuations for each room type, based on the results shown in Table 4.4, the following figures are presented showing the correlation between the throughput reduction and the signal attenuation.

Regarding High Integrated buildings, the available data suggests a growing throughput reduction with the number of penetrated walls in both simulated and measured results, showing an average reduction between room types, (3.14), of 15.20 % and 16.51 % for DL and UL, respectively. DL results are shown in Figure 4.5.a), although only IW and ID rooms were measured; for UL only IW rooms

were measured, Figure 4.5.b). Although the same reduction trend can be found, the measurements show a DL/UL throughput increase in IW rooms, whereas the simulation accounts for reduction. Since the measured and simulated sets do not have the same dimension, the correlation factor cannot be computed (even excluding DI rooms in DL, the set is too small to have a mathematical meaning).

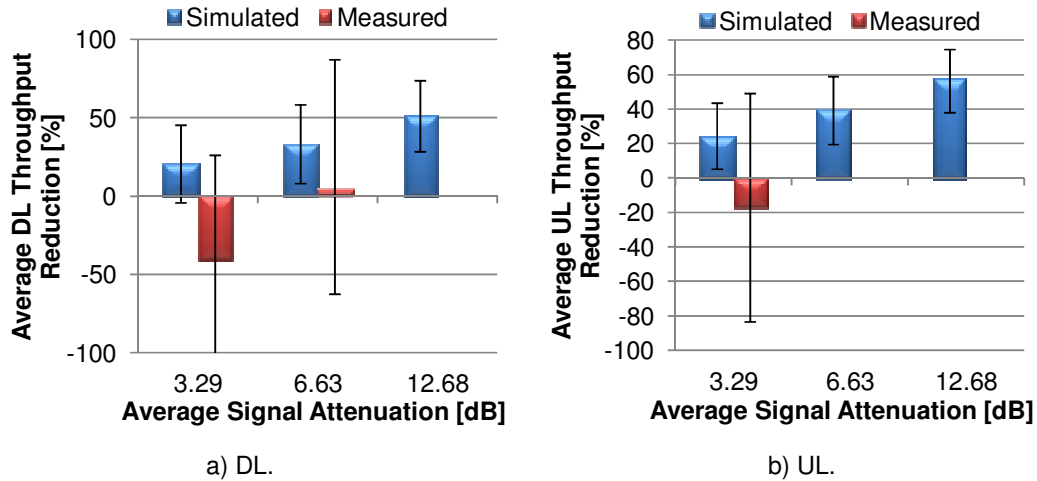


Figure 4.5. Mean throughput reductions comparison for High Integrated buildings.

Regarding High Isolated buildings, the available data also suggests a growing reduction with the number of penetrated walls in DL in both simulated and measured results, with an average reduction between room types, (3.14), of 16.07 % and 4.07 %, respectively, Figure 4.6.a). In UL, the same trend can be found, being the average reduction between room types 26.04 % for simulated and 21.43 % for measured results, Figure 4.6.b). Although the measurements show a throughput increase, the simulation accounts for reduction. This might be due to a TTI change in the measurement procedure (the outdoor measurement might have with a higher TTI, resulting in lower throughput). Both sets have good correlation factors, namely 0.847 for DL and 0.915 for UL, confirming the good trend approximation.

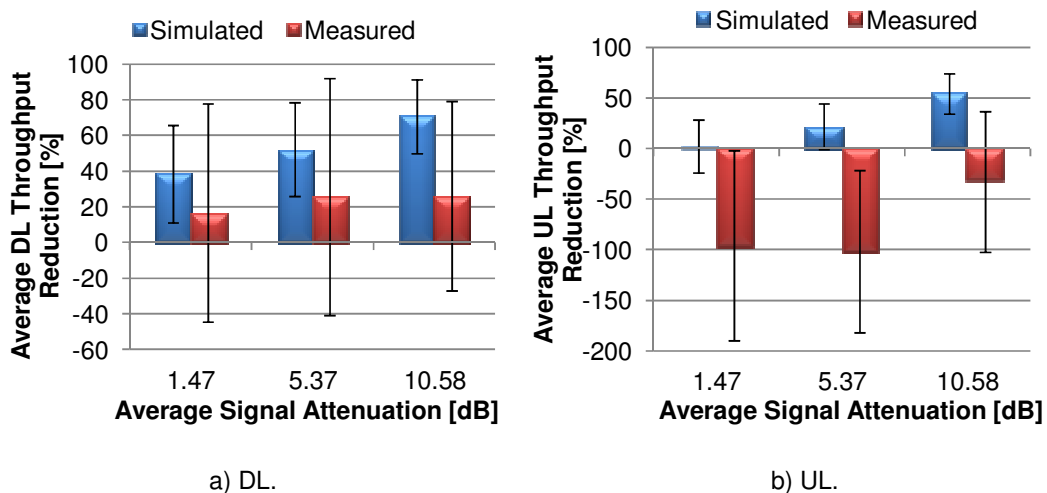


Figure 4.6. Mean throughput reductions comparison for High Isolated buildings.

Regarding Low Integrated buildings, the available data also suggests a growing reduction with the number of penetrated walls in both simulated and measured results, although the measured DI does not follow the trend in DL and UL, Figure 4.7. The simulated and measured average DL reductions between room types, (3.14), are 7.44 % and 5.17 %, respectively. Specifically in UL, the measurements show a throughput increase, whereas the simulation accounts for reduction, Figure 4.7.b). Again, this might be due to a TTI change in the measurement procedure. The reduction values in UL are 7.58 % and 3.29 %, for simulated and measured results, respectively. The strange behaviour in DI rooms might be due the difficulty in finding a correct room for that classification in this type of building, resulting in poor correlation factors: 0.504 for DL and 0.308 for UL.

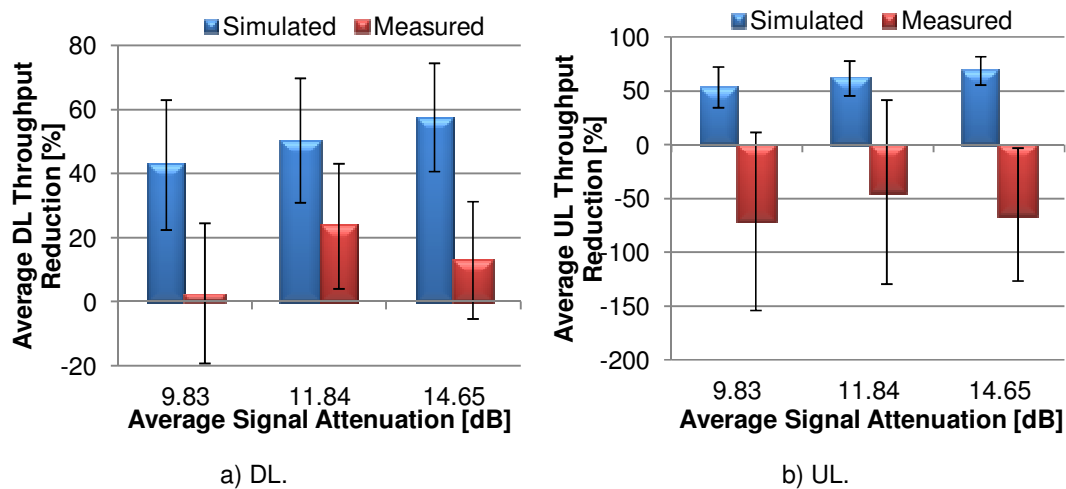


Figure 4.7. Mean throughput reductions comparison for Low Integrated buildings.

Lastly, for Low Isolated buildings, a similar behaviour to the previous analyses can be found. As it can be seen in Figure 4.8, the simulated results show a growing reduction for the inner rooms, for both DL and UL. The same trend can be seen in measured DL results, whereas in UL the trend is inverted, possibly due to specific propagation conditions or TTI change during the measurement procedure. The similar behaviour in DL results in a very good correlation factor, 0.999, whereas the inverted trend in UL shows an undesired correlation factor of -0.982. The simulated and measured average DL reductions between room types, (3.14), are 15.18 % and 6.38 %, respectively; in UL, these values are 23.13 % and -8.94 %, respectively.

A common fact on these comparisons is the higher standard deviation in the measured results than in the simulated ones. This indicates a greater variability of the measured results, which is in accordance with the stated conclusions in Subsection 4.2.2: its analysis is not only greatly dependent on the signal power, but also on the adopted modulation and the network load, which might not be constant.

Moreover, the difference between the average values is within the standard deviations' range, which lowers the degree of confidence when defining a trend line for both measured and simulated results. This is particularly critical in the measured ones, due to the even greater standard deviations. Regarding the simulated ones, the high standard deviations presented for the signal attenuation

model, Table 4.4, as well as the influence of fading margins, result in high standard deviations in the throughput reduction.

In the majority of cases, DL throughput simulated values are closer to the measured results than the UL ones. As stated earlier, the UL throughput accounts for another issue: the TTI variation may distort the results since the maximum available throughput changes.

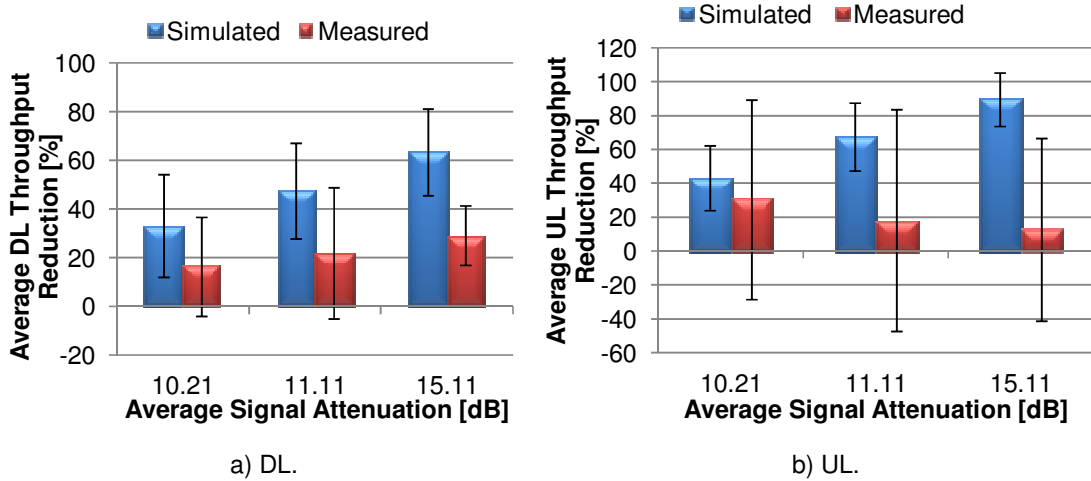


Figure 4.8. Mean throughput reductions comparison for Low Isolated buildings.

The correlation between throughput reduction and signal attenuation is shown in Table 4.5 for all building types, through (3.17). These results were obtained using a trend line for each building type, considering both simulated and measured results. The simulated results show very good correlation coefficients, whereas the measured ones show poor correlation, particularly in UL, due to the reasons stated in Subsection 4.2.2.

Table 4.5. Correlation between throughput reduction and signal attenuation for all building types.

| Building Type | DL                           |               |                              |               | UL                           |               |                              |               |
|---------------|------------------------------|---------------|------------------------------|---------------|------------------------------|---------------|------------------------------|---------------|
|               | Simulated                    |               | Measured                     |               | Simulated                    |               | Measured                     |               |
|               | $\Psi$ [%·dB <sup>-1</sup> ] | $\rho_{corr}$ |
| HInt          | 3.20                         | 0.998         | 13.33                        | 1.000         | 3.46                         | 0.996         | -                            | -             |
| HIso          | 3.53                         | 1.000         | 0.98                         | 0.848         | 5.75                         | 0.998         | 7.25                         | 0.866         |
| LInt          | 3.06                         | 0.994         | 1.77                         | 0.409         | 3.09                         | 0.985         | 0.81                         | 0.138         |
| LIso          | 5.53                         | 0.950         | 2.35                         | 0.960         | 8.23                         | 0.927         | -2.95                        | 0.840         |
| Average       | 3.83                         | 0.986         | 4.61                         | 0.804         | 5.13                         | 0.977         | 1.70                         | 0.461         |

### 4.3.2 Urban Scenarios Simulations

In this section, different urban scenarios are tested, changing both indoor and outdoor parameters, such as the outdoor configuration between BS and MT, Figure 3.2, the indoor desired coverage and both room and building types. Different analyses are performed in order to evidence the parameter changes. Only DL and UL throughputs are analysed, since previous works have already produced

signal power attenuations analysis.

The following results are analysed taking evidence of the most relevant facts in each analysis. Small changes in throughput variation may be due to the used signal attenuation model, which varies according to the building and room type.

For the reference scenario, the floor analysis is performed, Figure 4.9 for DL and Figure 4.10 for UL, as well as the room analysis, Figure 4.13. The floor throughput reduction analysis includes the average building attenuation comparison, taking the mean values of all available room types. The standard deviation is computed by (3.11), taking into account the standard deviation associated with the simulation in each floor (for the floor analysis) and room (for the room analysis).

One can notice the increasing DL throughput trend as the MT moves upper inside the building in Integrated buildings, whereas in Isolated cases the opposite occurs: the interference power in the Isolated buildings is increasingly higher in the upper floors due to LoS, forcing SINR and throughput reduction. Integrated buildings show a greater DL throughput reduction in the first floors, which is coherent with the absence of LoS and therefore a lower available received signal power. Concerning the standard deviation values, it is noticeable that the greater the throughput is, the lower standard deviation is obtained. This is due to the greater throughput variation for higher throughputs, as shown in Figure 2.3.

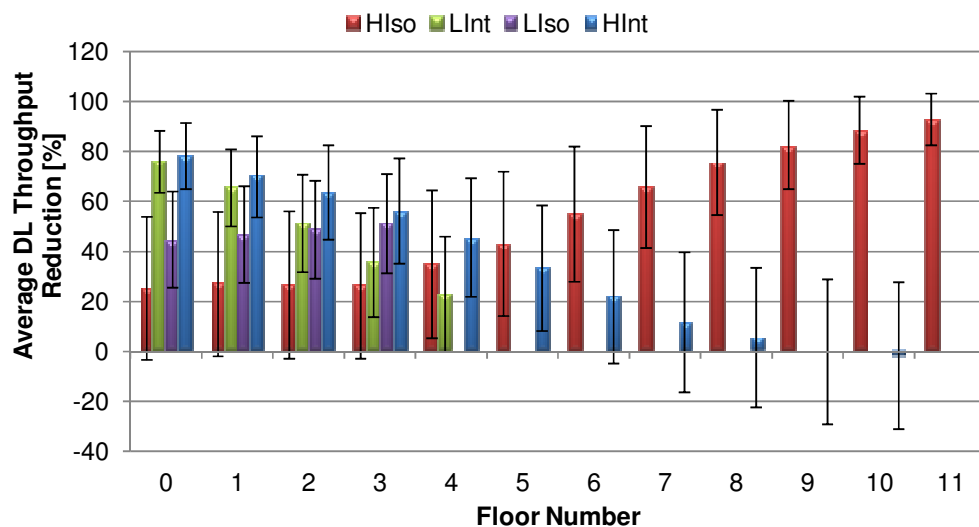


Figure 4.9. Average DL throughput reduction along the simulated building floors.

In UL, the same decreasing trend can be found, including for the Isolated buildings. The interference model presented in (3.4) shows a lower interference power in UL, which does not greatly influence the available SINR. A particular note must be addressed to the Low Isolated building throughput reduction: the model is a product of the measurement campaign and shows low fidelity (as seen in Subsection 4.2.2), therefore its results must be analysed carefully. In UL, one can notice the low slope compared to the other building types', being the reduction almost insensitive to the MT height inside

the building – this might be due to the low number of available rooms for measurements, Table 4.1. Again, Integrated buildings show the highest reductions, mostly in lower floors, where diffraction is responsible for great signal attenuation.

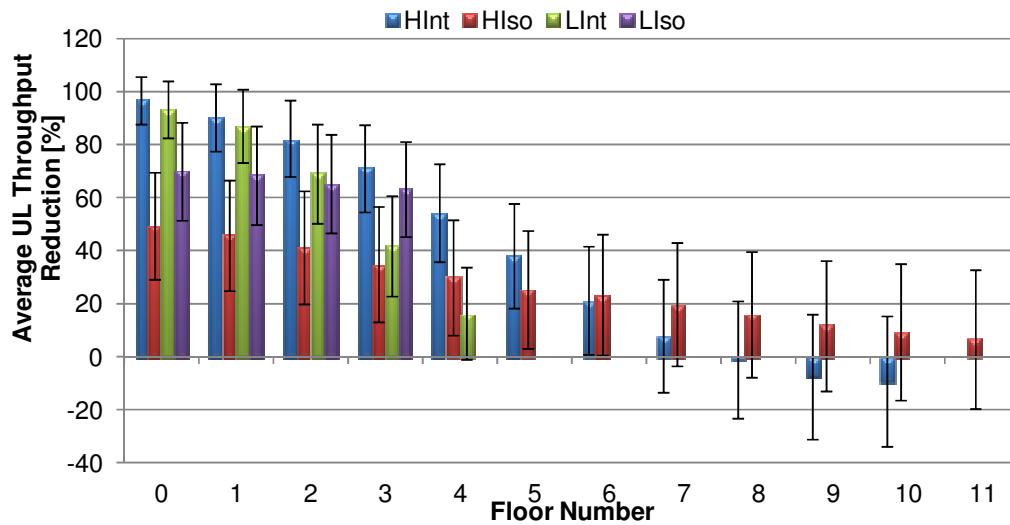


Figure 4.10. Average UL throughput reduction along the simulated building floors.

The average throughput reduction for the simulated building floors and the respective trend lines are presented in Figure 4.11 for DL and Figure 4.12 for UL. The correlation coefficients for each pair of curves are presented in Table 4.6. One can notice the high correlation factors, which allows a good trend linearization.

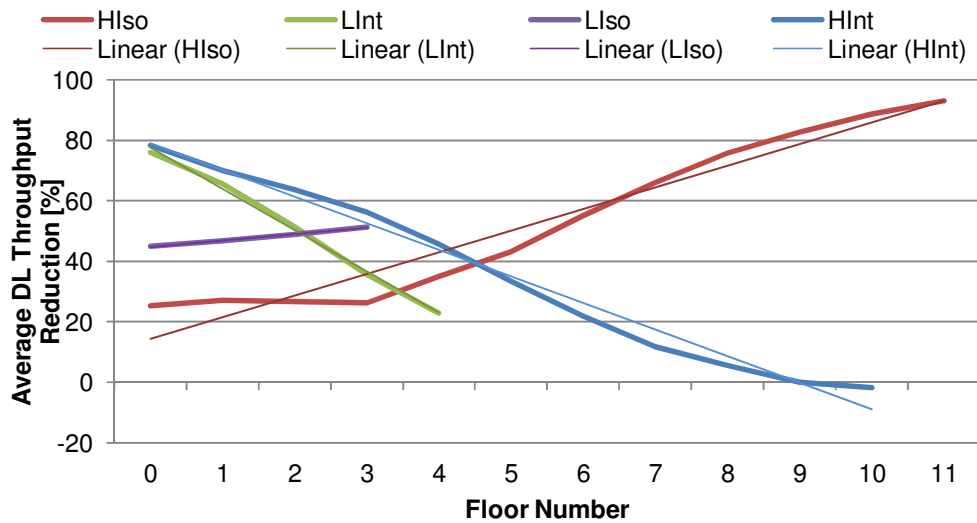


Figure 4.11. Average DL throughput reduction along building floors with the respective trend line.

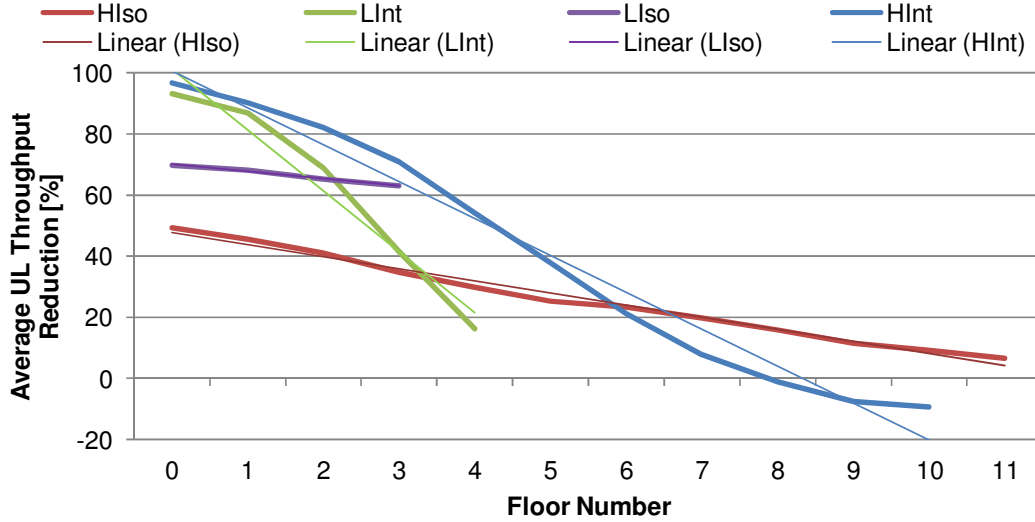


Figure 4.12. Average UL throughput reduction along building floors with the respective trend line.

Table 4.6. Correlation coefficients for throughput reduction functions along the building floors.

| Link | Correlation coefficient ( $\rho_{corr}$ ) |        |        |        |
|------|---|--------|--------|--------|
|      | HInt                                      | HIso   | LInt   | LIso   |
| DL   | 0.9920                                    | 0.9735 | 0.9980 | 0.9989 |
| UL   | 0.9889                                    | 0.9940 | 0.9780 | 0.9933 |

$$\begin{cases} \overline{\Delta R_b^{HInt}} [\%] = -8.79 \times F_N + 87.73, & \text{DL} \\ \overline{\Delta R_b^{HInt}} [\%] = -12.1 \times F_N + 112.85, & \text{UL} \end{cases} \quad (4.4)$$

$$\begin{cases} \overline{\Delta R_b^{HIso}} [\%] = 7.15 \times F_N + 7.25, & \text{DL} \\ \overline{\Delta R_b^{HIso}} [\%] = -3.95 \times F_N + 51.70, & \text{UL} \end{cases} \quad (4.5)$$

$$\begin{cases} \overline{\Delta R_b^{LInt}} [\%] = -13.62 \times F_N + 91.13, & \text{DL} \\ \overline{\Delta R_b^{LInt}} [\%] = -19.91 \times F_N + 121.14, & \text{UL} \end{cases} \quad (4.6)$$

$$\begin{cases} \overline{\Delta R_b^{LIso}} [\%] = 2.11 \times F_N + 42.66, & \text{DL} \\ \overline{\Delta R_b^{LIso}} [\%] = -2.31 \times F_N + 72.38, & \text{UL} \end{cases} \quad (4.7)$$

Concerning the room attenuation analysis, the mean value for all floors is presented in Figure 4.13 for each building type. As expected, the reduction is larger for the inner rooms in both DL and UL. In DL, Isolated buildings show a slightly greater throughput reduction due to the exposure to interference in the upper floors, with an average reduction of 53.73 % and 47.93 % reductions for High and Low, respectively. For the Integrated buildings, the average reduction is 34.97 % and 50.28 % for High and Low, respectively. The lower throughput reduction values in the High Integrated buildings are due to the increase of LoS, creating a throughput gain in the upper floors.

In UL, the influence of interference is not so evident, and therefore High Isolated building values are much lower than in DL. In fact, these values are the lowest of all since LoS conditions are greater than any other. High buildings show lower reductions, due to throughput availability in upper floors, lowering their average reduction to 40.25 % and 25.99 % for Integrated and Isolated, respectively. As for Low buildings, a throughput reduction of 61.42 % and 66.60 % is shown for Integrated and Isolated, respectively. Low Isolated building results show again unexpectedly high reductions, due to the poor model extracted from the measurements.

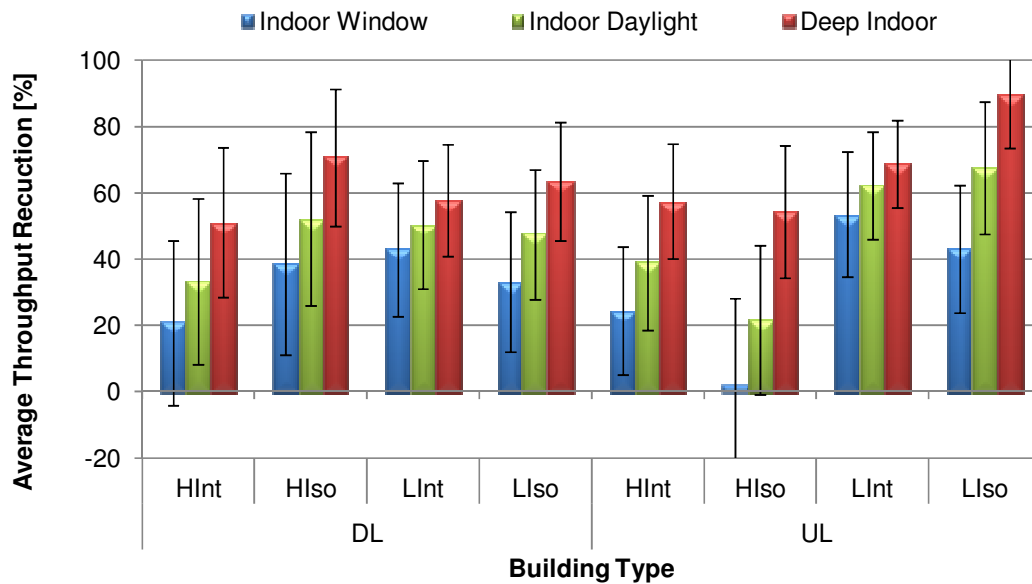


Figure 4.13. Average throughput reduction for all simulated room types.

The average difference of throughput reduction between consecutive floors, defined in (3.16), is presented in Table 4.7 for the reference scenario. Together with the shorter throughput range, as shown in (3.7), the lower transmitting power available in UL (which is reflected in the available SINR) increases the average throughput reduction.

Table 4.7. Average difference of throughput reduction between floors.

| Room Type       | $\overline{\Delta R_b^{floor}}$ [%] |              |
|-----------------|-------------------------------------|--------------|
|                 | DL                                  | UL           |
| Indoor Window   | -1.43                               | -8.22        |
| Indoor Daylight | -3.13                               | -9.18        |
| Deep Indoor     | -5.20                               | -9.55        |
| <b>Average</b>  | <b>-3.25</b>                        | <b>-8.99</b> |

Other analyses are performed in order to understand the system behaviour for other requirements. The outdoor reference signal power is greatly dependent on the distance to the BS. Therefore other configurations between the BS and MT are tested, as described in Table 4.2. Besides cases 2, 3 and 4 comparison, a shorter (30 m) and a longer distances (250 m) are compared to the reference

scenario, the latter being close to the average cell edge distance in a dense urban scenario [Voda11]. The shorter distance building does not account for any obstacle building (LoS - case 5), whereas the longer distance one accounts for two obstacle buildings (NLoS – case6). The decision to separate the first 3 cases (distanced up to 20 m from the BS) from the remaining is due to the favourable conditions in which they are inserted in, since at such short distance the results begin to saturate at the maximum throughput. Moreover, in the first 3 cases, the distance is not changed but only the BS antenna position relatively to the MT.

Figure 4.14 shows the different antenna position results for DL and UL. Due to the short distance to the MT, case 2 and 4 (both in LoS) have very low throughput reductions, in some buildings these cases can even have throughput increase. The same does not happen in the case 3 scenario, in which LoS is not existent. In fact, a great obstruction of the Fresnel ellipsoid leads to high throughput reductions, reaching almost 100 % in the most troublesome buildings (the Isolated ones, where interference reduces even more the available throughput).

One can notice the higher DL throughput reduction in the Isolated buildings for case 2, again due to the presence of undesired interference, which does not happen in the UL analysis (where the interference value is lower). However, this is not so evident in case 4 since the BS antenna is positioned in the building façade, increasing the available signal power in the outdoor reference position and increasing the SINR inside the building.

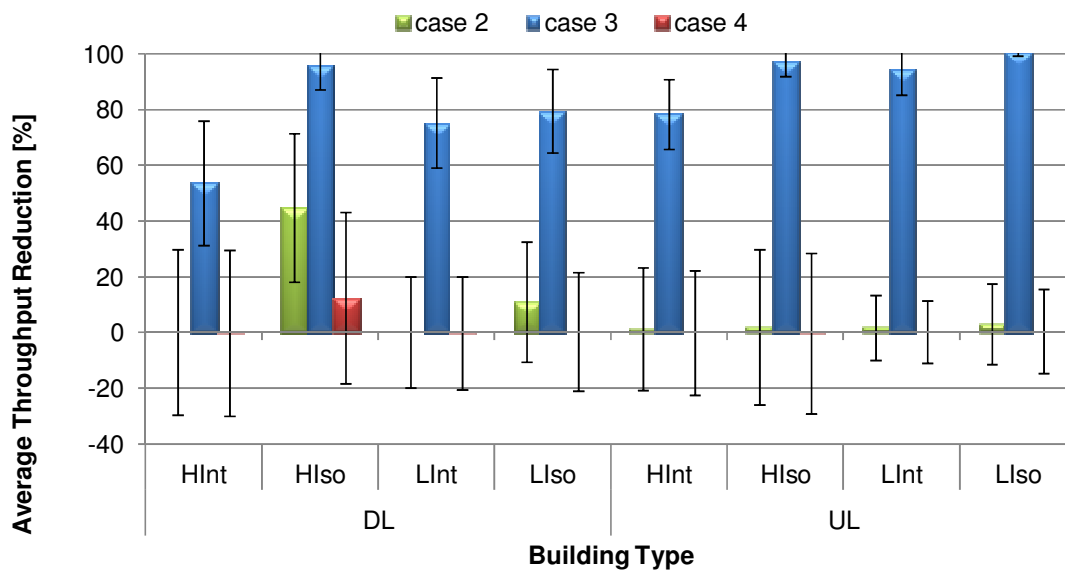


Figure 4.14. Average throughput reduction comparison for different antenna positions.

The results for the different distances (cases 5 and 6) are shown in Figure 4.15. The results show an increase of reduction when the MT is further away from the BS. General traces can be found, where Low buildings have slightly higher reductions due to the low availability of LoS, which would increase the simulated throughput. The High Isolated buildings are the exception: the presence of a great

interference power in the upper buildings makes the average throughput reduction rise.

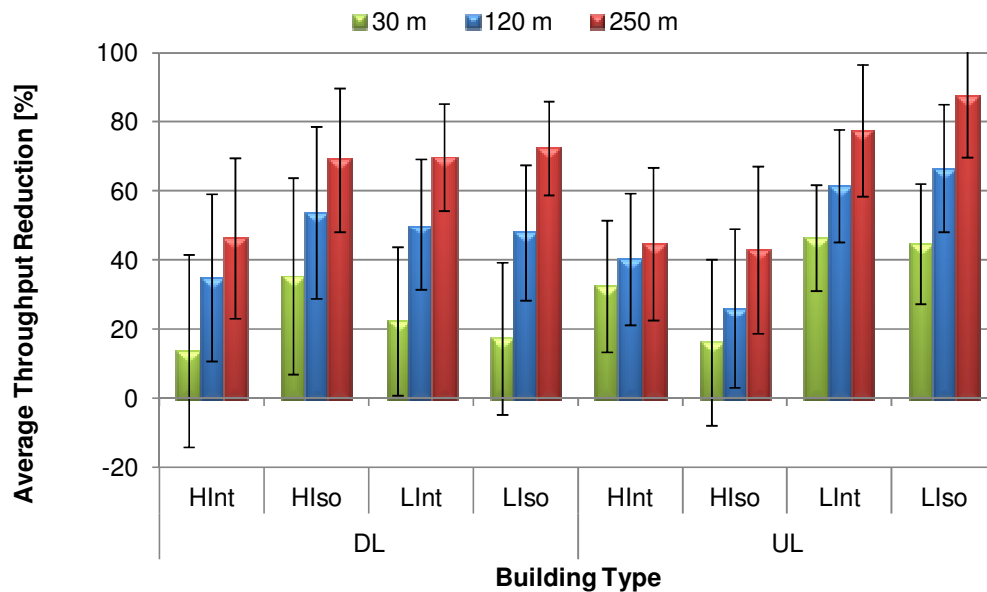


Figure 4.15. Average throughput reduction comparison for different distances.

In UL, the same conclusions can be taken, although in the High Isolated buildings the interference power is not as evident as in DL. In fact, the throughput reduction in these buildings is even lower than in the remaining building types, due to the exposure to LoS. Low Isolated buildings show in UL unexpected high results, in which great reductions are due to the poor signal attenuation model (the attenuation being almost insensitive to variations in the MT position inside the building).

The desired coverage is also tested. The reference scenario accounts for the average attenuation in each building, i.e., with a 50 % building coverage. Other scenarios with greater building coverage are simulated too: 90 % and 95 %, increasingly more demanding in signal and throughput requirements. The results are shown in Figure 4.16.

The results show the greater requirements in throughput availability when the desired coverage is increased. The reduction is greater in the Isolated buildings for higher coverage: since the throughput is so close to zero, the greater standard deviation values for these buildings (Table 4.4), particularly in Indoor Window rooms, cause a greater reduction comparing to other building types. This is mostly relevant in UL, where the Isolated buildings show a reduction of 100 %, which means that the UL throughput is reduced to zero.

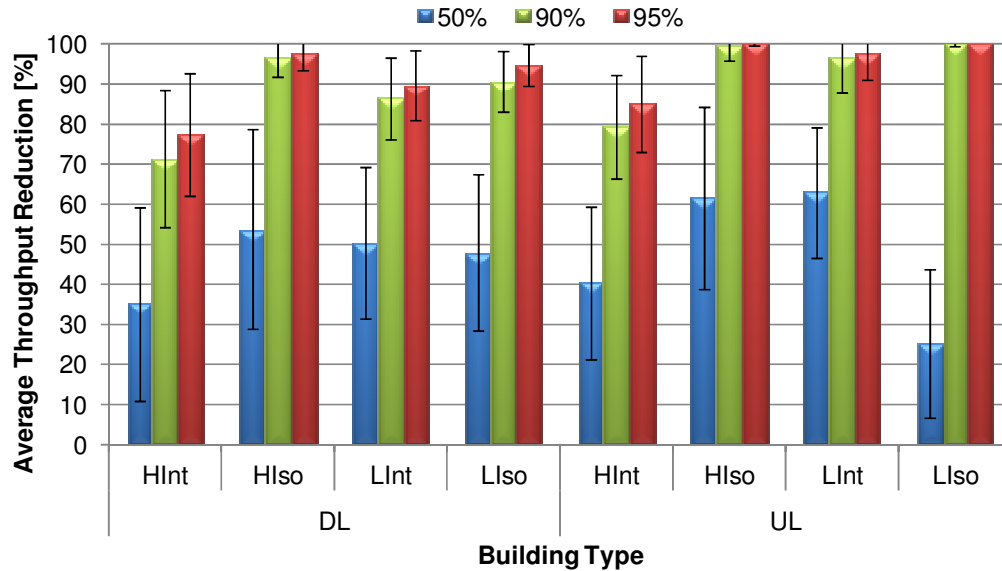


Figure 4.16. Average throughput reduction comparison for different coverage conditions.

The capacity analysis was also performed, according to the model suggested in Subsection 3.1.2. The three previously defined path loss scenarios were chosen: 30, 120 and 250 m. From the first three case scenarios in Figure 3.2, cases 2 and 4 were left out since the difference between the number of outdoor and indoor served users was below 0.01 % due to the high SINR available for both outdoors and indoors. Both DL and UL were tested for each distance. Besides the absolute number of users (indoor and outdoor) in the cell, an extra indicator is presented: the difference between the indoor and outdoor number of users, expressed in percentage, relative to the total possible number of users, expressed in (3.18).

Figure 4.17 shows the results for both outdoor and indoor DL. For lower throughput values the limitation factor is the number of codes, creating a saturated curve in 15 users. From that point on, the limitation is due to the available signal power and the present interference power, creating a small difference between the different curves. For higher throughputs, the number of served users is too low to notice relevant differences between the curves. One can notice the sensitivity in user reduction to distance mostly because of the orthogonality factor model presented in (2.6). Concerning the indoor variation, the random parameters (such as coverage percentage, building type, room position and MT height) create a wide spectrum of simulated scenarios, which is great enough to create statistical relevance. Therefore, these results represent an average number of served users in an urban environment for all building and room types, allowing the operator the correctly dimension the cell capacity.

The comparison between the indoor and outdoor curves for each distance is performed in Figure 4.18. Comparing the user reduction variation with the available throughput, the expected result would be a higher user reduction for the lower throughputs, since the number of users is greater. This does not happen due to the reason stated earlier: results are saturated, since the number of codes is limited,

and therefore the number of served users is also limited. Comparing the user reduction variation for the simulated distances, the results are in accordance with the expectations. In the 18 m and 30 m simulations, throughputs are highly saturated, and because of that no difference can be found between the outdoor and indoor served users. In the other two cases, the results are more significant, since the desired throughputs are more difficult to achieve: the required SINR is great and this is directly reflected in the number of users.

One should take into consideration the low user reduction values: 0.01 %, 0.03 %, 2.39 % and 2.96 % for 18 m, 30 m, 120 m and 250 m, respectively. This can be explained by the diversity of created scenarios: most of the cases show a throughput reduction, although some of them show an increase of throughput compared to the outdoor environment, particularly in the High buildings. These scenarios' results were averaged, being able to create a random urban environment and enhancing the results' usability in capacity dimensioning.

Figure 4.19 shows the results for both outdoor and indoor DL. In UL, the user saturation in the lower throughputs is not so evident, due to the lower transmitter power, lower processing gain and the presence of interference (through the ratio of inter- to intra-cell interferences,  $i_r$ ). This is visible in the user reduction analysis, Figure 4.20, where the higher variations are in the lower throughputs since the number of users is greater.

The same considerations can be taken for UL, in which the average user reduction values are 0.19 % for 18 m, 0.40 % for 30 m, 3.33 % for 120 m and 5.22 % for 250 m.

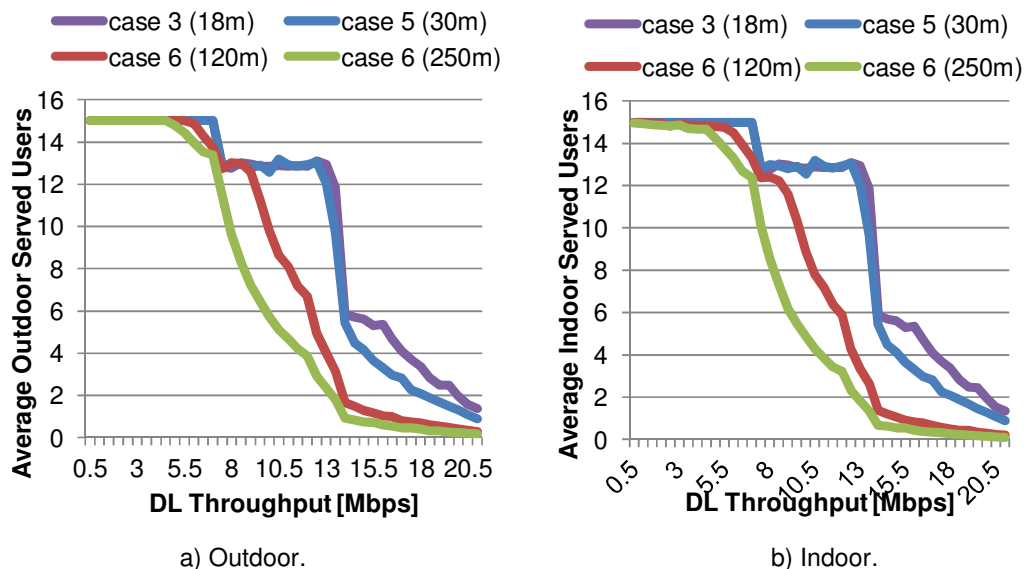


Figure 4.17. Served users for the available throughput values in DL for a SISO configuration.

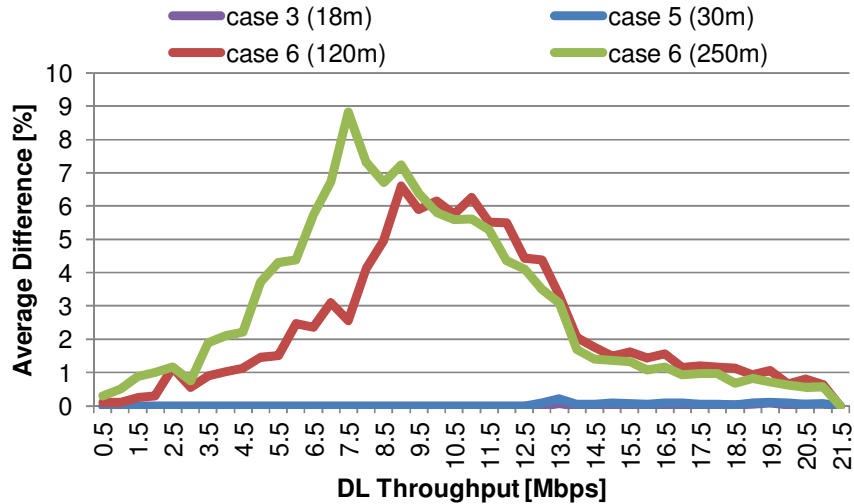


Figure 4.18. Average difference between outdoor and indoor served users in DL.

A comparison of the presented results with an earlier study is made [TaFi10]. Although its authors do not present the results in the same approach, some similarities can be found. The measurements in [TaFi10] show a 20 % to 40 % throughput reduction in low load period and less than 10 % reduction in high load period. In the given description, the low load period is defined by a noise-limited system, which corresponds to a typical Integrated building scenario, with the noise power being the limitation factor in the available SINR. On the other hand, the high load period can be associated to an Isolated building scenario.

Given this, these results are compared to the ones simulated in the reference scenario. In this work, the Isolated buildings show an average reduction of 53.73 % and 47.93 % for High and Low, respectively, whereas the Integrated buildings show an average reduction of 34.97 % and 50.28 % for High and Low, respectively. Averaging all room and building types, the average throughput reduction is 42.63 % for Integrated and 50.83 % for Isolated buildings. These values are much higher than the ones presented in [TaFi10]. However, the same conclusion can be taken: the presence of higher interference levels influences the throughput in about 10%, especially between higher buildings.

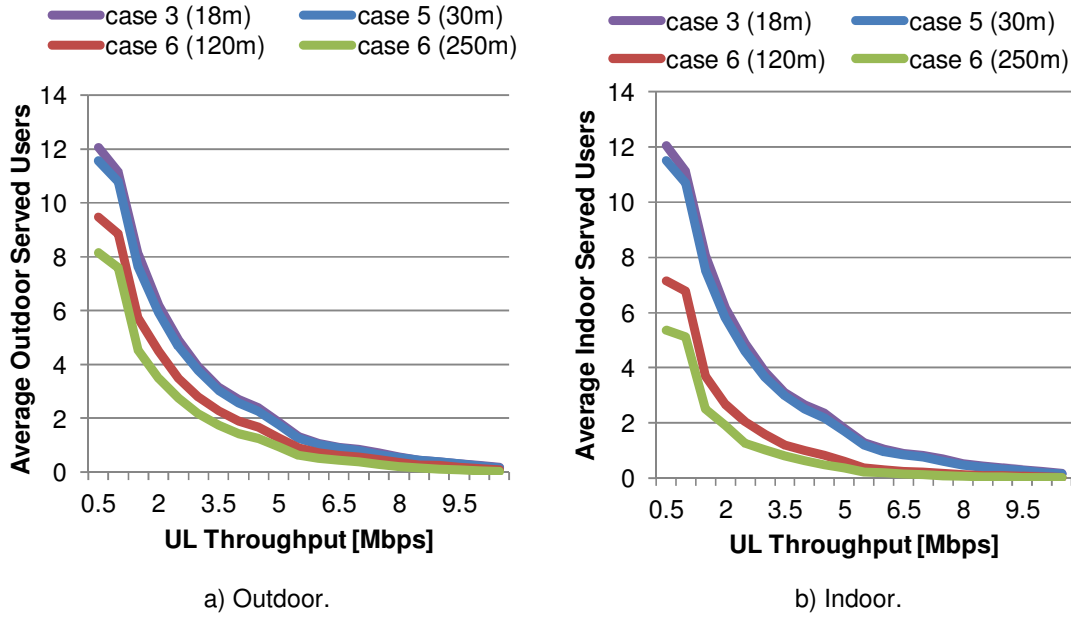


Figure 4.19. Served users for the available throughput values in UL for a SISO configuration.

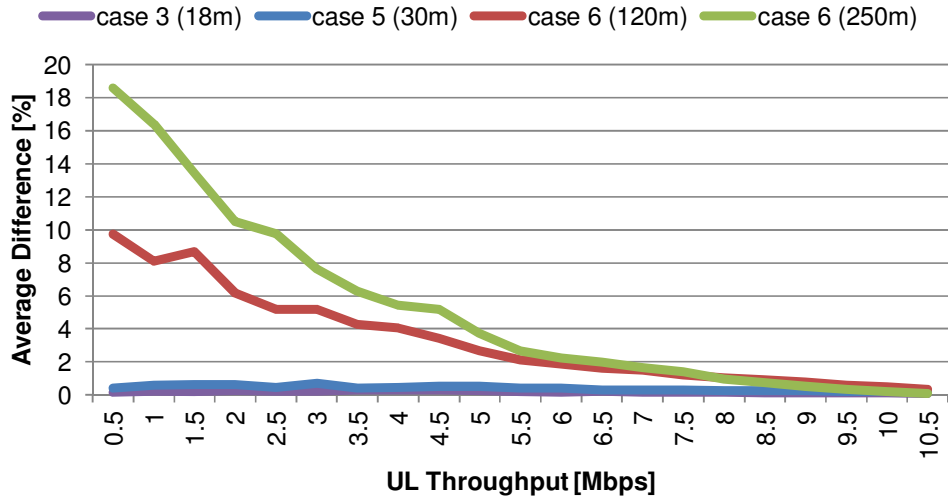


Figure 4.20. Average difference between outdoor and indoor served users in DL.

# Chapter 5

## Conclusions

In this chapter, the main conclusions of this thesis are pointed out, summing up a discussion and a critical analysis of the results, as well as some future work suggestions.

The main objective of this thesis was to study and quantify the data rate transmission performance for a UMTS/HSPA+ system in indoor scenarios, giving special emphasis to capacity and coverage aspects. These goals were accomplished through the development and implementation of two models: the Single-User and the Multi-User ones. A measurement campaign was conducted to obtain a model for indoor signal attenuation, which was input in both Single and Multi-User models.

Chapter 2 is focused on UMTS fundamental aspects, such as its basic aspects, the interference phenomenon and the propagation models used for network dimensioning. The first section includes the basic aspects of UMTS, more specifically its network elements, performance analysis and radio interface, considering all recent HSPA+ developments. The interference section includes a brief description of the interference phenomenon and shows the interference models available in literature. The propagation section also describes the types of propagation, indoor and outdoor, and shows several approaches for their calculation shown in previous works. Finally, the state-of-the-art is overviewed, considering the most relevant works in indoor data rate performance.

In Chapter 3, the developed models were presented. The Single-User model is intended to provide an understanding of the requirements needed to serve a user located indoors, considering different building and room types. It is possible to calculate the available throughput given for a Single-User, varying several parameters of both outdoor and indoor environments. The aim of the Multi-User model is to quantify the reduction in the number of users for a given throughput, assuming the users are uniformly distributed along the radius of the cell. Although the outdoor scenario is left unchanged, the model randomises the indoor scenario according to the available building and room types, building coverage and MT height. This model takes into account the both network and propagation restrictions: the number of available HSPA+ DL codes, the available signal and interference powers. These models were implemented in a C++ application, with an intuitive interface, allowing the user to easily create a scenario and perform simulations over it.

For the outdoor and indoor environments two different approaches were followed: the outdoor model was based on a previously developed model, whereas the indoor one was extracted from the measurement campaign (statistical), being both models based on empirical results. Both models take the interference phenomenon into account, combining two influencing factors in urban scenarios: the distance to the BS and the existence of LoS/NLoS.

Several parameters can be changed in the outdoor model: the BS and MT characteristics, the operating frequency and the distance between BS and MT. Concerning the indoor model, the user can decide the simulated building and room types, as well as the desired coverage and the building's number of floors. The simulator also allows computing both links (DL or UL) and different antenna configuration schemes, namely SISO, SIMO and MIMO. Although the three types were available, the latter two were not tested, mainly because the measuring equipment could only perform SISO. Nevertheless, throughput reduction was calculated in percentage, allowing a possible scaling process, in order to obtain SISO and MIMO values, assuming the inexistence of other relevant factors that

might influence the results.

In addition to the developed models, a measurement campaign was conducted. The results from the campaign were inserted in the indoor model for each building and room type, allowing a complete characterisation of the signal inside the building. However, and because the purpose of this work is to quantify the data rate performance, the indoor model is responsible to map the indoor signal attenuation onto an indoor throughput reduction model, by means of available SINR-to-throughput models. The campaign also included throughput measurements, both in DL and UL, which allowed an assessment of the simulated results.

In Chapter 4, the analyses of all measurements and simulations results were shown. Several buildings were measured, according to the proposed classification in [XaVe02]. After data processing, a signal attenuation model was created, taking as reference the outdoor measurements, and input in the model implementation. Additionally, the measurements' software provided information about the modulation usage in all measured sites, allowing the creation of another useful model to input in the simulator.

Not all measurements results were consistent, therefore some results had to be extracted from [SLCM05]. The specific propagations conditions and the lack of throughput stability did not allow to take good conclusions, although some trend could be identified. Generically, the floor height gain is verified for all building types, i.e., the upper floors have a greater available signal power than the lower ones. Among them, the High buildings show lower average building penetration attenuation due to the increase of signal availability in the upper floors (especially the Isolated case). In the measurements throughput analysis, the floor height gain is not true for all buildings though. Specifically, High Isolated ones have too much exposure to signal power, increasing not only the desired one, but also the interfering. SINR is therefore lowered and the throughput shows the opposite behaviour of signal power, being usually lower in the upper floors. The signal availability is greater in Isolated buildings, and so is UL throughput, since the interference power is not so influencing as in DL.

The measurement results were compared with the reference simulated scenario, showing similar trends in the majority of the cases: throughput suffers a greater reduction the inner the room is. The simulated results show good correlation with the measured ones most times, being the model for Low Isolated buildings the poorest one, and therefore the analyses need to be taken with caution. One should take into account that the measured throughput shows a great variability, either due to changes in TTI (UL), number of given codes (DL) or instantaneous network load changes (DL/UL). Signal attenuation can be correlated with throughput reduction, both in DL and UL. Increasing attenuation of 1 dB leads to average throughput reductions of 3.83 % in DL and 5.13 % in UL for simulation, and 4.61 % in DL and 1.70 % in UL for measurements.

In DL floor analysis, Integrated buildings have the greater throughput reduction in the lower floors, reaching 78.30 % in High and 75.98 % in Low buildings; with the floor height increase, the trend is to increase throughput, up to 22.85 % for Low and -1.71 % for High buildings. One should notice that High ones even reach negative reduction, i.e., throughput gains in the upper floors, due to the

exposure to higher signal power. In Integrated buildings, the trend is the opposite, since interference reduces the available SINR. In UL, interference power is not so influencing therefore all trends are towards lower throughput reductions. Low Isolated buildings show a very low reduction with increase of floor height, which is due to the low number of measured floors.

The room analysis was also performed, showing increasing throughput reductions the inner the room is. In DL, the results show higher average reductions in Isolated buildings (due to interference); in Integrated buildings, one can notice the influence of HInt's upper floors in lowering its average reduction. Regarding UL, interference is not so evident, and the most influencing factor starts to be the signal received in High buildings' upper floors, lowering their average reduction.

Also interesting is the computation of the average reduction per floor transition, enabling the quantification of the floor height gain in terms of throughput. Performing this analysis independently of the room type, the floor height gain is 3.25 % for DL and 8.99 % for UL. The lower transmitting power and the shorter throughput range increase UL throughput reduction in comparison to DL case.

For the cases where distance to the BS is lower than 20 meters, throughput reductions are lower in LoS cases. The higher result for the rooftop antenna in DL is explained by the reduction caused by interference in Isolated buildings, whereas this effect is not present in the façade antenna since the distance to MT is lower. One should take into consideration that, at such short distance, SINR is high enough to assure the highest possible throughput, the influence of indoor signal attenuation being low in the obtained throughput. In the NLoS case, the opposite behaviour is found: due to the obstruction of the Fresnel ellipsoid, SINR suffers a great outdoor loss, resulting in great throughput reductions.

Regarding distance variation, three tested distances include one LoS case (30 m) and two NLoS cases (120 m and 250 m). In all building types, throughput reduction is higher when the distance increases. In DL, the throughput reductions are almost independent of the building type. In UL, the effect of interference fades away, leaving the major cause of reduction the low height of the buildings and therefore poor LoS conditions.

Concerning coverage analysis, results show that a greater building coverage requires a greater throughput reduction. In both DL and UL, Isolated buildings show greater attenuations for 90 % and 95 % building coverage due to the greater standard deviations in the signal attenuation models, resulting in low throughput values. The exception to these great throughput reductions (between 80 % and 100 %) is the High Integrated case, which shows average reductions below 80 %, due to the absence of a great interference power level, particularly in DL.

The last analysis is the capacity one, using the developed Multi-User model. Both DL and UL were tested, assuming UL requests are made from the same users that require DL capabilities. Four distances were tested, using 18 m, 30 m, 120 m and 250 m. For lower throughputs, the number of served users is limited by the number of available HSPA+ DL codes (15 codes available for data transmission), whereas for medium and higher throughputs the limitation factors are the available

signal power and interference level in the network. The low user reduction values (most of them below 5 %) are explained by the diversity of simulated scenarios: most of the cases show a throughput reduction, although some of them show an increase of throughput compared to the outdoor environment, particularly in High buildings.

Summarising, the indoor data rate performance is highly dependent on several parameters. In DL the most influencing factor is the presence of interference, lowering the average indoor throughput in Isolated buildings; in UL, the available signal is the key factor, in which higher buildings have greater average throughputs, due to the higher availability of signal in the upper floors. The number of penetrated walls also decreases the data rate, as well as the desired coverage percentage. The floor height gain verified in terms of signal power is also present in the data rate, with an average data rate increase of 3.25 % in DL and 8.99 % in UL. Generically, the data rate reductions are greater in UL, due to the lower transmitting power and the shorter throughput range.

The simulator proves to be a powerful tool in the indoor data rate performance study, but it has its limitations. The interference model is based on simulations and lacks a realistic approach, only considering the distance to the BS and the presence of LoS/NLoS in the studied floor. The model also accounts for SIMO and MIMO characterisation, although the signal attenuation model was generated with a SISO system, therefore not being totally appropriate for other antenna configurations. The Multi-User model is based on a snapshot analysis, with users spread uniformly along the defined radius, not taking into consideration the real position of the user and the influence of its generated interference on other users. The number of measured buildings was enough to obtain good results, although an increase in the number of measured buildings would allow a more robust measurements' analysis.

For future work, it is suggested an improvement of the simulator in its limitations, previously described, as well as the new multiple-cell operation technologies. In addition, the measurement campaign could also be improved, with a higher number of measured buildings of each type and including all room types. Additionally, simulations could be performed for different services, taking into consideration their single requirements and specifications. Moreover, it would be interesting to include the possibility of performing more than one service simultaneously, and even to study DL and UL jointly. A comparison between the HSPA+ and the new technology LTE would also be of interest, mainly taking into account the better interference handling that LTE is known to have.



# Annex A – Link Budget

In a good cellular design, the calculation of the maximum path loss is necessary for the estimation of the cell range. This estimation is called link budget and throughout this thesis it is based on the Release 99 one, though taking into account the upgrades to HSPA+.

The path loss in (2.27) can be rewritten as [Corr09]:

$$L_p[\text{dB}] = EIRP_{[\text{dBm}]} - P_r[\text{dBm}] + G_{Rx}[\text{dBi}] \quad (\text{A.1})$$

where:

- $EIRP$  is the equivalent isotropic radiated power;
- $G_r$  can be decomposed in two gains,  $G_r + G_{div}$ , when diversity is used. Diversity can only be used in the UL, since in the DL the MT is not able to perform that function: the MT is too small for spatial diversity; and it has a limited transmission power, which does not allow polarisation diversity [Sant04].

The EIRP depends on the link: in the DL it can be estimated by (A.2) and in the UL it can be estimated by (A.3) [Corr09].

$$EIRP_{[\text{dBm}]}^{DL} = P_{Tx}[\text{dBm}] - L_c[\text{dB}] + G_{Tx}[\text{dBi}] \quad (\text{A.2})$$

$$EIRP_{[\text{dBm}]}^{UL} = P_{Tx}[\text{dBm}] - L_u[\text{dB}] + G_{Tx}[\text{dBi}] \quad (\text{A.3})$$

where:

- $L_c$  is the cable loss attenuation between the emitter and the BS antenna;
- $L_u$  is the user body loss attenuation, which values can be [3, 10] dB for voice and [0, 3] dB for data.

The receiver signal also depends on the link: in the DL it can be estimated by (A.4) and in the UL it can be estimated by (A.5) [Corr09].

$$P_{Rx}[\text{dBm}]^{DL} = P_r[\text{dBm}] - L_u[\text{dB}] \quad (\text{A.4})$$

$$P_{Rx}[\text{dBm}]^{UL} = P_r[\text{dBm}] - L_c[\text{dB}] \quad (\text{A.5})$$

In UMTS, the receiver sensitivity can be expressed as [Corr09]:

$$P_{Rx \min}[\text{dBm}] = N_{[\text{dBm}]} - G_p[\text{dB}] + SNR_{[\text{dB}]} \quad (\text{A.6})$$

where:

- $N$  is the total noise power, given by (A.7);
- $G_p$  is the processing gain, Table A.1;
- $SNR$  is the signal-to-noise ratio, Table A.1.

Table A.1. Processing gain and SNR definition for HSPA+ (adapted from [Jaci09]).

| System   | Processing gain       | SNR       |
|----------|-----------------------|-----------|
| HSPA+ DL | Fixed and equal to 16 | $\rho_N$  |
| HSPA+ UL | $R_c/R_b$             | $E_b/N_0$ |

For the UL, the processing gain must be two or higher, since at least one of the codes must be dedicated to control and signalling. For this work it was considered that all resources were available in the UL, therefore the processing gain is equal to two.

The total noise power is given by [Corr09]:

$$N_{[\text{dBm}]} = -174 + 10 \log(\Delta f_{[\text{Hz}]}) + F_{[\text{dB}]} \quad (\text{A.7})$$

where:

- $\Delta f$  is the signal bandwidth (in UMTS it is equal to  $R_b$ );
- $F$  is the receiver's noise figure.

For the sensitivity calculation, the  $E_b/N_0$  is obtained using  $E_c/N_0$  [Corr09]:

$$E_b/N_{0[\text{dB}]} = E_c/N_{0[\text{dB}]} + G_p[\text{dB}] \quad (\text{A.8})$$

In HSPA+ UL, manipulating (A.6) and (A.8) and introducing the interference power, the  $E_b/(N_0 + I_0)$  for a certain user's distance is given by:

$$E_b/(N_0 + I_0)_{[\text{dB}]} = P_{R_{\text{min}}}[\text{dBm}] - (N + I)_{[\text{dBm}]} + G_p[\text{dB}] \quad (\text{A.9})$$

For HSPA+ DL, rearranging (A.6) and introducing the interference power, the SINR associated to a certain user distance is calculated by:

$$\rho_{IN[\text{dB}]} = P_{R_x}[\text{dBm}] - (I + N)_{[\text{dBm}]} + G_p[\text{dB}] \quad (\text{A.10})$$

Some more margins can be taken into account, which can be expressed as [Corr09]:

$$M_p[\text{dB}] = M_{SF}[\text{dB}] + M_{FF}[\text{dB}] \quad (\text{A.11})$$

where:

- $M_{SF}$  represents the margin due to slow fading;
- $M_{FF}$  represents the margin due to fast fading.

The fast and slow fading can be modelled by Rayleigh and Log-Normal distributions respectively, and are introduced in order to guarantee more realistic results. Expression (A.12) stands for the cumulative distribution function (CDF) of the Rayleigh distribution, while the Gaussian distribution CDF is given by (A.13) [Corr09].

$$P(x) = 1 - e^{-x_{[\text{dB}]}^2 / \langle x_{[\text{dB}]}^2 \rangle} \quad (\text{A.12})$$

where:

- $\langle x^2 \rangle$  is the mean square error, defined by:

$$\langle x_{[\text{dB}]}^2 \rangle = \frac{4\sigma_{[\text{dB}]}}{4 - \pi} \quad (\text{A.13})$$

with  $\sigma$  being the standard deviation.

$$P(x) = \frac{1 + \operatorname{erf}\left(\frac{x_{[\text{dB}]} - \langle x_{[\text{dB}]} \rangle}{\sqrt{2}\sigma_{[\text{dB}]}}\right)}{2} \quad (\text{A.14})$$

where:

- $\langle x \rangle$  is the mean value;
- $\operatorname{erf}()$  is the error function, defined by:

$$\operatorname{erf}(v) \cong 1 - \sqrt{\pi} \frac{e^{-v^2}}{(\pi - 1)v + \sqrt{v^2 + \pi}}, v > 0 \quad (\text{A.15})$$

Finally, the total path loss can be expressed as [Corr09]:

$$L_{ref} [\text{dB}] = L_p [\text{dB}] + M_p [\text{dB}] \quad (\text{A.16})$$



# Annex B – COST231 Walfisch-Ikegami

This annex describes the COST231 - Walfisch-Ikegami (WI) model, which is the most suited propagation model used in urban and sub-urban scenarios and therefore the one used on this thesis. The parameters for this model for path loss prediction are: buildings height ( $h_{Roof}$ ), roads width ( $w_s$ ), building separation ( $w_b$ ) and road orientation with respect to the direct radio path ( $\varphi$ ), as shown in Figure B.1 and Figure B.2. This model also distinguishes LoS from NLoS. For LoS propagation ( $\varphi=0$ ) the loss is calculated by (B.1). For NLoS propagation the loss is composed by three terms: free space loss ( $L_0$ ), multiple screen diffraction loss ( $L_{msd}$ ), and roof-top-to-street diffraction and scatter loss ( $L_{rts}$ ). The NLoS the prediction is calculated by (B.2).

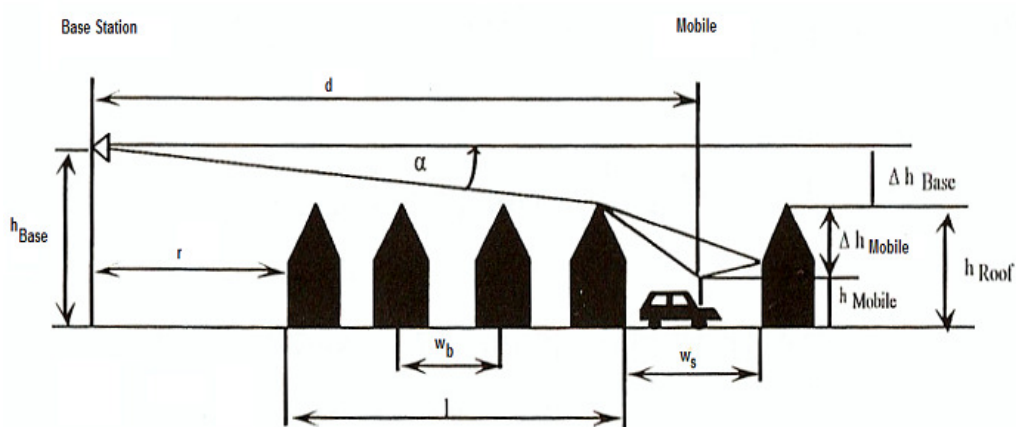


Figure B.1. Definition of the parameters used in the COST 231 - WI model (extracted from [DaCo99]).

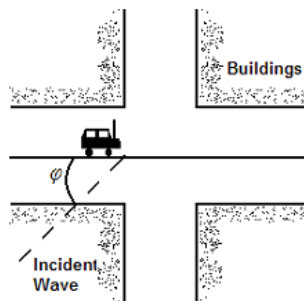


Figure B.2. Definition of the street orientation angle  $\varphi$  (extracted from [DaCo99]).

$$L_p[\text{dB}] = 42.6 + 26\log(d_{[\text{km}]}) + 20\log(f_{[\text{MHz}]}) , \text{ for } d \geq 0.02 \text{ km} \quad (\text{B.1})$$

$$L_p [\text{dB}] = \begin{cases} L_0 [\text{dB}] + L_{rts} [\text{dB}] + L_{msd} [\text{dB}] & \text{for } L_{rts} + L_{msd} > 0 \\ L_0 [\text{dB}] & \text{for } L_{rts} + L_{msd} \leq 0 \end{cases} \quad (\text{B.2})$$

The free-space loss is given by

$$L_0 [\text{dB}] = 32.4 + 20 \log(d_{[\text{km}]}) + 20 \log(f_{[\text{MHz}]}) \quad (\text{B.3})$$

The term  $L_{rts}$  basically describes the loss between last roof-top and MT. This parameter is mainly based on Ikegami's model (accounting street orientation and its width). However, rather than Ikegami, COST231 applies a different street-orientation function.

$$L_{rts} [\text{dB}] = -16.9 - 10 \log(w_s [\text{m}]) + 10 \log(f_{[\text{MHz}]}) + 20 \log(\Delta h_{\text{Mobile}} [\text{m}]) + L_{Ori} [\text{dB}] \quad (\text{B.4})$$

where:

- $\Delta h_{\text{Mobile}}$  is the difference between the roof height and the mobile height:

$$\Delta h_{\text{Mobile}} [\text{m}] = h_{\text{Roof}} [\text{m}] - h_{\text{Mobile}} [\text{m}] \quad (\text{B.5})$$

- $L_{Ori}$  is the street orientation loss:

$$L_{Ori} [\text{dB}] = \begin{cases} -10 + 0.354 \varphi_{[\text{deg}]} & \text{for } 0^\circ \leq \varphi \leq 35^\circ \\ 2.5 + 0.075(\varphi_{[\text{deg}]} - 35) & \text{for } 35^\circ \leq \varphi \leq 55^\circ \\ 4.0 + 0.114(\varphi_{[\text{deg}]} - 55) & \text{for } 55^\circ \leq \varphi \leq 90^\circ \end{cases} \quad (\text{B.6})$$

The  $L_{msd}$  parameter describes the loss between BS antennas and the last roof-top. It shows up as an extension of the Walfisch-Bertoni original model by COST231 for BS antennas height below the roof-top levels, using an empirical function based on measurements.

$$L_{msd} [\text{dB}] = L_{bsh} [\text{dB}] + k_a + k_d \log(d_{[\text{km}]}) + k_f \log(f_{[\text{MHz}]}) - 9 \log(w_b [\text{m}]) \quad (\text{B.7})$$

where:

- $L_{bsh}$  are the losses due to the fact that BS antennas are above or below the roof-top level:

$$L_{bsh} [\text{dB}] = \begin{cases} -18 \log(1 + \Delta h_{\text{base}} [\text{m}]) & \text{for } h_{\text{base}} > h_{\text{Roof}} \\ 0 & \text{for } h_{\text{base}} \leq h_{\text{Roof}} \end{cases} \quad (\text{B.8})$$

with  $\Delta h_{\text{base}}$  being the difference between the BS antenna height and the roof-top height:

$$\Delta h_{\text{base}} [\text{m}] = h_{\text{base}} [\text{m}] - h_{\text{Roof}} [\text{m}] \quad (\text{B.9})$$

- $k_a$  represents the increase of the path loss for BS antennas below the roof tops of the adjacent buildings:

$$k_a = \begin{cases} 54 & \text{for } h_{\text{base}} > h_{\text{Roof}} \\ 54 - 0.8 \Delta h_{\text{base}} & \text{for } d \geq 0.5 \text{ km and } h_{\text{base}} \leq h_{\text{Roof}} \\ 54 - 1.6 \Delta h_{\text{base}} d_{[\text{km}]} & \text{for } d < 0.5 \text{ km and } h_{\text{base}} \leq h_{\text{Roof}} \end{cases} \quad (\text{B.10})$$

- $k_d$  controls the dependence of the multi-screen diffraction loss versus distance:

$$k_d = \begin{cases} 18 & \text{for } h_{base} > h_{Roof} \\ 18 - 15 \frac{\Delta h_{base}}{h_{Roof}} & \text{for } h_{base} \leq h_{Roof} \end{cases} \quad (\text{B.11})$$

- $k_f$  controls the dependence of the multi-screen diffraction loss versus frequency:

$$k_f = \begin{cases} -4 + 0.7 \left( \frac{f_{[\text{MHz}]}}{925} - 1 \right) & \text{for } \begin{cases} \text{medium sized city} \\ \text{suburban centres with medium tree density} \end{cases} \\ -4 + 1.5 \left( \frac{f_{[\text{MHz}]}}{925} - 1 \right) & \text{for metropolitan centres} \end{cases} \quad (\text{B.12})$$

If the structure environment data is unknown the following values are recommended [Corr09]:

$$\left\{ \begin{array}{l} h_{Roof}[\text{m}] = 3 \times \{\text{number of floors}\} + \text{roof - height}[\text{m}] \\ \text{roof - height}[\text{m}] = \begin{cases} 3 & \text{for pitched} \\ 0 & \text{for flat} \end{cases} \\ w_b[\text{m}] \in [20, 50] \\ w_s[\text{m}] = \frac{w_b[\text{m}]}{2} \\ \varphi = 90^\circ \end{array} \right.$$

This COST 231 – WI model has the following restrictions:

$$\left\{ \begin{array}{l} f_{[\text{MHz}]} \in [800, 2000] \\ d_{[\text{km}]} \in [0.02, 5] \\ h_{base}[\text{m}] \in [4, 50] \\ h_{Mobile}[\text{m}] \in [1, 3] \end{array} \right.$$

The standard deviation of this model takes values in [4, 7] dB and the error increases when  $h_{base}$  decreased relatively to  $h_{Roof}$  [Corr09]. As one can notice, one of the limitations is the short distance of estimation. Moreover, the UMTS frequencies are not covered thoroughly by the system frequency spectrum.



# Annex C – UMTS Categories

This annex describes both UMTS/HSPA+ DL and UL MT categories. Each category has an associated maximum peak data rate, modulation and Transport Block Size (TBS). The categories are presented up to 3GPP's Release 9.

Table C.1 presents the DL MT categories for FDD HS-DSCH physical layer categories, covering up to Release 9. 3GPP standardised 28 categories for the DL, with the latest 4 including DC operation together with MIMO.

Table C.1. FDD HS-DSCH physical layer terminal categories (adapted from [3GPP10b]).

| MT Category | Maximum number of HS-DSCH codes received | Supported Modulations | Supported Modulations with MIMO     | Supported Modulations with DC operation                      | Supported Modulations with MIMO and DC operation                                | Maximum $N_b$ on a HS-DSCH TBS | Maximum theoretical peak data rate [Mbps] |       |       |             |       |       |
|-------------|--|-----------------------|-------------------------------------|--|---|--------------------------------|---|-------|-------|-------------|-------|-------|
| 1           | 5  | QPSK, 16QAM           | Not applicable (MIMO not supported) | Not applicable (aggregated carriers operation not supported) | Not applicable (aggregated carriers operation together with MIMO not supported) | 7298                           | 1.22                                      |       |       |             |       |       |
| 2           |  |                       |                                     |  |   | 7298                           | 1.22                                      |       |       |             |       |       |
| 3           |  |                       |                                     |  |   | 7298                           | 1.82                                      |       |       |             |       |       |
| 4           |  |                       |                                     |  |   | 7298                           | 1.82                                      |       |       |             |       |       |
| 5           |  |                       |                                     |  |   | 7298                           | 3.65                                      |       |       |             |       |       |
| 6           |  |                       |                                     |  |   | 7298                           | 3.65                                      |       |       |             |       |       |
| 7           | 10                                       |                       |                                     |  |   |                                |   |       | 14411 | 7.21        |       |       |
| 8           |  |                       |                                     |  |   |                                |   |       | 14411 | 7.21        |       |       |
| 9           | 15                                       |                       |                                     |  |   |                                |   |       | 20251 | 10.20       |       |       |
| 10          |  |                       |                                     |  |   |                                |   |       | 27952 | 14.40       |       |       |
| 11          | 5  | QPSK                  |                                     |  |   | 3630                           | 0.91                                      |       |       |             |       |       |
| 12          |  |                       |                                     |  |   | 3630                           | 1.82                                      |       |       |             |       |       |
| 13          | 15                                       | QPSK, 16QAM, 64QAM    |                                     |  |   | 35280                          | 17.64                                     |       |       |             |       |       |
| 14          |  |                       |                                     |  |   | 42192                          | 21.10                                     |       |       |             |       |       |
| 15          |  | QPSK, 16QAM           |                                     |  |   |                                | 23370                                     | 23.37 |       |             |       |       |
| 16          |  |                       |                                     |  |   |                                | 27952                                     | 27.95 |       |             |       |       |
| 17          |  | QPSK, 16QAM, 64QAM    | QPSK, 16QAM                         |  |   |                                | 35280                                     | 23.37 |       |             |       |       |
| 18          |  |                       |                                     |  |   |                                | 42192                                     | 27.95 |       |             |       |       |
| 19          |  | QPSK, 16QAM, 64QAM    |                                     |  |   |                                | 35280                                     | 35.28 |       |             |       |       |
| 20          |  |                       |                                     |  |   |                                | 42192                                     | 42.20 |       |             |       |       |
| 21          |  |                       |                                     |  | QPSK, 16QAM   |                                | 23370                                     | 23.37 |       |             |       |       |
| 22          |  |                       |                                     |  | 27952   |                                | 27.95                                     |       |       |             |       |       |
| 23          |  |                       |                                     |  | 35280   |                                | 35.28                                     |       |       |             |       |       |
| 24          |  |                       |                                     |  | 42192   |                                | 42.20                                     |       |       |             |       |       |
| 25          |  |                       |                                     |  | -   |                                | -   |       |       | QPSK, 16QAM | 23370 | 46.74 |
| 26          |  |                       |                                     |  |   |                                |   |       |       | 27952       | 55.90 |       |
| 27          |  | 35280                 | 70.56                               |  |   |                                |   |       |       |             |       |       |
| 28          |  |                       |                                     |  | QPSK, 16QAM, 64QAM  | 42192                          | 84.38                                     |       |       |             |       |       |

The computation of the maximum theoretical peak data rate is done according to the maximum number of HS-DSCH transport block bits ( $N_b$ ) received within a TTI, as shown in (C.1). In the cases of variable TTI for the same category (UL), the resulting throughput was calculated for the maximum system performance case.

$$R_{b \max [\text{Mbps}]} = \frac{\max(N_b)}{\min(TTI_{[\text{ms}]})} \quad (\text{C.1})$$

One ought to notice that these are the maximum available throughput values. The performance indicators, such as CQI, in a real system are lower to the ones presented in each table. For the UL, 3GPP includes 9 categories for Release 9, already including DC operation in the latest 2 categories. Table C.2 shows UMTS HSPA+ MT categories in the UL.

Table C.2. FDD E-DCH physical layer terminal categories (adapted from [3GPP10b]).

| MT Category | Maximum number of E-DCH codes transmitted | TTI length [ms]     | Supported Modulations                 | Minimum SF         | Maximum $N_b$ on a E-DCH TBS | Maximum theoretical peak data rate [Mbps] |
|-------------|---|---------------------|---------------------------------------|--------------------|------------------------------|---|
| 1           | 1   | 10                  | QPSK                                  | SF <sub>4</sub>    | 7110                         | 0.71                                      |
| 2           | 2   | 2, 10               |                                       | 2×SF <sub>4</sub>  | 14484 (TTI = 10 ms)          | 1.45                                      |
| 3           |   | 10                  |                                       |                    | 2798 (TTI = 2 ms)            |   |
| 4           |   | 2, 10               |                                       | 2×SF <sub>2</sub>  | 14484                        | 1.45                                      |
| 5           | 10  | 20000 (TTI = 10 ms) |                                       |                    | 2.89                         |   |
| 6           | 4   | 2, 10               | 2×SF <sub>4</sub> + 2×SF <sub>2</sub> | 5772 (TTI = 2 ms)  |                              | 2.00                                      |
| 7           |   |                     |                                       | 10                 | 20000 (TTI = 10 ms)          |   |
| 8           |   | 2                   |                                       | QPSK, 16QAM        | 11484 (TTI = 2 ms)           | 11.50                                     |
| 9           |   |                     |                                       | QPSK, 16QAM        | 20000 (TTI = 10 ms)          |   |
|             |   |                     |                                       | 22996 (TTI = 2 ms) |                              |   |

# Annex D – HSPA+ Throughput Models

The current annex presents the HSPA+ data rate models, which accurate the SINR and throughput of each considered system for several configurations. These models are referred to the physical layer of the Open Systems Interconnection (OSI) Reference Layer model; therefore they do not take into account the necessary throughput reductions of the upper layers, such as overhead and BLER requirements.

HSPA+ theoretical throughput values are presented in Figure 2.3 for a Pedestrian A channel. Previous works, such as [Jaci09] and [Preg08], have produced interpolated experimental expressions to precise SINR,  $\rho_{IN}$ , as a function of throughput,  $R_b$ , and vice-versa for several types of antenna configurations and modulations. These experimental expressions are supported by Ericsson, [3GPP06a] and [3GPP06b], and Huawei [3GPP06c] measurements, and remain valid up to this date, without any other contribution from the manufacturers. As stated before, all throughputs obtained are valid for the physical layer, and the authors ensure the extrapolations do not have relative mean errors greater than 5 %, which are acceptable for this kind of approximations. Some minor errors present in the equations were corrected, such as discontinuities between curves and the absence of saturation curves.

Although most of the curves were already available in previous works, the expressions for QPSK in the DL were produced in Matlab taking as reference the 16QAM curves. To produce these curves, some requirements had to be fulfilled [HoTo10]: the QPSK bit rate is half compared to 16QAM by transmitting 2 bits per symbol instead of 4 and the difference in the required SNR is approximately 6 dB between 16QAM and QPSK. The same steps to produce the expressions were used, also ensuring relative mean errors below 5 %.

The current expressions were taken from the measurements of Pedestrian A channel, since these are able to provide a good estimation for the signal arriving at a static equipment, which is most of the times the standard case for HSPA+ terminals. Estimations for Vehicular channel were not done, because this type of environment is not in the scope of this thesis. As for the Indoor channel, the propagation models already take into account the attenuation caused by an indoor environment.

As mentioned before, the following models consider 15 HS-PDSCH codes contrary to the real 14 available for data, since there was no available data for the latter number of codes.

Considering a SISO configuration with QPSK, for DL, one has:

$$\rho_{IN} \text{ [dB]} = \begin{cases} -0.0271 \times R_b^6 + 0.47465 \times R_b^5 - 3.36 \times R_b^4 + 12.33 \times R_b^3 \\ -24.86 \times R_b^2 + 27.77 \times R_b - 14.74, & 0.7 \leq R_b \text{ [Mbps]} < 4.5 \\ -0.0649 \times R_b^4 + 1.581 \times R_b^3 - 13.81 \times R_b^2 + 53.78 \times R_b \\ -76.46, & 4.5 \leq R_b \text{ [Mbps]} \leq 7.2 \end{cases} \quad (\text{D.1})$$

Considering a SISO configuration with 16QAM, for DL, one has:

$$\rho_{IN} \text{ [dB]} = \begin{cases} -0.0541 \times R_b^6 + 0.9494 \times R_b^5 - 6.7214 \times R_b^4 + 24.6466 \times R_b^3 \\ -49.805 \times R_b^2 + 55.0299 \times R_b - 31.1894, & 0.7 \leq R_b \text{ [Mbps]} < 4.5 \\ -0.0319 \times R_b^2 + 1.7534 \times R_b - 6.9882, & 4.5 \leq R_b \text{ [Mbps]} < 9.7 \\ 0.1529 \times R_b^3 - 5.1218 \times R_b^2 + 57.816 \times R_b - 211.471, & 9.7 \leq R_b \text{ [Mbps]} \leq 14.4 \end{cases} \quad (\text{D.2})$$

For a SISO configuration with 64QAM, for DL, the SINR is given by:

$$\rho_{IN} \text{ [dB]} = \begin{cases} -0.0541 \times R_b^6 + 0.9499 \times R_b^5 - 6.7214 \times R_b^4 + 24.6466 \times R_b^3 \\ -49.805 \times R_b^2 + 55.0299 \times R_b - 31.1894, & 0.7 \leq R_b \text{ [Mbps]} < 3.7 \\ 1.3691 \times R_b - 5.8516, & 3.7 \leq R_b \text{ [Mbps]} < 8.7 \\ 0.9565 \times R_b - 2.3371, & 8.7 \leq R_b \text{ [Mbps]} < 20.0 \\ 0.0332 \times R_b^2 + 0.0799 \times R_b + 1.9286, & 20.0 \leq R_b \text{ [Mbps]} \leq 21.6 \end{cases} \quad (\text{D.3})$$

In a SIMO 1x2 configuration with QPSK modulation, for DL, the SINR can be calculated by:

$$\rho_{IN} \text{ [dB]} = \begin{cases} 0.373 \times R_b^6 - 4.59 \times R_b^5 + 22.68 \times R_b^4 - 57.03 \times R_b^3 \\ + 75.55 \times R_b^2 - 45.01 \times R_b - 0.8666, & 1.0 \leq R_b \text{ [Mbps]} < 3.1 \\ 0.0671 \times R_b^4 - 1.2777 \times R_b^3 + 8.947 \times R_b^2 - 24.65 \times R_b + 20.22, & 3.1 \leq R_b \text{ [Mbps]} < 5 \\ -0.1809 \times R_b^3 + 4.233 \times R_b^2 - 28.42 \times R_b + 62.05, & 5.8 \leq R_b \text{ [Mbps]} < 7.2 \end{cases} \quad (\text{D.4})$$

In a SIMO 1x2 configuration with 16QAM modulation, for DL, the SINR can be calculated by:

$$\rho_{IN} \text{ [dB]} = \begin{cases} -0.0012 \times R_b^6 - 0.0171 \times R_b^5 + 0.0476 \times R_b^4 + 0.4255 \times R_b^3 \\ -3.251 \times R_b^2 + 10.0299 \times R_b - 17.1838, & 1.0 \leq R_b \text{ [Mbps]} < 1.8 \\ -0.4437 \times R_b^2 + 4.3888 \times R_b - 13.5340, & 1.8 \leq R_b \text{ [Mbps]} < 3.2 \\ 0.0661 \times R_b^4 - 1.2758 \times R_b^3 + 8.8721 \times R_b^2 \\ -24.7943 \times R_b + 19.3601, & 3.2 \leq R_b \text{ [Mbps]} < 5.9 \\ -0.1323 \times R_b^3 + 2.7646 \times R_b^2 - 17.8122 \times R_b + 36.0243, & 5.9 \leq R_b \text{ [Mbps]} < 8.3 \\ 0.0208 \times R_b^3 - 0.6278 \times R_b^2 + 7.276 \times R_b - 26.0464, & 8.3 \leq R_b \text{ [Mbps]} < 13.5 \\ 3.3333 \times R_b^2 - 87.6667 \times R_b + 585.0, & 13.5 \leq R_b \text{ [Mbps]} \leq 14.4 \end{cases} \quad (\text{D.5})$$

Considering SIMO 1x2 configuration with 64 QAM, for DL, one has:

$$\rho_{IN} \text{ [dB]} = \begin{cases} -0.0012 \times R_b^6 - 0.0171 \times R_b^5 + 0.0476 \times R_b^4 + 0.4255 \times R_b^3 \\ -3.251 \times R_b^2 + 10.0299 \times R_b - 17.1838, & 1.0 \leq R_b \text{ [Mbps]} < 2.2 \\ -0.1349 \times R_b^2 + 2.7519 \times R_b - 11.4313, & 2.2 \leq R_b \text{ [Mbps]} < 5.9 \\ -0.0148 \times R_b^4 + 0.2876 \times R_b^3 - 1.6684 \times R_b^2 \\ + 2.8789 \times R_b - 0.07, & 5.9 \leq R_b \text{ [Mbps]} < 7.4 \\ -0.0381 \times R_b^2 + 1.7802 \times R_b - 9.1641, & 7.4 \leq R_b \text{ [Mbps]} < 12.4 \\ -0.0158 \times R_b^2 + 1.4895 \times R_b - 9.0373, & 12.4 \leq R_b \text{ [Mbps]} < 18.5 \\ 0.6466 \times R_b^2 - 23.7609 \times R_b + 231.2882, & 18.5 \leq R_b \text{ [Mbps]} \leq 21.6 \end{cases} \quad (\text{D.6})$$

In a MIMO 2x2 configuration, using QPSK, for DL, the SINR is given by:

$$\rho_{IN} \text{ [dB]} = \begin{cases} 0.0699 \times R_b^5 - 1.229 \times R_b^4 + 8.639 \times R_b^3 \\ -30.48 \times R_b^2 + 56.03 \times R_b - 49.1, & 1.7 \leq R_b \text{ [Mbps]} < 3.4 \\ -0.0276 \times R_b^2 + 1.988 \times R_b - 9.967, & 3.4 \leq R_b \text{ [Mbps]} < 5.6 \\ -0.0579 \times R_b^2 + 1.979 \times R_b - 9, & 5.6 \leq R_b \text{ [Mbps]} < 7.0 \\ 0.0003 \times R_b^4 - 0.0059 \times R_b^3 + 0.0178 \times R_b^2 + 2.144 \times R_b \\ -12.6, & 7.0 \leq R_b \text{ [Mbps]} < 12.0 \\ 0.0205 \times R_b^3 - 0.6132 \times R_b^2 + 8.363 \times R_b - 35.7, & 12.0 \leq R_b \text{ [Mbps]} < 14.4 \end{cases} \quad (\text{D.7})$$

For a MIMO 2x2 configuration, with 16QAM, for DL, the SINR is given by:

$$\rho_{IN} \text{ [dB]} = \begin{cases} -0.0052 \times R_b^6 + 0.1479 \times R_b^5 - 1.7114 \times R_b^4 + 10.2135 \times R_b^3 \\ -33.3531 \times R_b^2 + 58.6222 \times R_b - 50.9322, & 1.7 \leq R_b \text{ [Mbps]} < 3.4 \\ -0.0642 \times R_b^2 + 1.9468 \times R_b - 10.8835, & 3.4 \leq R_b \text{ [Mbps]} < 5.6 \\ -0.0579 \times R_b^2 + 2.1091 \times R_b - 12.0231, & 5.6 \leq R_b \text{ [Mbps]} < 7.0 \\ -0.0704 \times R_b^2 + 2.3595 \times R_b - 13.1371, & 7.0 \leq R_b \text{ [Mbps]} < 12.0 \\ -0.0043 \times R_b^3 + 0.1489 \times R_b^2 - 0.8793 \times R_b + 1.6067, & 12.0 \leq R_b \text{ [Mbps]} < 14.2 \\ -0.0170 \times R_b^2 + 1.1714 \times R_b - 6.3410, & 14.2 \leq R_b \text{ [Mbps]} < 19.3 \\ -0.0016 \times R_b^3 + 0.1082 \times R_b^2 - 1.6755 \times R_b + 13.4935, & 19.3 \leq R_b \text{ [Mbps]} < 25.8 \\ 0.5533 \times R_b^2 - 28.4577 \times R_b + 380.712, & 25.8 \leq R_b \text{ [Mbps]} \leq 28.8 \end{cases} \quad (\text{D.8})$$

In a MIMO 2x2 configuration with 64QAM, for DL, the SINR can be calculated by:

$$\rho_{IN} \text{ [dB]} = \begin{cases} -0.0673 \times R_b^6 + 1.5397 \times R_b^5 - 14.3404 \times R_b^4 + 69.4089 \times R_b^3 \\ -184.0043 \times R_b^2 + 255.3831 \times R_b - 154.0503, & 1.7 \leq R_b \text{ [Mbps]} < 3.5 \\ -0.0202 \times R_b^4 + 0.5189 \times R_b^3 \\ -4.7933 \times R_b^2 + 20.2255 \times R_b - 37.2841, & 3.5 \leq R_b \text{ [Mbps]} < 6.4 \\ -0.0202 \times R_b^4 + 0.5189 \times R_b^3 \\ -0.0579 \times R_b^2 + 2.1091 \times R_b - 14.0231, & 6.4 \leq R_b \text{ [Mbps]} < 7.0 \\ -0.0817 \times R_b^2 + 2.4592 \times R_b - 13.2108, & 7.0 \leq R_b \text{ [Mbps]} < 7.8 \\ -0.0933 \times R_b^3 + 2.5064 \times R_b^2 - 21.1894 \times R_b + 57.9987, & 7.8 \leq R_b \text{ [Mbps]} < 9.5 \\ 0.8613 \times R_b - 5.1806, & 9.5 \leq R_b \text{ [Mbps]} < 14.1 \\ -0.0042 \times R_b^2 + 0.7262 \times R_b - 2.4267, & 14.1 \leq R_b \text{ [Mbps]} < 34.5 \\ 0.0482 \times R_b^2 - 2.879 \times R_b + 60.0064, & 34.5 \leq R_b \text{ [Mbps]} < 42.5 \\ 0.2984 \times R_b^2 - 21.9131 \times R_b + 417.3976, & 42.5 \leq R_b \text{ [Mbps]} \leq 43.2 \end{cases} \quad (\text{D.9})$$

For QPSK, in UL direction, one has:

$$(E_c/N_0) \text{ [dB]} = \begin{cases} -3.33 \times R_b - 10.0, & 0 \leq R_b \text{ [Mbps]} < 1.5 \\ -0.5998 \times R_b^2 + 5.0194 \times R_b - 11.1447, & 1.5 \leq R_b \text{ [Mbps]} < 3.4 \\ -5.2083 \times R_b^3 + 62.5 \times R_b^2 - 244.7917 \times R_b + 313.5, & 3.4 \leq R_b \text{ [Mbps]} < 4.2 \\ -4.3821 \times R_b^3 + 65.5602 \times R_b^2 \\ -321.7734 \times R_b + 521.6365, & 4.2 \leq R_b \text{ [Mbps]} \leq 5.5 \end{cases} \quad (\text{D.10})$$

Considering 16QAM for UL, the  $E_c/N_0$  is given by (D.8). Since the equation in [Jaci09] was not continuous, a modified version of the equation in [Preg08] is presented.

$$(E_c/N_0) \text{ [dB]} = \begin{cases} -1.5432 \times R_b^3 + 6.9444 \times R_b^2 - 6.9444 \times R_b - 3.0, & 0.6 \leq R_b \text{ [Mbps]} < 1.6 \\ 2.0 \times R_b - 6.0, & 1.6 \leq R_b \text{ [Mbps]} < 3.8 \\ 0.1307 \times R_b^4 - 3.041 \times R_b^3 + 26.0522 \times R_b^2 \\ -95.8265 \times R_b + 129.0191, & 3.8 \leq R_b \text{ [Mbps]} < 7.7 \\ 0.1386 \times R_b^3 - 3.5025 \times R_b^2 + 30.979 \times R_b - 87.2192, & 7.7 \leq R_b \text{ [Mbps]} \leq 11.0 \end{cases} \quad (\text{D.11})$$

It is also important to present the inverted expressions, i.e., the throughput as a function of SINR for DL and as a function of  $E_c/N_0$  for UL. Regarding the SISO configuration with QPSK, for DL, the expression is defined by:

$$R_b \text{ [Mbps]} = \begin{cases} 0.0072 \times \rho_N^2 + 0.1743 \times \rho_N + 1.383, & -10 \leq \rho_N \text{ [dB]} < -6 \\ 0.025 \times \rho_N^2 + 0.425 \times \rho_N + 2.25, & -6 \leq \rho_N \text{ [dB]} < -1 \\ 0.00779 \times \rho_N^2 + 0.368 \times \rho_N + 2.193, & -1 \leq \rho_N \text{ [dB]} < 10 \\ -0.0148 \times \rho_N^2 + 0.499 \times \rho_N + 3.0, & 10 \leq \rho_N \text{ [dB]} < 16 \\ 7.2, & \rho_N \text{ [dB]} \geq 16 \end{cases} \quad (\text{D.12})$$

For a SISO configuration with 16QAM, one has:

$$R_b [\text{Mbps}] = \begin{cases} 0.0143 \times \rho_N^2 + 0.3486 \times \rho_N + 2.7657, & -10 \leq \rho_N [\text{dB}] < -6 \\ 0.05 \times \rho_N^2 + 0.85 \times \rho_N + 4.5, & -6 \leq \rho_N [\text{dB}] < -1 \\ 0.0223 \times \rho_N^2 + 0.631 \times \rho_N + 4.3203, & -1 \leq \rho_N [\text{dB}] < 10 \\ -0.05 \times \rho_N^2 + 1.5757 \times \rho_N + 1.9286, & 10 \leq \rho_N [\text{dB}] < 16 \\ 14.4, & \rho_N [\text{dB}] \geq 16 \end{cases} \quad (\text{D.13})$$

For a SISO configuration with 64QAM, the throughput is given by:

$$R_b [\text{Mbps}] = \begin{cases} 0.0143 \times \rho_N^2 + 0.3586 \times \rho_N + 2.7657, & -10 \leq \rho_N [\text{dB}] < -6 \\ 0.0005 \times \rho_N^3 + 0.0208 \times \rho_N^2 + 0.6167 \times \rho_N + 4.3131, & -6 \leq \rho_N [\text{dB}] < 11 \\ -0.0652 \times \rho_N^2 + 2.87 \times \rho_N - 9.7048, & 11 \leq \rho_N [\text{dB}] < 20 \\ 21.6, & \rho_N [\text{dB}] \geq 20 \end{cases} \quad (\text{D.14})$$

In a SIMO 1x2 scheme with QPSK, the expression is defined by:

$$R_b [\text{Mbps}] = \begin{cases} 0.017 \times \rho_N^2 + 0.416 \times \rho_N + 2.973, & -10 \leq \rho_N [\text{dB}] < 3 \\ -0.0404 \times \rho_N^2 + 0.9318 \times \rho_N + 1.824, & 3 \leq \rho_N [\text{dB}] < 13 \\ 7.2, & \rho_N [\text{dB}] \geq 13 \end{cases} \quad (\text{D.15})$$

For a SIMO 1x2 configuration with 16QAM, the throughput can be computed by:

$$R_b [\text{Mbps}] = \begin{cases} 0.03 \times \rho_N^2 + 0.7823 \times \rho_N + 5.8266, & -10 \leq \rho_N [\text{dB}] < 3 \\ -0.0626 \times \rho_N^2 + 1.6255 \times \rho_N + 3.813, & 3 \leq \rho_N [\text{dB}] < 13 \\ 14.4, & \rho_N [\text{dB}] \geq 13 \end{cases} \quad (\text{D.16})$$

Considering a SIMO 1x2 configuration with 64QAM, one has:

$$R_b [\text{Mbps}] = \begin{cases} 0.0255 \times \rho_N^2 + 0.7265 \times \rho_N + 5.6914, & -10 \leq \rho_N [\text{dB}] < -1 \\ 0.0105 \times \rho_N^2 + 0.8517 \times \rho_N + 5.783, & -1 \leq \rho_N [\text{dB}] < 13 \\ -0.0542 \times \rho_N^2 + 2.2154 \times \rho_N - 0.9696, & 13 \leq \rho_N [\text{dB}] < 19 \\ 21.6, & \rho_N [\text{dB}] \geq 19 \end{cases} \quad (\text{D.17})$$

For a MIMO 2x2 scheme with QPSK, the throughput is defined by:

$$R_b [\text{Mbps}] = \begin{cases} -0.00695 \times \rho_N^3 - 0.1357 \times \rho_N^2 - 0.6502 \times \rho_N + 0.9762, & -10 \leq \rho_N [\text{dB}] < -5 \\ -0.00042 \times \rho_N^3 + 0.0151 \times \rho_N^2 + 0.435 \times \rho_N + 3.592, & -5 \leq \rho_N [\text{dB}] < 10 \\ -0.0523 \times \rho_N^2 + 2.009 \times \rho_N - 4.904, & 10 \leq \rho_N [\text{dB}] < 20 \\ 14.4, & \rho_N [\text{dB}] \geq 20 \end{cases} \quad (\text{D.18})$$

For a MIMO 2x2 configuration with 16QAM, one has:

$$R_b [\text{Mbps}] = \begin{cases} -0.0139 \times \rho_N^3 - 0.2714 \times \rho_N^2 - 1.3004 \times \rho_N + 1.9524, & -10 \leq \rho_N [\text{dB}] < -5 \\ 0.0021 \times \rho_N^3 + 0.0209 \times \rho_N^2 + 0.7905 \times \rho_N + 7.0537, & -5 \leq \rho_N [\text{dB}] < 10 \\ -0.0722 \times \rho_N^2 + 3.1463 \times \rho_N - 5.2526, & 10 \leq \rho_N [\text{dB}] < 20 \\ 28.8, & \rho_N [\text{dB}] \geq 20 \end{cases} \quad (\text{D.19})$$

In a MIMO 2x2 configuration with 64QAM, the physical throughput is given by:

$$R_b [\text{Mbps}] = \begin{cases} -0.0083 \times \rho_N^3 - 0.1357 \times \rho_N^2 - 0.2131 \times \rho_N + 4.8057, & -10 \leq \rho_N [\text{dB}] < -6 \\ 0.0005 \times \rho_N^4 + 0.0018 \times \rho_N^3 \\ + 0.0089 \times \rho_N^2 + 0.7812 \times \rho_N + 7.0784, & -6 \leq \rho_N [\text{dB}] < 1 \\ -0.001 \times \rho_N^3 + 0.0657 \times \rho_N^2 + 0.5792 \times \rho_N + 7.211, & 1 \leq \rho_N [\text{dB}] < 4 \\ 0.008 \times \rho_N^3 - 0.0593 \times \rho_N^2 + 0.8046 \times \rho_N + 6.0472, & 4 \leq \rho_N [\text{dB}] < 13.5 \\ -0.0757 \times \rho_N^2 + 4.3661 \times \rho_N - 19.392, & 13.5 \leq \rho_N [\text{dB}] < 26.5 \\ 43.2, & \rho_N [\text{dB}] \geq 26.5 \end{cases} \quad (\text{D.20})$$

For UL, for QPSK configuration, the physical throughput as a function of  $E_c/N_0$  is given by:

$$R_b [\text{Mbps}] = \begin{cases} 0.0643 \times (E_c/N_0)^2 + 0.8557 \times (E_c/N_0) + 4.18, & -5 \leq (E_c/N_0)_{[\text{dB}]} < -1 \\ -0.05 \times (E_c/N_0)^2 + 0.31 \times (E_c/N_0) + 3.77, & -1 \leq (E_c/N_0)_{[\text{dB}]} < 2 \\ 0.0417 \times (E_c/N_0)^3 - 0.5429 \times (E_c/N_0)^2 \\ + 2.5012 \times (E_c/N_0) + 1.04, & 2 \leq (E_c/N_0)_{[\text{dB}]} < 6 \\ 5.5, & (E_c/N_0)_{[\text{dB}]} \geq 6 \end{cases} \quad (\text{D.21})$$

For UL, for 16QAM configuration, the physical throughput can be computed by:

$$R_b [\text{Mbps}] = \begin{cases} -0.0087 \times (E_c/N_0)^4 - 0.0669 \times (E_c/N_0)^3 - 0.0936 \times (E_c/N_0)^2 \\ + 0.6056 \times (E_c/N_0) + 3.0522, & -5 \leq (E_c/N_0)_{[\text{dB}]} < -3 \\ 0.0333 \times (E_c/N_0)^4 + 0.1 \times (E_c/N_0)^3 - 0.0333 \times (E_c/N_0)^2 \\ + 0.4 \times (E_c/N_0) + 3.0, & -3 \leq (E_c/N_0)_{[\text{dB}]} < 1 \\ 0.0583 \times (E_c/N_0)^3 - 0.575 \times (E_c/N_0)^2 \\ + 2.3667 \times (E_c/N_0) + 1.66, & 1 \leq (E_c/N_0)_{[\text{dB}]} < 5 \\ -0.0003 \times (E_c/N_0)^3 - 0.0195 \times (E_c/N_0)^2 \\ + 0.9558 \times (E_c/N_0) + 2.1899, & 5 \leq (E_c/N_0)_{[\text{dB}]} < 14 \\ 11.0, & (E_c/N_0)_{[\text{dB}]} \geq 14 \end{cases} \quad (\text{D.22})$$

# Annex E – User’s Manual

This annex describes the simulator user interface step by step. The graphical interface was developed to be as intuitive as possible.

When opening the program’s executable, one can notice the first window presenting the title and author of the simulator. The second window is the one corresponding to the main window, where the user has access to several menus that execute different options of the software. These menus are: *File*, *Outdoor Environment*, *Outdoor Parameters* and *Indoor Simulation*. In the beginning, only the *File* and *Outdoor Environment* menus are available, Figure E.1. These options can be selected by clicking on the menus.



Figure E.1. Main window of the UMTSIndCov simulator.

On the *File* menu, one can exit the program (File->Exit). On the *Outdoor Environment* menu, one can define the BS and obstacle buildings’ characteristics, such as antenna’s and buildings’ height,  $w_s$ ,  $w_b$  and number of obstacle buildings, Figure E.2. The user can check a tick box to mark that the MT is on the same building as the BS. After all values are filled in, one can click in the *OK* button to save the information. When the characteristics are defined, the *Outdoor Parameters* menu is enabled.

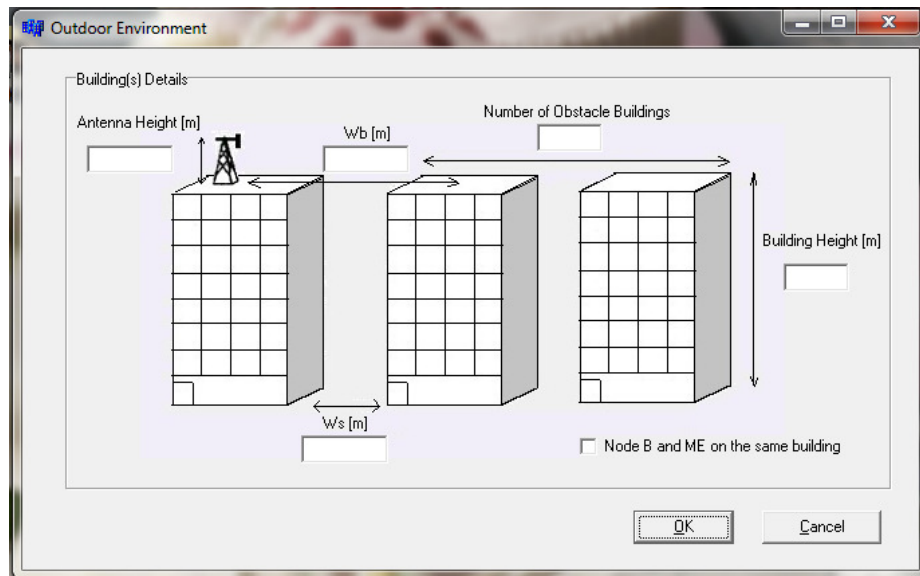


Figure E.2. Outdoor Environment window.

On the *Outdoor Parameters* menu, one can define the environment characteristics, such as the antenna configuration, the fast fading distribution standard deviation, the slow fading margin, the BS transmission power and radiation pattern (by importing a Kathrein antenna file [Kath11]), the MT transmission power and antenna gain, the receiver's noise figure, the user body and cable losses, the antenna tilt and its variation, Figure E.3. The user can fill in these parameters or press the *Default* button, in combination with the *Downlink/Uplink* option. This option sets the specific parameters for each type of link.

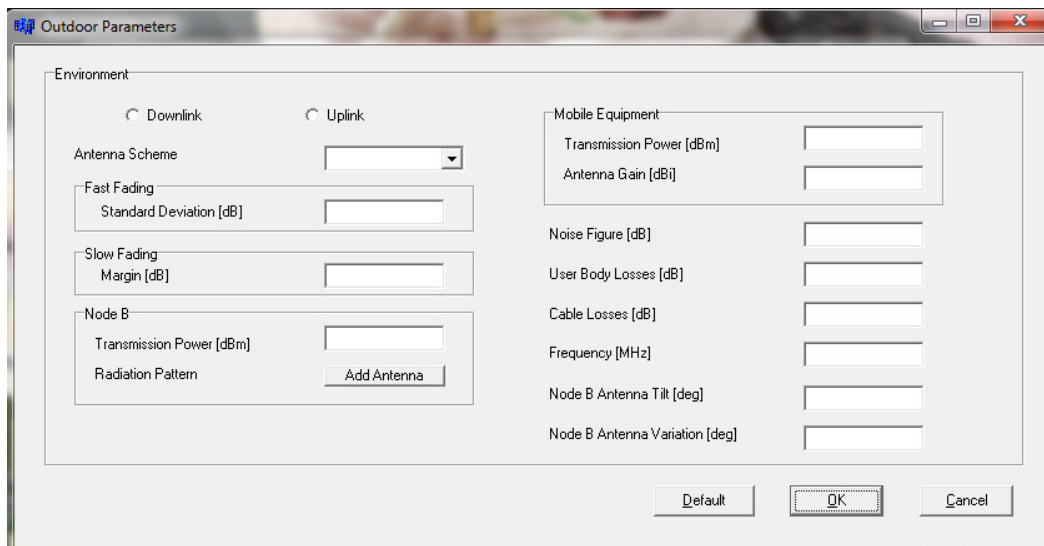


Figure E.3. Other Parameters window.

After introducing the outdoor variables, one can select the type of simulation on the *Indoor Simulation* menu. The two options are *Coverage Simulation* (File->Coverage Simulation) and *Capacity Simulation*

(File->Capacity Simulation). While the former is the implementation of the Single-User Model, the latter implements the Multi-User Model, both described in Section 3.2.

For the *Coverage Simulation*, one is able to choose the building type (High/Low and Integrated/Isolated), the room category (IW, ID or DI), the MT building number of floors and the desired coverage in percentage, Figure E.4. The *Run!* button starts the computation and its completion is marked by the full progress bar. The *Open Output File* button is highlighted when the simulation is over and can be pressed, allowing the user to see the simulation results.

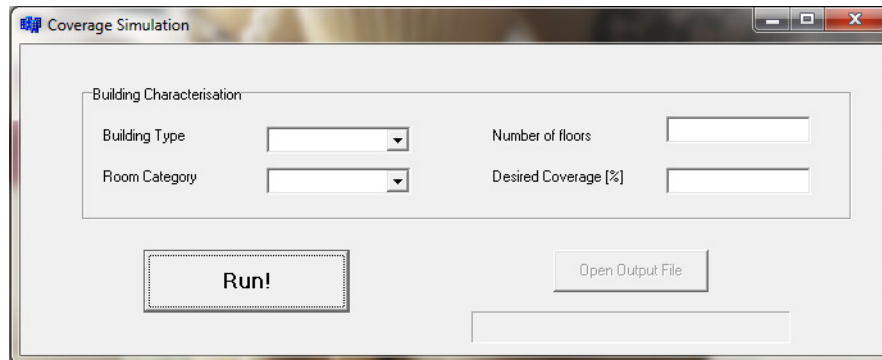


Figure E.4. Coverage Simulation window.

In the *Capacity Simulation*, the user is prompted to choose the desired simulation mode, according to the model overviewed in Subsection 3.2.2. The *Auto* mode allows the program to cover all the available data rates for the defined HSPA+ configuration and proceed with the computations (through the use of the *Run!* button). After the simulation completion, the *Open Output File* button becomes available and the user is able to see the simulation results. The *Manual* mode is able to deliver the output instantaneously by inserting the desired data rate, Figure E.5. The *Run!* button starts the computation and its completion is marked by the full progress bar.

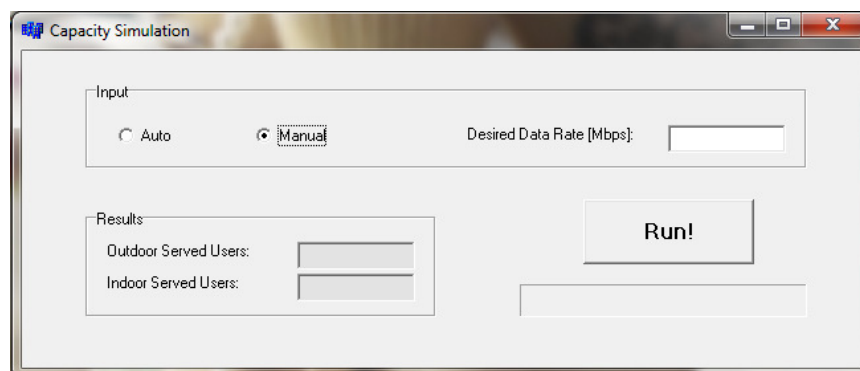


Figure E.5. Capacity Simulation window.



# Annex F – Measurements Results

In this annex, measurements results for each building are analysed, using graphs to show the main indicators and curve tendencies. A brief building description is done and any particularity concerning the values is referred in the text, such as the measured floors and rooms, and the explanation for any unexpected result.

The results were grouped by building type, as mentioned in Section 3.1. Concerning room attenuation, the mean and standard deviation values were calculated for each building type, according to (3.10) and (3.11). Regarding floor attenuation, the floor mean value is presented for all room types.

Figure F.1, Figure F.2, Figure F.3 and Figure F.4 show the average RSCP attenuation values for all four building types. Results show there is a virtual RSCP gain between building floors for most buildings, mainly due to the increase of LoS when moving to upper floors. Nevertheless, most Deep Indoor rooms show poor results, as the attenuation increases with the increase of MT height. This behaviour is also present in other room types for Low Isolated buildings: the attenuation increases in upper floors possibly due to poor propagation inside the buildings (influence of curtains and other materials inside the rooms).

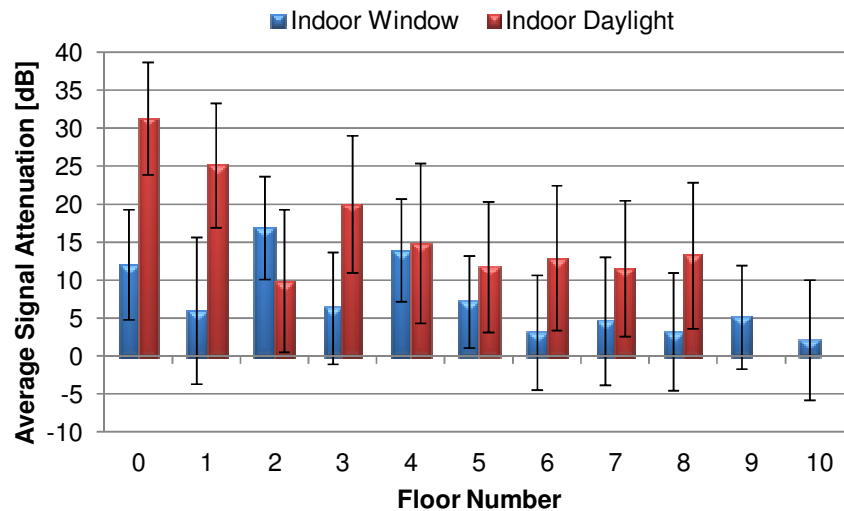


Figure F.1. RSCP attenuation values for High Integrated buildings in floor transitions.

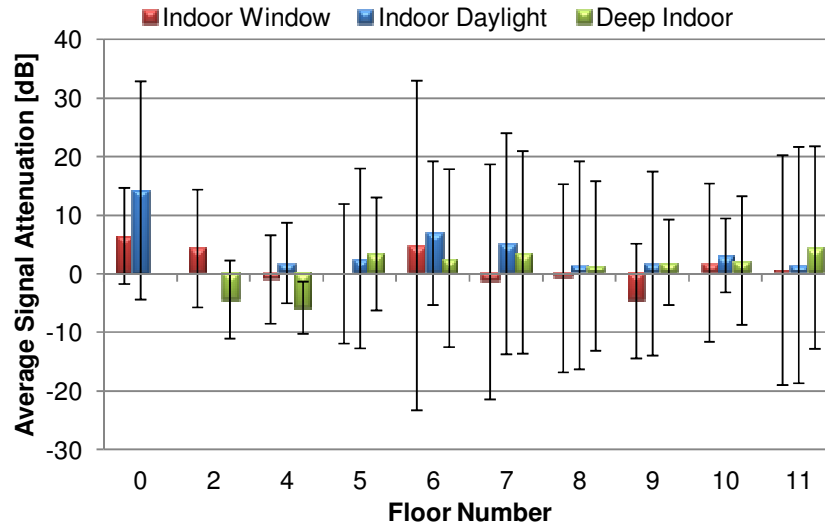


Figure F.2. RSCP attenuation values for High Isolated buildings in floor transitions.

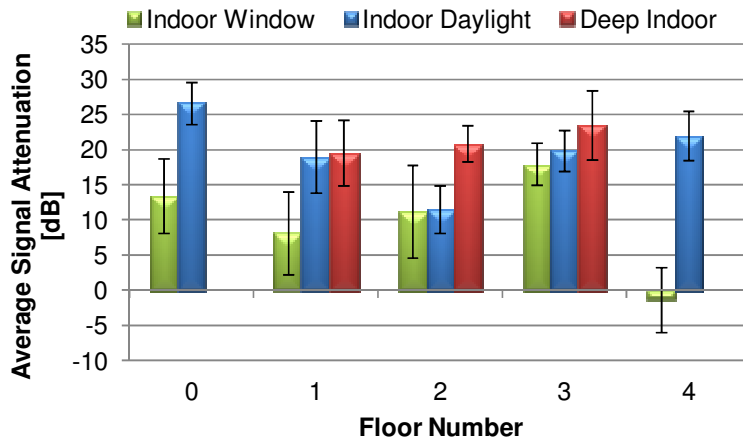


Figure F.3. RSCP attenuation values for Low Integrated buildings in floor transitions.

Figure F.5, Figure F.6, Figure F.7 and Figure F.8 show DL throughput attenuation values for all four building types. Similarly to RSCP, there is a virtual throughput gain between building floors for most buildings. High Isolated buildings show the opposite behaviour though: the interference power is high due to the greater exposure to several BSs, resulting in a reduction in SINR and therefore in throughput. Low Isolated buildings also show an increase of attenuation, although the interference is not as influencing as in High buildings: it might be caused by a reduction of the number of codes given to the user or a sudden increase on the network's load. Particularly for Low Integrated buildings, upper floor shows an unexpected throughput loss, which might also be due to the reasons explained earlier.

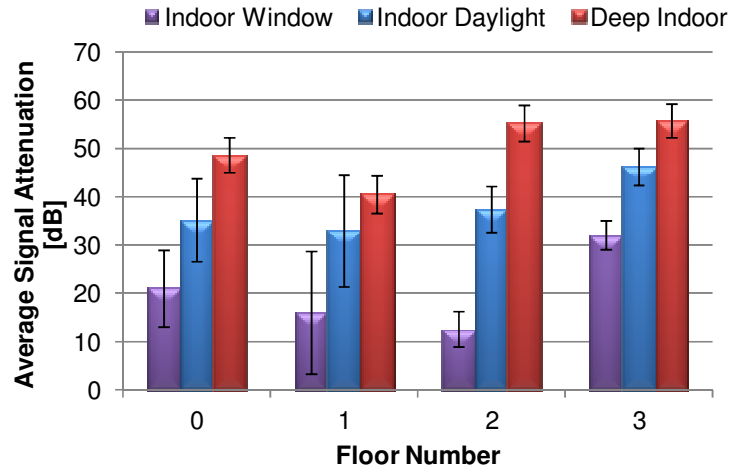


Figure F.4. RSCP attenuation values for Low Isolated buildings in floor transitions.

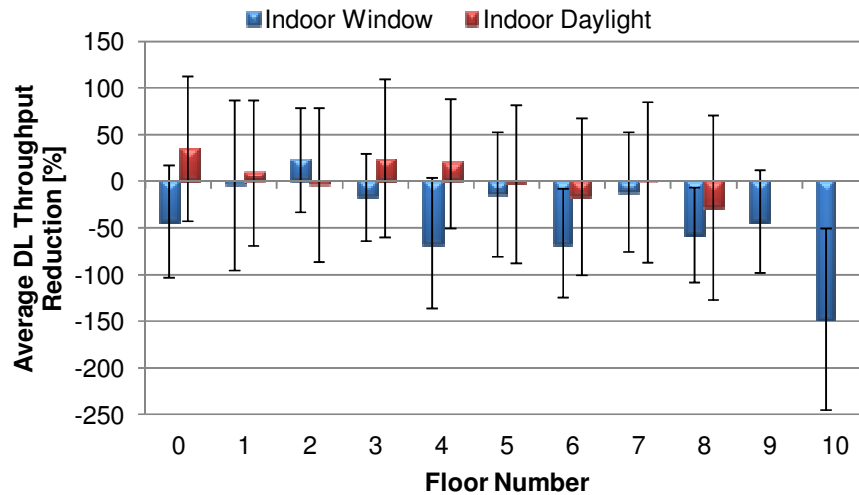


Figure F.5. DL throughput attenuation values for High Integrated buildings in floor transitions.

Figure F.9, Figure F.10, Figure F.11 and Figure F.12 show UL throughput attenuation values for all four building types. In High Isolated buildings, UL was not measured for Indoor Daylight rooms because the UL measuring software was not mastered yet by the author. Results show a great similarity with DL throughput ones, with a increasing gain when the MT height increases. The only exception is Low Integrated results, which show a growing attenuation: this can be explained by the change in the TTI value, which limits the UL maximum throughput, as stated in Subsection 4.2.2.

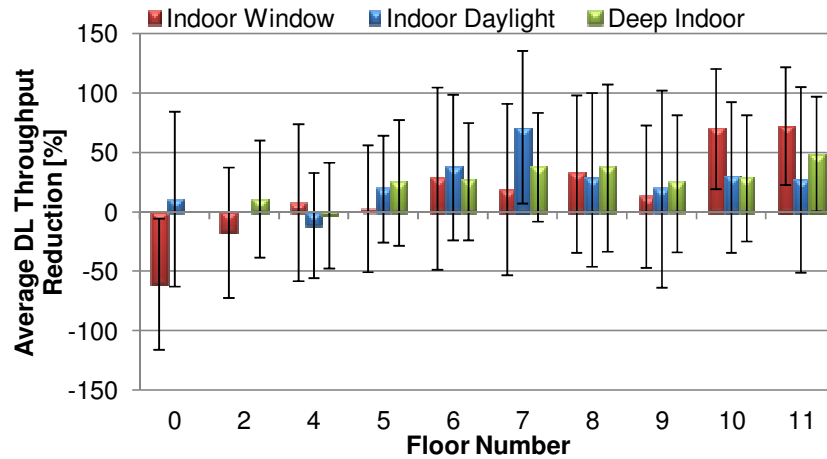


Figure F.6. DL throughput attenuation values for High Isolated buildings in floor transitions.

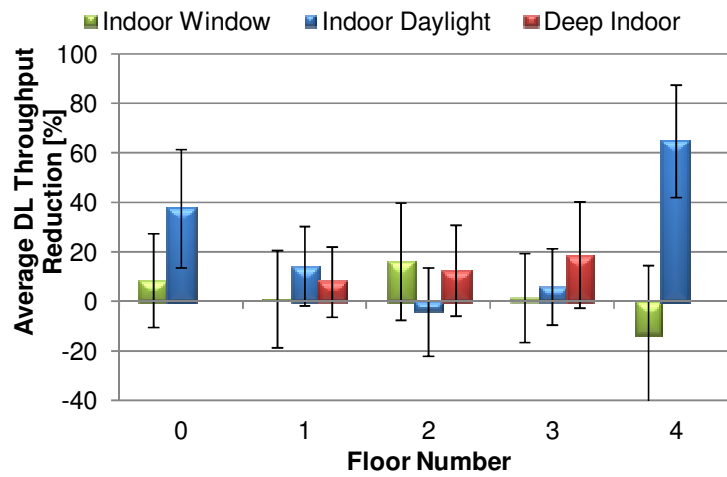


Figure F.7. DL throughput attenuation values for Low Integrated buildings in floor transitions.

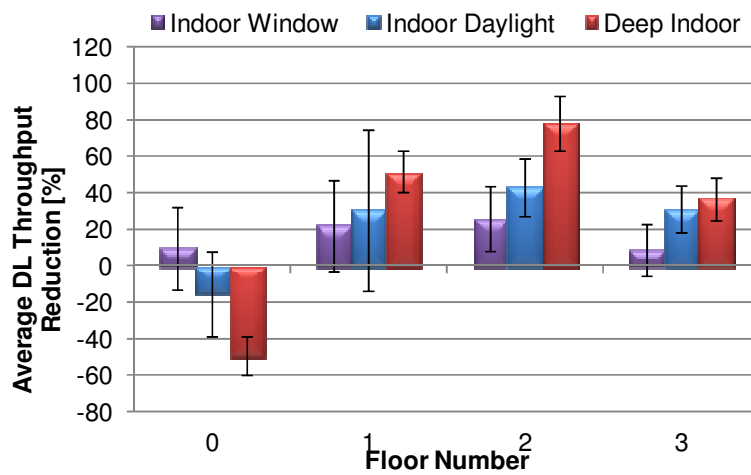


Figure F.8. DL throughput attenuation values for Low Isolated buildings in floor transitions.

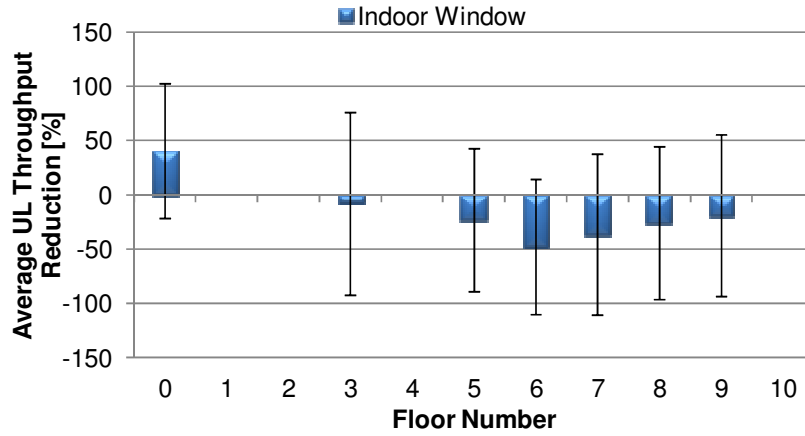


Figure F.9. UL throughput attenuation values for High Isolated buildings in floor transitions.

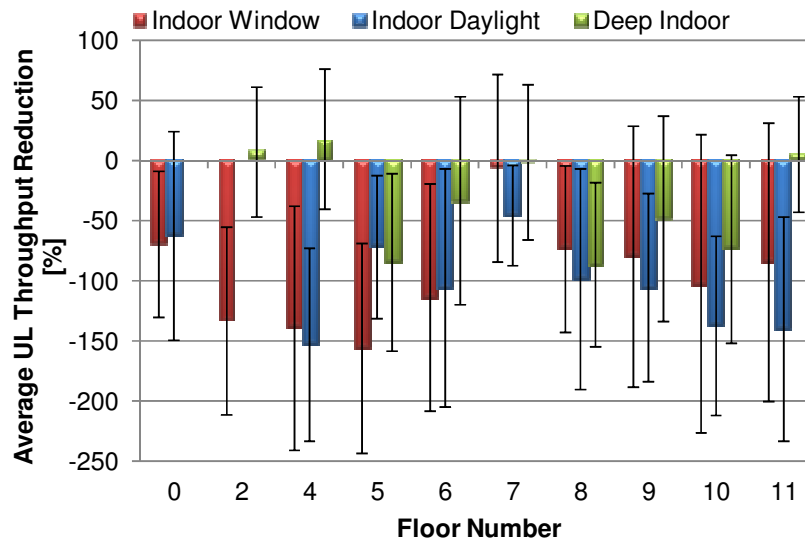


Figure F.10. UL throughput attenuation values for High Integrated buildings in floor transitions.

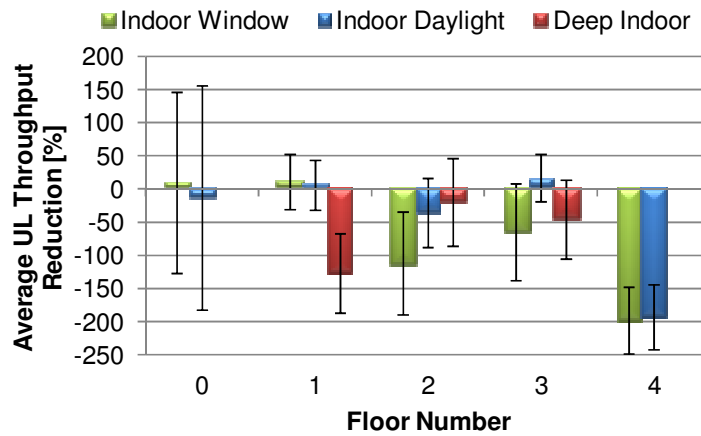


Figure F.11. UL throughput attenuation values for Low Isolated buildings in floor transitions.

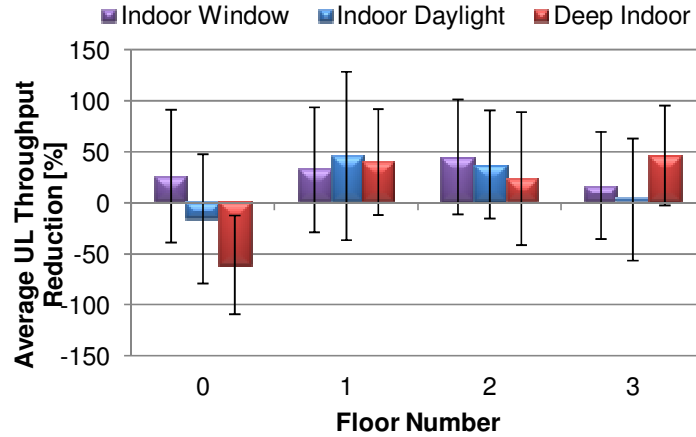


Figure F.12. UL throughput attenuation values for Low Integrated buildings in floor transitions.

The standard deviation quadratic mean was performed for all floors and presented in Table F.1, calculated by (3.11). One can notice that the standard deviations for UL throughput are generically higher than the ones for DL mainly due to TTI change in the measurement procedure. More, High buildings show greater throughput variations than the Low ones, which might be due to the interference exposure, and therefore throughput loss.

Table F.1. Standard deviations for the measured attenuations.

| Building Type | Standard Deviation    |       |       |                       |       |       |                       |       |       |
|---------------|-----------------------|-------|-------|-----------------------|-------|-------|-----------------------|-------|-------|
|               | $\Delta R_{SCP}$ [dB] |       |       | $\Delta R_b$ (DL) [%] |       |       | $\Delta R_b$ (UL) [%] |       |       |
|               | IW                    | ID    | DI    | IW                    | ID    | DI    | IW                    | ID    | DI    |
| <b>HInt</b>   | 7.54                  | 9.07  |       | 66.86                 | 83.13 |       | 66.26                 |       |       |
| <b>HIso</b>   | 15.74                 | 15.43 | 12.34 | 61.16                 | 66.47 | 52.97 | 93.85                 | 80.22 | 69.70 |
| <b>LInt</b>   | 5.22                  | 3.68  | 4.18  | 21.90                 | 19.54 | 18.28 | 82.78                 | 85.49 | 61.78 |
| <b>LIso</b>   | 7.88                  | 7.83  | 3.73  | 20.36                 | 26.92 | 12.26 | 58.95                 | 65.59 | 54.09 |

The room transition is performed according to the room classification in Section 3.1. For each building type, the attenuation between the outdoor reference value and the respective indoor room is presented. For all measured attenuations, (3.10) was used to compute the mean value of each room type.

Figure F.13 presents the RSCP attenuation values for all room transitions. One can notice increasing RSCP loss for inner rooms. The lower attenuations in High buildings are due to more intense exposure to the BS. The greater attenuations shown in Low Isolated buildings are mainly due to the thick walls that cause a greater signal power loss. The lack of values for Deep Indoor rooms in High Integrated buildings is explained by the absence of this room type inside these buildings.

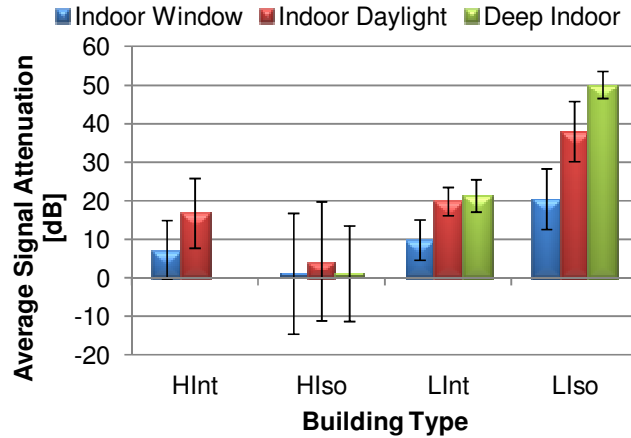


Figure F.13. RSCP attenuation values in room transitions.

Figure F.14 presents DL throughput attenuation values for all room transitions. Again, the presented values are relative and not absolute in order to scale these results to other HSPA+ configurations. The similarity between the absolute and the relative variation is evident, therefore only the relative analysis is performed. Most results follow the same trend as the RSCP variation, with some exceptions: the High Integrated buildings were located in highly dense urban areas, where the presence of high interference power decreases significantly the outdoor available throughput. In these cases, the indoor placement benefits throughput due to interference attenuation. This is also noticeable in Deep Indoor rooms of High Isolated buildings.

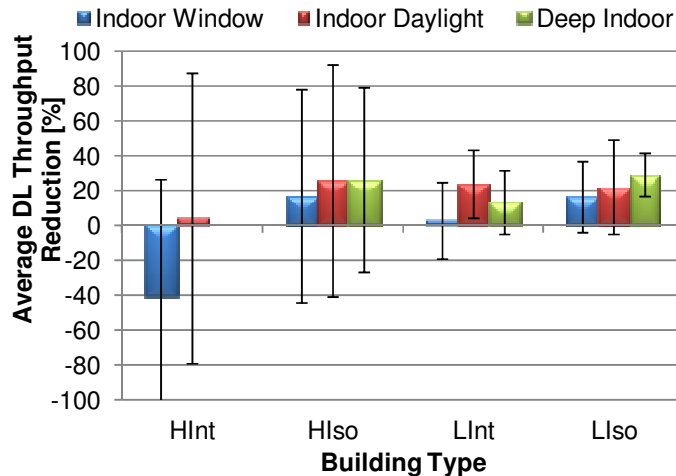


Figure F.14. DL throughput attenuation values in room transitions.

Figure F.15 presents UL throughput attenuation values for all room transitions. The results for HInt and Llso are roughly coherent with RSCP variation, whereas for Hlso and LInt one cannot find the same relation. The UL throughput gain shown in Hlso and LInt buildings might be greatly due to changes in TTI, which inserts a limit in the maximum UL throughput. Despite this hypothesis, the UL

analysis has to be carefully made, following the reasons stated in Subsection 4.2.2.

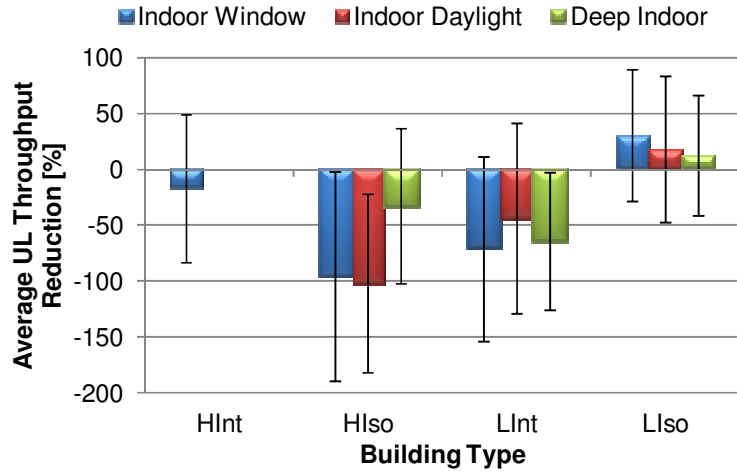


Figure F.15. UL throughput attenuation values in room transitions.

Regarding DL modulation usage, Figure F.16, Figure F.17, Figure F.18 and Figure F.19 present the measured values for each building type. These values are averages of all samples in a specific room type for each building type. Since the modulation scheme can be changed every TTI, the software only shows the percentage of each modulation usage in each sample, which is a good parameter for the measurements analysis. The standard deviation is not presented since its values are mathematically inconsistent (the usage percentage could be over 100 %).

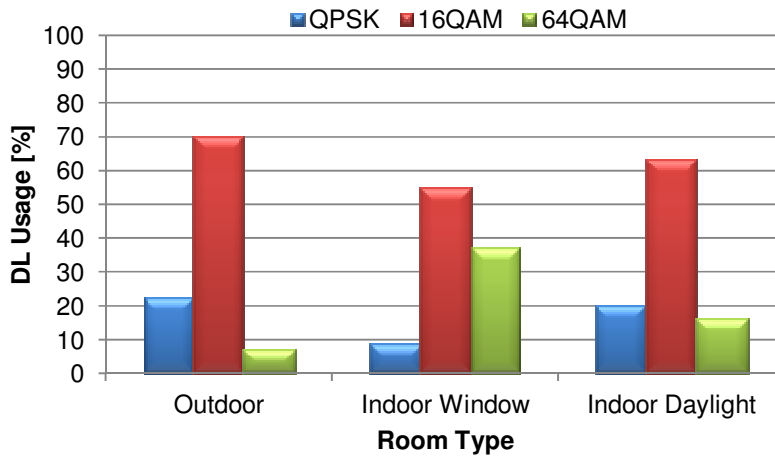


Figure F.16. DL modulation usage for High Integrated buildings.

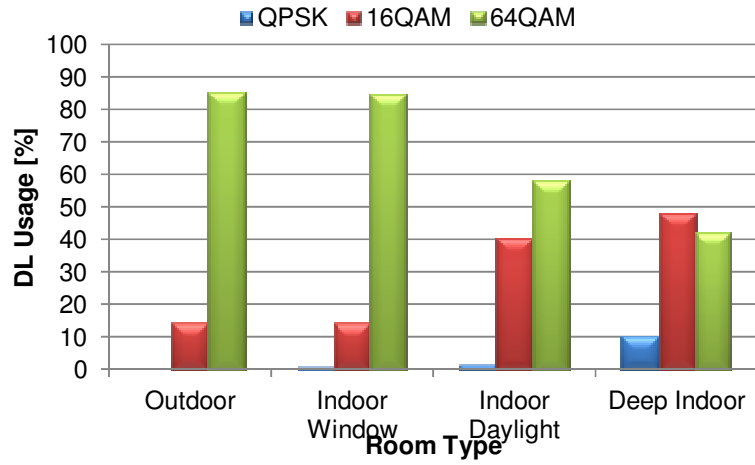


Figure F.17. DL modulation usage for High Isolated buildings.

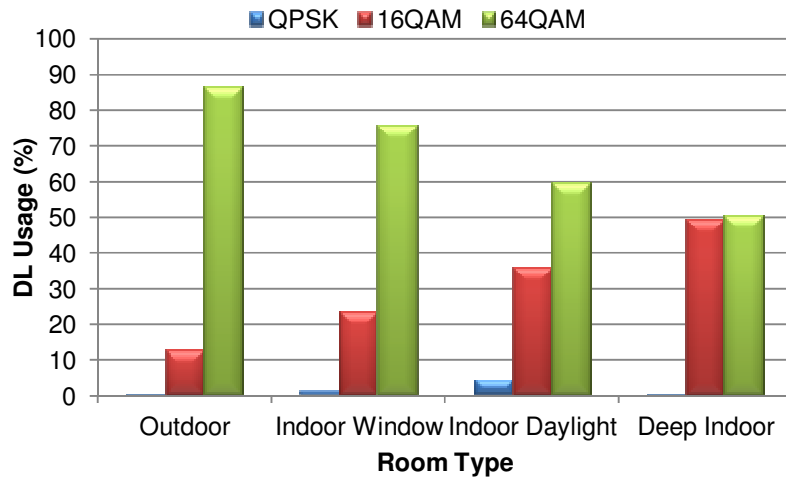


Figure F.18. DL modulation usage for Low Integrated buildings.

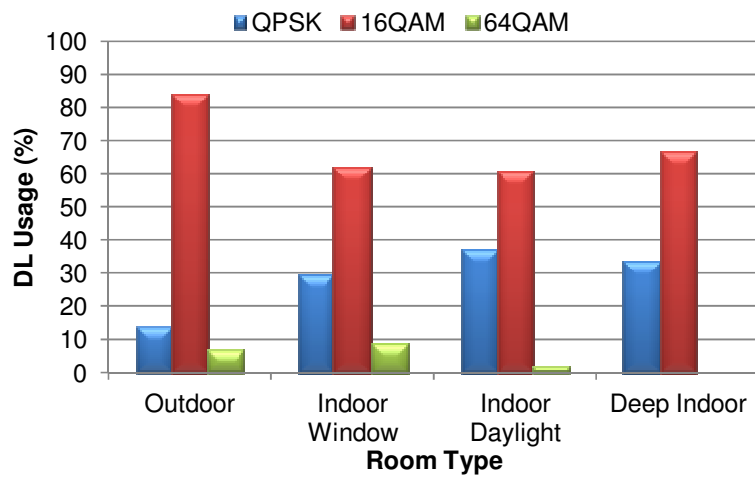


Figure F.19. DL modulation usage for Low Isolated buildings.

In the room comparison, almost all buildings show a decrease in the modulation index usage percentage when going inner inside the building, since signal power decreases due to wall attenuation. All High buildings show a great usage of 16QAM (more than 50 % for all rooms). Integrated ones show a greater percentage of 64QAM (usually above 30 %), whereas in Isolated ones, it is more likely to find QPSK (also roughly 30 %), mainly due to increase of the average interference power in upper floors, that is significantly higher in Isolated cases and where a more robust modulation is required. Low buildings show a great usage of 64QAM mostly due to the proximity to BS, in most cases being higher than 50 %. 16QAM is the second preferred modulation in these buildings. QPSK has a residual percentage in Low buildings, which indicates signal quality.

Concerning UL, the equipment does not perform other modulations other than QPSK, not using the full potentialities of HSPA+ UL. Therefore, UL modulation usage is the same as DL one, but only considering QPSK and 16QAM as possible modulations.

The measurements software was also capable of measuring SIR in each sample. Despite being an interesting parameter to analyse, its value is measured on the pilot channel (HS-DPCCH) and not on the data channel (HS-DSCH). As it can be seen in Figure 2.3, increase of SIR leads to throughput increase. Since SIR is measured on the pilot channel, the effect is the opposite: when SIR rises, more requests are made, and therefore availability in terms of throughput decreases. Figure F.20 shows the measured curves on the pilot channel for each building type, and also the theoretical ones obtained for the data channel, indicating in which channel each one is measured.

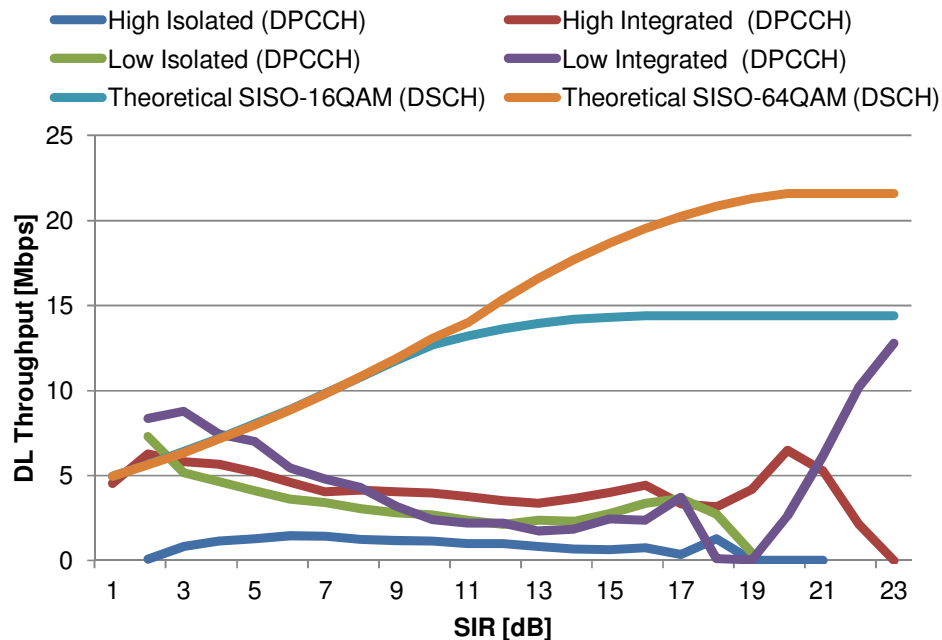


Figure F.20. Mapping between SIR and DL throughput for the different building types.

# Annex G – Application Layer Throughput

The purpose of this annex is to evaluate the performance of HSPA+ in the application layer, rather than in the physical layer, according to the OSI Reference Model [Zimm80]. Although the measured throughputs are referred to the physical layer, one should consider that the actual throughput given to the MT user is referred to the application layer. Therefore, several overheads must be considered, each one introduced by the respective layer. Moreover, the throughputs presented in the physical layer consider the use of all the HS-PDSCH codes, though this might not always happen in a real situation. It is then necessary to obtain the throughput per code.

For HSPA+ DL, from (G.1) one can compute the maximum throughput at the physical layer for a given modulation per HS-PDSCH code. For instance, using 16QAM (4 symbols per bit) with a SISO configuration, the maximum throughput at the physical layer per HS-PDSCH code is 0.96 Mbps, which means 4.8, 9.6 and 14.4 Mbps for 5, 10 and 15 codes, respectively. Although the usual assumption is to have 15 HS-PDSCH codes for data in the MT, only 14 codes are truly available. The remaining 2 HS-SCCH codes are used for signalling and control functions. From now on, it is referred 15 HS-PDSCH codes, although the analysis performed considers that only 14 HS-PDSCH codes are available for data. Thus, the maximum throughput achieved at the physical layer is 13.44 Mbps for 16QAM with a SISO configuration.

$$SF_{16} = \frac{R_c [\text{Mcps}]}{S_R [\text{MHz}]} = \frac{R_c [\text{Mcps}]}{R_{b/code} / S_b} \Leftrightarrow R_{b/code} = \frac{R_c [\text{Mcps}]}{SF_{16} / S_b} \quad (\text{G.1})$$

where:

- $S_R$  is the symbol rate;
- $S_b$  is the symbols per bit;
- $R_{b/code}$  is the physical layer throughput per code.

As stated before, the real throughput achieved by the MT user is not the one measured at the physical layer, mainly because of the overheads in each OSI layer and the coding rate. The following overheads are taken into account, in DL: RLC (2.5 % for an average packet size of 656 bits) and MAC (3.125 % for an average packet size of 792 bits), according to [3GPP07]; application (5 %); and BLER requirements (10 %). This indicates that a total overhead of 19.24 % is present at the physical throughput, i.e., the application throughput is 80.76 % of the physical throughput. For UL, the same overheads apply, with a small change in the RLC one (0.625 % for an average packet size of 2576 bits) [3GPP07]. The total overhead in UL is therefore 17.69 % of the physical throughput.

As for the coding rate, it is assumed that the radio channel conditions are well-known, which means that the coding rate is 100 %. This way it is possible to know the maximum range of the cell for a determined service throughput.

The maximum application throughput is limited by both modulation and configuration chosen. The maximum DL throughputs at the physical layer and at the application level for different modulation schemes and antenna configurations are presented in Table G.1.

Table G.1. Maximum physical and application throughput for different configurations in HSPA+ DL  
(extracted from [Preg08]).

| <b>Configuration</b> | <b>Modulation</b> | <b>Maximum throughput [Mbps] (physical layer) – 15 codes</b> | <b>Maximum throughput [Mbps] (physical layer) – 14 codes</b> | <b>Throughput [Mbps] (application layer)</b> |
|----------------------|-------------------|--|--|--|
| 1×1 (SISO)           | 16QAM             | 14.4   | 13.44  | 10.89  |
| 1×1 (SISO)           | 64QAM             | 21.6   | 20.16  | 16.33  |
| 2×2 (MIMO)           | 16QAM             | 28.8   | 26.88  | 21.77  |
| 2×2 (MIMO)           | 64QAM             | 43.2   | 40.32  | 32.66  |

# Annex H – Normal Distribution Validation

In order to input the RSCP transition values in the model and also compare the simulated throughput with the measured one, the Log-Normal distribution assumption (stated in Section 3.1) needs to be verified. Not only must the measured distributions for RSCP and throughputs be validated, but most importantly the distribution of the difference between each floor/room, i.e., the transitions in the horizontal and vertical axis. The cross-correlation gives the probability density of the difference between two independent random variables. Figure H.1 and Figure H.2 show the upper floor outdoor-IW transition probability density function (PDF) in Torre Norte for RSCP and DL/UL throughputs, respectively. In order to quantify the similarity of these distributions with the normal one, a statistical hypothesis test was performed for each distribution, namely the Student's  $t$ -test. The tested hypothesis was the similarity between the difference distribution and a randomly generated normal distribution with the same mean and equal standard deviation.

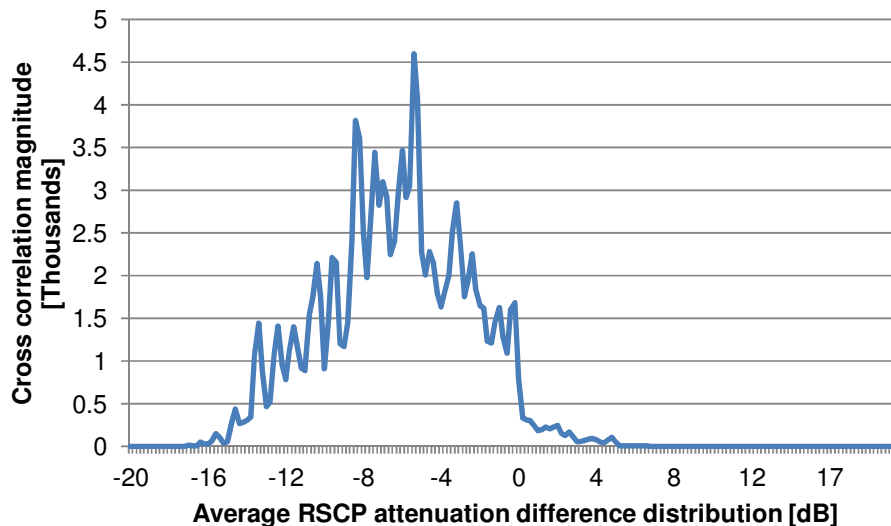


Figure H.1. PDF of the signal attenuation between outdoor and IW scenarios (Torre Norte, 11<sup>th</sup> floor).

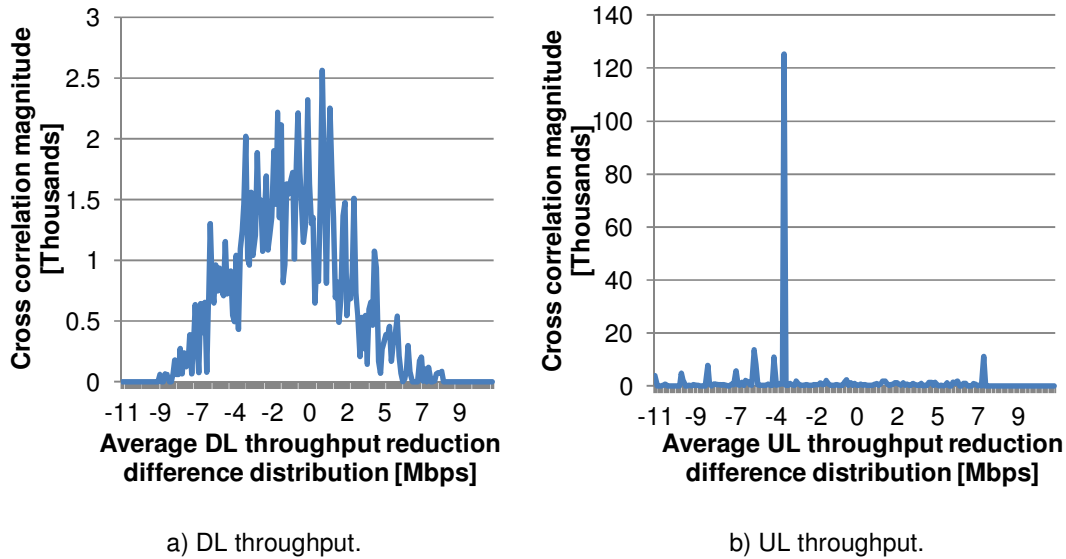


Figure H.2. PDF of the throughput attenuation distribution between outdoor and IW (Torre Norte - 11<sup>th</sup> floor).

Several tests were performed although only a few representative ones are presented. All tests were performed at a 5 % significance level. The resulting p-value indicates the probability of obtaining a statistic test at least as extreme as the one that was actually observed. The correspondent p-values for the presented distributions are presented in Table H.1.

Table H.1. Hypothesis test results.

| Parameter | $\Delta R_{SCP}$ | $\Delta R_b$ (DL) | $\Delta R_b$ (UL) |
|-----------|------------------|-------------------|-------------------|
| p-value   | 0.601            | 0.599             | 0.634             |

All presented p-values are greater than the significance level (0.05) therefore one should not reject the null hypothesis, i.e., the similarity of the resulting distribution with a normal one. Despite this, the visual analysis of the distributions does not show the same results. Although both the RSCP and DL throughput show a good approximation, the UL throughput cannot be approximated as a normal distribution, resulting in a single relevant value, as shown in Figure H.2.b). Therefore, all conclusions concerning the UL throughput should be taken carefully later on.

# Annex I – Indoor Signal Attenuation

## Model Validation

For the purpose of this work, the indoor signal attenuation model has to be constructed based on the measurements campaign since the previous works on indoor attenuation are not satisfactory. Although the campaign has produced some outputs, the low number of measured buildings and the lack of some types of rooms in those buildings make the results less significant than one could expect. [SLCM05] complements this thesis results since more measurements were taken, providing a more significant analysis. Since some results presented in Annex F are not robust enough, the models for these are extracted from [SLCM05]. Furthermore, the existing results in Annex F are to be compared with the ones in [SLCM05] in order to verify if the correct model usage.

The signal penetration results in [SLCM05] were made for GSM900, therefore are not in the same frequency band as the measurements in this work. The authors in [SLCM05] also made measurements in the UMTS band and suggest a 1.9 dB correction to the presented values, being the attenuation in the UMTS bands greater than the GSM ones. The presented values are the corrected ones.

Figure I.1 and Figure I.2 show the signal attenuation value in each floor for the measurements in the current work (UMTS) and the measurements in [SLCM05] (GSM), considering the Indoor Window rooms inside High Integrated buildings. One can notice the same behaviour in both trend lines therefore the results in [SLCM05] may be used in the indoor signal attenuation model. Figure I.3, Figure I.4, Figure I.5 and Figure I.6 show the remaining comparisons for the adopted models in Table 4.4. The same behaviour can be found in these figures despite the differences in the absolute values.

Since the measured floor numbers are not the same as the measured in [SLCM05] performing the correlation factor would be conceptually incorrect. Therefore the choice is not to analyse the measured values but the trend lines graphically, in order to understand their mutual behaviour.

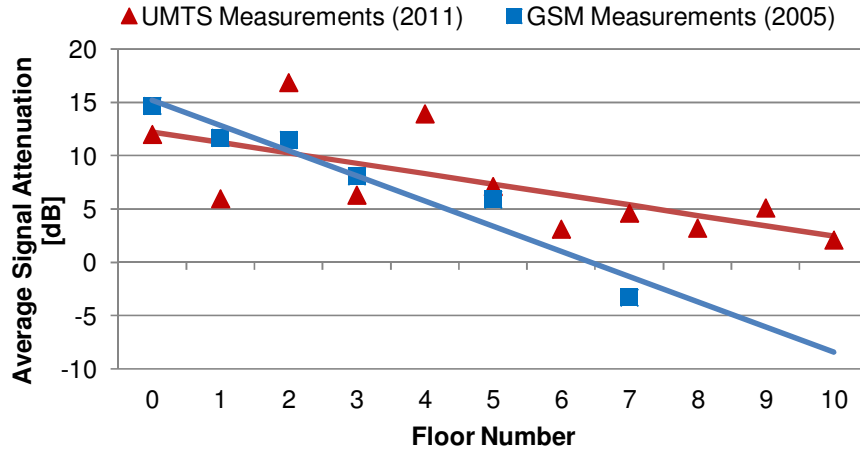


Figure I.1. Signal attenuation values for Indoor Window rooms in High Integrated buildings.

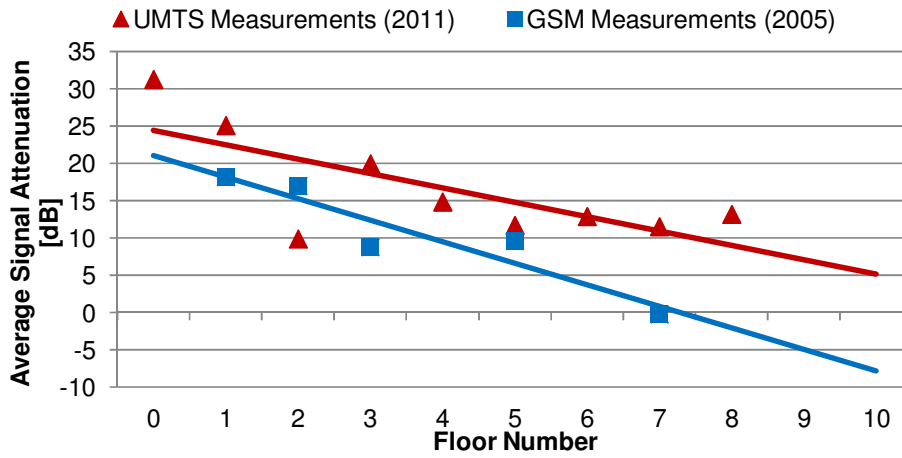


Figure I.2. Signal attenuation values for Indoor Daylight rooms in High Integrated buildings.

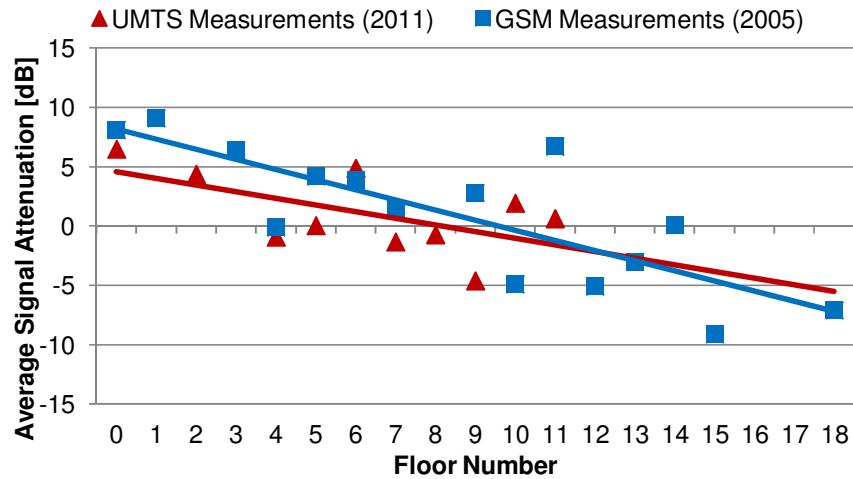


Figure I.3. Signal attenuation values for Indoor Window rooms in High Isolated buildings.

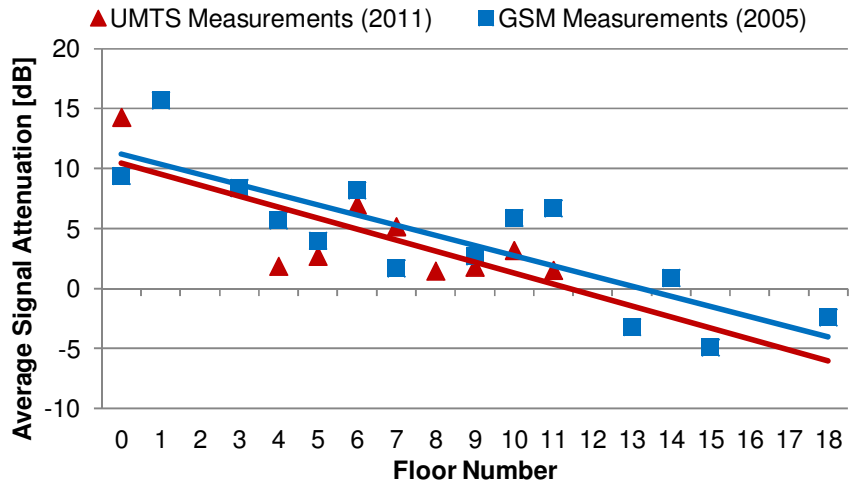


Figure I.4. Signal attenuation values for Indoor Daylight rooms in High Isolated buildings.

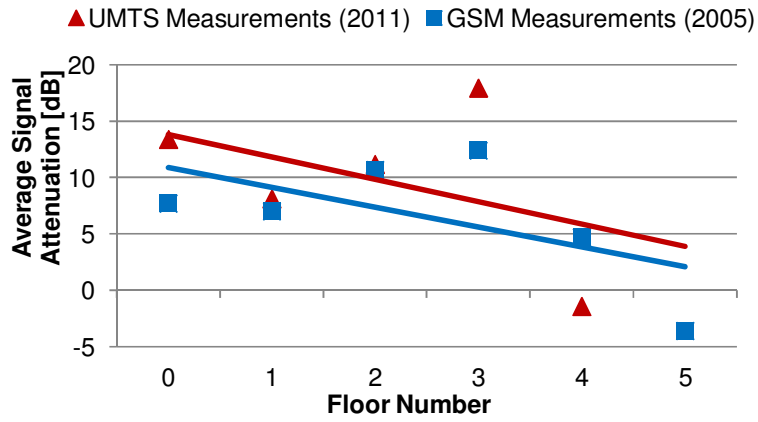


Figure I.5. Signal attenuation values for Indoor Window rooms in Low Integrated buildings.

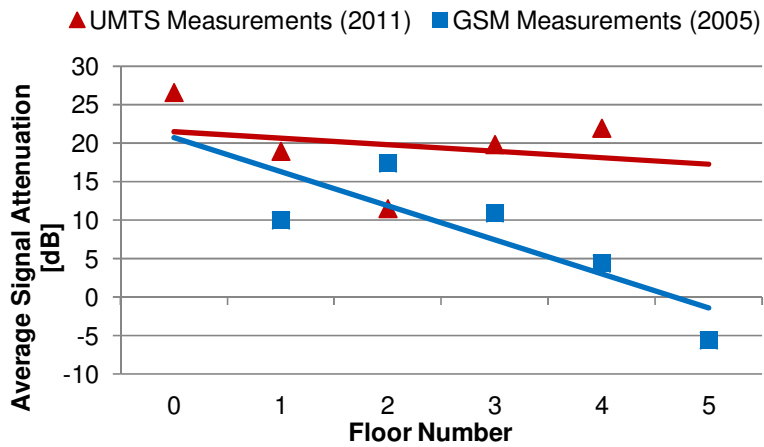


Figure I.6. Signal attenuation values for Indoor Daylight rooms in Low Integrated buildings.

# References

- [3GPP02a] 3GPP, Technical Specification Group Radio Access Network, *UTRAN Overall Description (Release 99)*, Report TS 25.401, Version 3.10.0, June 2002 (<http://www.3gpp.org/ftp/Specs/html-info/25401.htm>).
- [3GPP02b] 3GPP, Technical Specification Group Services and System Aspects, *Quality of Service (QoS) concept and architecture (Release 99)*, Report TS 23.107, V3.9.0, Sep. 2002 (<http://www.3gpp.org/>).
- [3GPP06a] 3GPP, Technical Specification Group – RAN WG1 (Radio Layer 1), *64QAM for HSDPA - Link-Level Simulation Results*, Meeting no. 46, Tallinn, Estonia, Sep. 2006 ([http://www.3gpp.org/ftp/tsg\\_ran/WG1\\_RL1/TSGR1\\_46/Docs/R1-062264.zip](http://www.3gpp.org/ftp/tsg_ran/WG1_RL1/TSGR1_46/Docs/R1-062264.zip)).
- [3GPP06b] 3GPP, Technical Specification Group – RAN WG1 (Radio Layer 1), *16QAM for HSUPA - Link-Level Simulation Results*, Meeting no. 46, Tallinn, Estonia, Sep. 2006 ([http://www.3gpp.org/ftp/tsg\\_ran/WG1\\_RL1/TSGR1\\_46/Docs/R1-062266.zip](http://www.3gpp.org/ftp/tsg_ran/WG1_RL1/TSGR1_46/Docs/R1-062266.zip)).
- [3GPP06c] 3GPP, Technical Specification Group – RAN WG1 (Radio Layer 1), *D-TxAA with 64QAM for HSDPA – Link-Level Simulation Results*, Meeting no. 47, Riga, Latvia, Nov.2006 ([http://www.3gpp.org/ftp/tsg\\_ran/WG1\\_RL1/TSGR1\\_47/Docs/R1-063115.zip](http://www.3gpp.org/ftp/tsg_ran/WG1_RL1/TSGR1_47/Docs/R1-063115.zip)).
- [3GPP07] 3GPP, Technical Specification Group – RAN WG2 (Radio Layer 2), *HSPA+ User Plane Enhancements*, Report R2-070125, Sorrento, Italy, Jan. 2007 ([ftp://ftp.3gpp.org/tsg\\_ran/WG2\\_RL2/TSGR2\\_56bis/Documents/R2-070125.zip](ftp://ftp.3gpp.org/tsg_ran/WG2_RL2/TSGR2_56bis/Documents/R2-070125.zip)).
- [3GPP09] 3GPP, Technical Specification Group Services and System Aspects, *Technical Specifications and Technical Reports for a UTRAN-based 3GPP system (Release 99)*, Report TS 21.101, Version 3.18.0, Dec. 2009 (<http://www.3gpp.org/ftp/Specs/html-info/21101.htm>).
- [3GPP10a] 3GPP, Technical Specification Group Services and System Aspects, *Service aspects, Services and Service Capabilities (Release 9)*, Technical Specification Group Services and System Aspects, Report TS 22.105, V9.1.0, Oct. 2010 (<http://www.3gpp.org/ftp/Specs/html-info/22105.htm>).
- [3GPP10b] 3GPP, Technical Specification Group Radio Access Network, *UE Radio Access*

capabilities (Release 9), Report TS 25.306, V9.5.0, Dec. 2010 (<http://www.3gpp.org/ftp/Specs/html-info/25306.htm>).

- [Asco11] <http://www.ascom.com/en/tems-investigation-3.htm>, May 2011.
- [BEGG08] Bergman,J., Ericson,M., Gerstenberger,D., Göransson,B., Peisa,J. and Wager,S., *HSPA Evolution – Boosting the performance of mobile broadband access*, Ericsson Review, Vol. 85, No. 1, 2008, pp.32-37.
- [BrHo10] Braz,G. and Hoefel,R., “Indoor WCDMA/HSDPA: Field and Analytical Results on Coverage and Throughput”, in *Proc. of 7<sup>th</sup> International IEEE Symposium on Wireless Communication Systems*, Jersey City, New Jersey, USA, Sep. 2010.
- [Carr11] Carreira,P., *Data Rate Performance Gains in UMTS Evolution to LTE at the Cellular Level*, M.Sc. Thesis, Instituto Superior Técnico, Lisbon, Portugal, Oct. 2011.
- [CEGH02] Catreux,S., Erceg,V., Gesbert,D. and Heath,R.W. Jr., “Adaptive Modulation and MIMO Coding for Broadband Wireless Data Networks”, *IEEE Communications Magazine*, Vol. 40, No. 6, June 2002, pp.108-115.
- [ChAn08] Chandrasekhar,V. and Andres,J., “Femtocell networks: a survey”, *IEEE Communications Magazine*, Vol. 46, No. 9, Sep. 2008, pp.59-67.
- [Chen03] Chen,Y., *Soft Handover Issues in Radio Resource Management for 3G WCDMA Networks*, Ph. D. Thesis, Queen Mary College - University of London, London, UK, 2003.
- [Code11] <http://www.codegear.com/>, Apr. 2011.
- [Corr09] Correia,L.M., *Mobile Communications Systems – Lecture Notes*, Instituto Superior Técnico, Lisbon, Portugal, 2009.
- [DaCo99] Damosso,E. and Correia,L.M., *Digital Mobile Radio Towards Future Generation Systems (COST 231 Final Report)*, COST Telecom Secretariat, European Commission, Brussels, Belgium, 1999.
- [DPSB08] Dahlman,E., Parkvall,S., Sköld,J., Beming,P., *3G Evolution – HSPA and LTE for Mobile Broadband (2<sup>nd</sup> edition)*, Academic Press, Oxford, UK, 2008.
- [EsPe06] Esteves,H., Pereira,M., *Impact of Intra- and Inter-Cell Interference on UMTS-FDD (in Portuguese)*, Graduation Project, Instituto Superior Técnico, Lisbon, Portugal, 2006.
- [Gold05] Goldsmith,A., *Wireless Communications*, Cambridge University Press, Stanford, California, USA, 2005.
- [Hata80] Hata,M., “Empirical Formula for Propagation Loss in Land Mobile Radio Services”, *IEEE*

*Trans. on Vehicular Technology*, Vol. 29, No.3, Aug. 1980, pp. 317-325.

- [HoTo04] Holma,H. and Toskala,A., *WCDMA for UMTS (3<sup>rd</sup> Edition)*, John Wiley & Sons, Chichester, UK, 2004.
- [HoTo06] Holma,H. and Toskala,A., *HSDPA/HSUPA for UMTS*, John Wiley & Sons, Chichester, UK, 2006.
- [HoTo07] Holma,H. and Toskala,A., *WCDMA for UMTS – HSPA Evolution and LTE (4<sup>th</sup> Edition)*, John Wiley & Sons, Chichester, UK, 2007.
- [HoTo10] Holma,H. and Toskala,A., *WCDMA for UMTS – HSPA Evolution and LTE (5<sup>th</sup> Edition)*, John Wiley & Sons, Chichester, UK, 2010.
- [IkYo84] Ikegami,F., Yoshida,S., Takeuchi,T. and Umehira,M., “Propagation Factors Controlling Mean Field Strength on Urban Streets”, *IEEE Trans. on Antennas and Propagation*, Vol. AP-32, No. 8, Aug. 1984, pp. 882-889.
- [IsLe07] Isotalo,T. and Lempiäinen,J., “HSDPA measurements for Indoor DAS”, in *Proc. of 65<sup>th</sup> IEEE Vehicular Technology Conference*, Dublin, Ireland, Apr. 2007.
- [Jaci09] Jacinto,N., *Performance Gains Evaluation from UMTS/HSPA+ to LTE at the Radio Network Level*, M. Sc. Thesis, Instituto Superior Técnico, Lisbon, Portugal, 2009.
- [Kath11] <http://www.kathrein.de/en/mcs/index.htm>, June 2011.
- [Lope08] Lopes,J., *Performance Analysis of UMTS/HSDPA/HSUPA at the Cellular Level*, M. Sc. Thesis, Instituto Superior Técnico, Lisbon, Portugal, 2008.
- [Marq08] Marques,A., *Modelling of Building Height Interference Dependence in UMTS*, M. Sc. Thesis, Instituto Superior Técnico, Lisbon, Portugal, 2008.
- [Nguy05] Nguyen,S., *Capacity and Throughput Optimization in Multi-Cell 3G WCDMA Networks*, M.Sc. Thesis, University of North Texas, Denton, Texas, USA, 2005.
- [OkOh68] Okumura,Y., Ohmori,E. and Kawano,T., “Field Strength and Its Variability in VHF and UHF Land-Mobile Service”, *Review of the Electrical Communication Laboratory*, Vol. 16, no. 9-10, Oct. 1968, pp. 825-873.
- [Preg08] Preguiça,R., *Comparison between UMTS/HSPA+ and WiMAX/IEEE 802.16e in Mobility Scenarios*, M.Sc. Thesis, Instituto Superior Técnico, Lisbon, Portugal, Sep. 2008.
- [PWST07] Peisa,J., Wager,S., Sågfors,M., Torsner,J., Göransson,B., Fulghum,T., Cozzo,C. and Grant,S., “High Speed Packet Access Evolution – Concept and Technologies”, in *Proc. of 65<sup>th</sup> IEEE Vehicular Technology Conference*, Dublin, Ireland, Apr. 2007.

- [Rahm68] Rahman,N.A., *A Course in Theoretical Statistics*, Charles Griffin and Company, London, UK, 1968.
- [RMSp87] Rao,D.N., Murthy,M.J.K., Sarkar,S.K., Pasricha,P.K., Dutta,H.N. and Reddy,B.M., "Hilly Terrain LOS Fadeouts and Fresnel Zone Considerations from Ray Tracing Techniques", *IEEE Trans. on Antennas and Propagation*, Vol. AP-35, No. 11, Nov. 1987, pp. 1330-1333.
- [Sant04] Santo,L., *UMTS Performance in Multi-Service Non-Uniform Traffic Networks*, M.Sc. Thesis, Instituto Superior Técnico, Lisbon, Portugal, 2004.
- [SLCM05] Sebastião,D., Ladeira,D., Carpinteiro,G., Martins,G., Esteves,H., Ferreira,L., Pereira,M., Kuipers,M., Costa,P., Correia,S. and Correia,L.M., *Characterisation of signal penetration into buildings for GSM900, GSM1800 and UMTS-FDD*, Instituto de Telecomunicações, Lisboa, Portugal, Nov. 2005.
- [SRAA03] Sallent,O., Ruiz,S., Agusti,R., Adelantado,F., Diaz-Guerra,M.A., Montero,J., Gago,E., Miranda,J.L., "Using measurements extracted from GSM/UMTS networks for 3G planning and RRM evaluation", *IEEE Wireless Communications and Networking*, Vol. 3, Mar. 2003, pp.1448-1452.
- [SKYM03] Sugano,M., Kou,L., Yamamoto,T. and Murata,M., "Impact of Soft Handoff on TCP Throughput over CDMA Wireless Cellular Networks", in *Proc. of VTC 2003 Fall – IEEE Vehicular Technology Conference*, Orlando, Florida, USA, Oct. 2003.
- [TaFi10] Tang,Z. and Fitzpatrick,P., "Measurement of the Impact of Building Penetration Loss on HSDPA Performance", in *6<sup>th</sup> International Conference on Wireless Communications Networking and Mobile Computing (WiCOM)*, Chengdu, China, Sep. 2010.
- [TaPi93] Tanis,W.J., Pilato,G.J., "Building penetration characteristics of 880 MHz and 1922 MHz radio waves", in *Proceedings of VTC'93 – 43rd IEEE Vehicular Technology Conference*, Secausus, New Jersey, USA, May 1993.
- [ToTP98] Toledo,A.F, Turkami,A.M.D., Parsons,J.D., "Estimation coverage of radio transmission into and within buildings at 900, 1800 and 2300 MHz", in *IEEE Personal Communications*, Vol. 5, No. 2, Apr. 1998, pp. 40-47.
- [Telm08] Batista,T., *Capacity Increase in UMTS/HSPA+ Through The Use of MIMO Systems*, M. Sc. Thesis, Instituto Superior Técnico, Lisbon, Portugal, 2008.
- [TPTe11] <http://tptest.sourceforge.net/index.php>, June 2011.
- [Voda11] Vodafone Portugal, *Internal communication*, Sep. 2011.

- [XaVe02] Xavier,D.M. and Venes,J.M., *Characterisation of signal penetration loss into buildings for GSM* (in Portuguese), Graduation Project, Instituto Superior Técnico, Lisbon, Portugal, Sep. 2002.
- [WaBe88] Walfisch,J. and Bertoni,H., "A Theoretical Model of UHF Propagation in Urban Environments", *IEEE Trans. on Antennas and Propagation*, Vol. 36, No. 12, Dec. 1988, pp. 1788-1796.
- [Wire11] <http://wirelesshabitat.eu/archives/104>, Sep. 2011.
- [Zimm80] Zimmermann,H., "OSI Reference Model – The ISO Model Architecture for Open Systems Interconnection", *IEEE Transactions on Communications*, Vol. 28, No. 4, Apr. 1980, pp. 425-432.